

BEXYL
BEYOND XYLELLA

Identification of the molecular mechanisms of resistance to *Xylella fastidiosa* across main perennial crops

Deliverable 4.2

30 June 2026

Author(s): Ofir Bahar (P11-ARO-VOL), Maria Saponari, Pasquale Saldarelli, Annalisa Giampetruzzi, Soraya Mousavi, Roberto Mariotti (P5-CNR), Silke Robatzek (P12-LMU), Leonardo de la Fuente (P9-AU)

Funded by the European Union

DELIVERABLE INFORMATION

Start of the project:	01 Sep 2022
Duration:	48 months
Coordinator:	Blanca B. Landa
Deliverable title:	Identification of the molecular mechanisms of resistance to *Xylella fastidiosa* across main perennial crops
Deliverable n°:	D4.2
Nature of the deliverable:	Report
Dissemination level:	Sensitive
WP contributing:	WP4
Lead beneficiary:	P11-ARO-VOL
Due date of deliverable:	30 June 2026
Actual submission date:	30 June 2026

Deliverable status

Ver.	Status	Date	Author(s)
1.0	Final	30 June 2026	Ofir Bahar (P11-ARO-VOL), Maria Saponari, Pasquale Saldarelli, Annalisa Giampetruzzi, Soraya Mousavi, Roberto Mariotti (P5-CNR), Silke Robatzek (P12-LMU), Leonardo de la Fuente (P9-AU)

Disclaimer

The content of this deliverable does not necessarily reflect the official opinions of the European Commission or other institutions of the European Union.

Funded by the European Union

Table of contents_

1. **INTRODUCTION** 5

2. **MATERIALS AND METHODS** 6

2.1 Transcriptomic analysis of resistant and susceptible almond cultivars in response to Xylella fastidiosa *infection* *6*

2.2. Genome sequencing and immune profiling of the immune receptor landscape of olive 6

2.2.1 Genome assembly 6

2.2.2 Protein-coding gene annotation 7

2.2.3 Domain-based prediction of the PRRome and NLRome 7

2.2.4 Protein phylogenetic trees 8

2.2.5 Synteny analysis 8

2.2.6 Identification of orthologs 8

2.2.7 *Olea europea* phylogenetic tree and gene family expansion/contraction analysis 8

2.2.8 Molecular cloning 9

2.2.9 Transient and stable transformation of plants 9

2.2.10 ROS assay 9

2.2.11 MAPK phosphorylation assay 9

2.3. Genome Wide Association Study (GWAS) of olive cultivars and progeny *10*

2.3.1 Probe design for single-primer enrichment technology 10

2.3.2 DNA extraction, library preparation and sequencing 11

2.3.3 Short read mapping and SNP detection for SPET benchmark 13

2.3.4 SPET benchmark data analysis 13

2.3.5 Genome-wide association study for *Xf* phenotypes 13

2.4 Characterization of the molecular response of resistant and susceptible olive cultivars to Xylella fastidiosa *infection* *14*

2.4.1 Plant inoculations and RNA-Seq analysis 14

2.4.2 Bioinformatic analysis 14

2.5 Characterization of the mineral element concentrations (ionome) in susceptible and resistant almond and olive cultivars. *15*

3. **RESULTS** 16

3.1 Transcriptomic analysis of resistant and susceptible almond cultivars in response to Xylella fastidiosa *subsp.* fastidiosa *inoculation* *16*

3.2 Genome sequencing and immune profiling of the immune receptor landscape of olive *20*

Funded by the European Union

3.2.1 Genome assembly and gene model prediction of *Olea europaea* cultivars 'Leccino' and 'Ogliarola salentina' 20
3.2.2 Genome features of *Olea europaea* cultivars 21
3.2.3 Defining the *Olea europaea* cultivar immune receptor repertoire 21
3.2.4 The PTI landscape of the *Olea europaea* cultivars and *Xylella fastidiosa* responses 26
3.3 Genome wide association study (GWAS) of olive cultivars and progeny 30
3.3.1 SNP and phenotypic data merging for GWAS analysis 30
3.3.2 Evaluation of quantitative bacterial load (Cq) associated loci 30
3.3.3 Evaluation of Plant Disease Severity Classification Associated Loci 32
3.3.4 Bioinformatic Integration and Literature Cross-Validation 35
3.3.5 Variant Effect Prediction (VEP) and High-Impact Mutation Profiling 35
3.3.6 Characterization of the water stress-responses 36
3.4 Characterization of the molecular response of resistant and susceptible olive cultivars to Xylella fastidiosa *infection 37*
3.5 Characterization of the mineral element concentrations (ionome) in susceptible and resistant plants 42
3.5.1 Ionome analysis of susceptible and resistant almonds cultivars 42
3.5.2 Ionome analysis of susceptible and resistant olive cultivars 48
4. **DISCUSSION** 51
4.1 Transcriptomic analysis of resistant and susceptible almond cultivars in response to Xylella fastidiosa *infection 51*
4.2 Haplotype-resolved genomes and immune profiling of the immune receptor landscape of olive 52
4.3 Genome Wide Association Study (GWAS) of olive cultivars and progeny 53
4.4 Characterization of the molecular response of resistant and susceptible olive cultivars to Xylella fastidiosa *infection. 54*
4.5 Characterization of the mineral element concentrations (ionome) in susceptible and resistant plants 56
5. **CONCLUSIONS** 58
6. **REFERENCES** 58
7. **SUPPLEMENTARY MATERIAL** 68

Funded by the European Union

1. INTRODUCTION

Xylella fastidiosa (*Xf*) is a xylem-limited bacterial pathogen that threatens numerous economically important perennial crops worldwide, including olive, almond, grapevine, citrus, and several ornamental and forest species. Since its introduction into Europe, *Xf* has caused severe economic and environmental damage, most notably through Olive Quick Decline Syndrome (OQDS) in southern Italy, but also through disease outbreaks affecting almond, grapevine and other hosts in several Mediterranean regions. The absence of effective curative treatments has highlighted the urgent need to identify and deploy durable sources of resistance as a sustainable disease management strategy.

Thus far, host species that are immune to *Xf* infection have not been reported. However, quantitative resistance to *Xf* has been identified in several crop species, including grapevine, olive, and almond, indicating that resistance to *Xf* is likely a complex trait involving multiple layers of host defense. Successful resistance may depend on the ability of plants to recognize pathogen-derived molecules, activate innate immune responses, restrict bacterial colonization and movement within the xylem, reinforce structural barriers, and modulate physiological responses associated with disease development. Recent advances in genomics, transcriptomics, and functional biology have created new opportunities to dissect these mechanisms and identify the genetic determinants underlying differential host susceptibility.

Natural variation in disease response has been observed among cultivars of several perennial crops. In olive, cultivars such as 'Leccino' display reduced susceptibility to *Xf* infection compared with highly susceptible cultivars, suggesting the presence of genetic factors that enhance pathogen recognition and immune activation. Similarly, in almond, resistant cultivars exhibit reduced symptom development and lower bacterial colonization relative to susceptible genotypes, indicating the existence of defense mechanisms that limit disease progression. Understanding the molecular basis of these contrasting responses is essential for accelerating breeding programs and developing innovative strategies for disease control.

This report brings together complementary studies aimed at identifying the molecular mechanisms associated with resistance to *Xf* across major perennial crops. The work integrates comparative genomics, transcriptomics, immune phenotyping, and physiological analyses to characterize host responses at multiple biological levels. By comparing resistant and susceptible genotypes, we sought to identify candidate genes, signaling pathways, immune receptors, and defense-related processes associated with resistance. Particular attention was given to mechanisms involved in pathogen perception, activation of plant immunity, cell wall remodeling, hormone-mediated defense signaling, and the restriction of bacterial colonization.

The combined results provide new insights into both conserved and crop-specific mechanisms of resistance to *Xf*. These findings contribute to a broader understanding of host-pathogen interactions in perennial crops and establish a foundation for the development of resistant cultivars and future disease management strategies.

Funded by the European Union

2. MATERIALS AND METHODS

2.1 Transcriptomic analysis of resistant and susceptible almond cultivars in response to *Xylella fastidiosa* infection

The objective of this experiment was to identify differentially expressed genes (DEGs) associated with the resistance mechanism to *Xf* by comparing the transcriptomic response of two almond cultivars (susceptible – 'UEF'; and resistant - 'Lauranne') to *Xf* subsp. *fastidiosa* infection.

Two-year-old almond trees of the susceptible cultivar UEF and the resistant cultivar 'Lauranne' were grown under net-house conditions and inoculated with *Xf* subsp. *fastidiosa* (*Xff*) strain SN17-4 of ST1 by using the pin-prick method (Zecharia et al. 2022). Four treatment groups were established: non-inoculated 'UEF' (Uc), inoculated 'UEF' (Ui), non-inoculated 'Lauranne' (Lc), and inoculated 'Lauranne' (Li). Leaf samples were collected two weeks after inoculation from three biological replicates (plants) per treatment.

Total RNA was extracted from leaf tissue using the EURx RNA Purification Kit (EURx, Gdańsk, Poland) according to the manufacturer's instructions. Briefly, leaf samples were homogenized, lysed, and applied to silica membrane spin columns, where RNA was selectively bound, washed, and eluted. RNA quality and integrity were assessed prior to sequencing. Libraries were prepared and sequenced by Syntezza Bioscience Ltd. (Jerusalem, Israel). Raw reads were quality-filtered and mapped to the almond reference genome (Lauranne Genome v1.0; GCA_008632915.2). Differential gene expression analysis was performed using DESeq2 (Love et al., 2014). Genes were considered significantly differentially expressed when the adjusted *p*-value (padj) was < 0.05 and the absolute $\log_2$ fold change was ≥ 1. Functional enrichment analyses of Gene Ontology (GO) terms and KEGG pathways were performed to identify biological processes and pathways associated with resistance and susceptibility responses to *Xff*.

2.2. Genome sequencing and immune profiling of the immune receptor landscape of olive

To investigate the molecular basis of resistance to *Xf* subsp. *pauca* in olive, comparative genomic and functional analyses were conducted using the resistant cultivar 'Leccino' and the susceptible cultivar 'Ogliarola salentina'. High-quality haplotype-resolved genome assemblies were generated for both cultivars and used to characterize their repertoires of pattern recognition receptors (PRRs) and nucleotide-binding leucine-rich repeat receptors (NLRs). In parallel, immune responses were evaluated by assessing the ability of pathogen-associated molecular patterns (PAMPs) and bacterial extracts to trigger pattern-triggered immunity (PTI). The integration of genomic and immune phenotyping approaches enabled the identification of differences in immune receptor composition and defense responses associated with resistance and susceptibility to *Xf*.

2.2.1 Genome assembly

We aimed to generate nuclear genome assemblies for each 'Leccino' and 'Ogliarola salentina' haplotype, excluding sequence originating from organelles, contaminants, or sequencing

Funded by the European Union

errors. We generated phased genome assemblies from PacBio HiFi reads and Illumina paired-end Hi-C reads using hifiasm (Cheng et al. 2021) (version 0.16.0-r369), producing an initial set of contigs for each haplotype. To identify contigs originating from sequencing errors, we aligned PacBio HiFi reads against the initial sets with minimap2 (Li 2018) (version 2.24-r1122) and computed the median read depth of each contig using mosdepth (Pederson et al. 2018) (version 0.3.2). We excluded contigs with a median read depth lower than 6, considering these technical noise or contamination. To distinguish between nuclear and non-nuclear sequence, we aligned contigs against the RefSeq plant, mitochondrion, and plastid genomic databases (Steinegger and Söding 2017) (FTP release 210) using mmseqs2 (version 3bcbdbab3debafa8750e38834fc387863fe9bec8). We excluded contigs with a best hit against an organellar sequence or no hit at all. To help prevent removing genuine nuclear contigs, we did not exclude those containing at least one highly conserved single-copy ortholog of the BUSCO (Manni et al. 2021) (version 5.2.2) embryophyta_odb10 database.

We then set out to generate chromosome-level sequences out of the sets of filtered contigs. We aligned Hi-C reads to each set of contigs using a workflow consisting of bwa mem (Li 2013) (version 0.7.17-r1188), pairtools (Open2C et al. 2024) (version 0.3.0), samtools (Danecek et al. 2021) (version 1.6), and bedtools (Quinlan and Hall 2010) (version 2.30.0). We subsequently used SALSA2 (Ghurye et al. 2019) (version 2.3) to scaffold the sets according to the Hi-C alignments. To help determine how the scaffolds should be placed into chromosomes, we aligned scaffolds against the 'Leccino' assembly of Lv *et al.* using nucmer (Marçais et al. 2018) (version 4.0.0beta2). We used Juicebox Assembly Tools (Dudchenko et al. 2018) to place scaffolds in chromosome-level sequences, using the Hi-C contact maps and the alignments against the assembly of Lv *et al.* as guidance. We gave precedence to the Hi-C contact maps over the alignments if they disagreed with each other. This resulted in 23 chromosome-level sequences and a set of all unplaced scaffolds for each haplotype. To ease comparisons between the haplotypes, all chromosome-level sequences follow the orientation of their homologous counterparts in the Lv *et al.* assembly. We assessed the quality of the final genome assemblies using QUAST (Mikheenko et al. 2018) (version 5.0.2) and Merqury (Rhie et al. 2020) (version 1.3).

2.2.2 Protein-coding gene annotation

Helixer (Holst et al. 2026) (version 0.3.4) with the land_plant model (version land_plant_v0.3_a_0080.h5). We excluded gene models lacking valid open reading frames using AGAT (Dainat et al. 2026) (version 1.4.1) and gffread (Pertea and Pertea 2020) (version 0.12.7). Following recommended filtering strategies (Vuruputoor et al. 2023), we retained gene models encoding proteins containing a known protein domain, according to Interproscan (Jones et al. 2014) (version 5.70-102.0), and/or have 0.8 reciprocal overlap with a RefSeq plant protein (FTP release 226), determined using mmseqs2 (Steinegger and Söding 2017) (version 3bcbdbab3debafa8750e38834fc387863fe9bec8). We assessed the quality of the final gene annotations using BUSCO (Manni et al. 2021) (version 5.2.2), ran with the embryophyta_odb10 database, and gFACs (Caballero and Wegrzyn 2019) (version 1.1.2).

2.2.3 Domain-based prediction of the PRRome and NLRome

All protein sequences from the four assembled haplotypes were obtained with agat_sp_keep_longest_isoform.pl from AGAT (Dainat et al. 2026) (version 1.5.1) and gffread

Funded by the European Union

(Pertea and Pertea 2020) (version 0.12.7). Identification of RLKs, RLPs and NLRs were identified using a domain-based pipeline inspired by Ngou et al. (2022) (Ngou et al. 2022). Domains were identified via HMMER (version 3.4, hmmer.org) and transmembrane (TM) domain prediction via deepTM 1.0 web interface (Hallgren et al. 2022) LRR-RLKs were defined as proteins containing an LRR domain, a TM domain and a kinase domain and with a minimum protein length of 250 amino acids. LRR-RLK-XIIs were further defined based on their similarity with Arabidopsis known as class XII, performed with domain alignments and phylogenetic trees, as detailed in the next part. LRR-RLPs were defined as proteins containing an LRR domain, a TM domain, the absence of a kinase domain, the presence of a C3F domain (Fritz-Laylin et al. 2005) and a minimum protein length of 150 amino acids. The custom HMM C3F profile was built from a multiple alignment of Arabidopsis LRR-RLPs following Ngou et al., (2022) (Ngou et al. 2022). LysM-RLKs were defined as proteins containing LysM domains, a TM domain, a kinase domain and a minimum protein length of 150 amino acids. LysM-RLPs were defined as proteins containing LysM domains, a TM domain, the absence of a kinase domain and a minimum protein length of 150 amino acids. NLRs were defined as proteins containing an NB-ARC domain, a LRR domain and at least one of the following domains: TIR, CC or RPW8. NLRs were further classified in CNLs, TNLS RPW8-NLs and only NLs according to their domains.

2.2.4 Protein phylogenetic trees

Trees were inferred from alignments of either the full protein sequences, the ectodomains, or trimmed domains. LRR domains were trimmed according to their coordinates given in the HMM output (version 3.4, hmmer.org) and ectodomains were trimmed according to the transmembrane domain coordinates given by deepTM (Hallgren et al. 2022) (version 1.0), both with a custom bash script. Sequence alignments were done with MAFFT (Katoh and Standley 2013) (version 7.526) and trimmed with trimAL (Capella-Gutiérrez et al. 2009) (version 1.5.1). Phylogenetic trees were inferred using IQ-TREE (Wong et al. 2026) (Version 3.0.1) and visualisation and annotation were performed in R using the ggtree package.

2.2.5 Synteny analysis

Synteny analysis across the four haplotype assemblies was performed using SyRi (Goel et al. 2019) and visualization using plotsr (Goel and Schneeberger 2022) (version 1.1.1). As SyRi compares in a pairwise manner, comparisons of all haplotypes against all were generated.

2.2.6 Identification of orthologs

To identify olive orthologs of Arabidopsis and Solanaceae species, or orthologs across the four haplotypes themselves, OrthoFinder (Emms and Kelly 2015; Emms and Kelly 2019) (version 2.5.5) was run on published proteomes and Olive putative proteomes generated with AGAT (Dainat et al. 2026) (version 1.5.1) and gffread (Pertea and Pertea 2020) (version 0.12.7. When possible, used proteomes contained only the longest isoforms.

2.2.7 *Olea europaea* phylogenetic tree and gene family expansion/contraction analysis

We used CAFE5 (Mendes et al. 2021) to analyse changes in gene family size in a way that accounts for phylogenetic history and provides a statistical foundation for evolutionary

Funded by the European Union

inferences. Input files for CAFE5 were generated by OrthoFinder (SpeciesTree_rooted.txt & Orthogroups.GeneCount.tsv). The species tree was transformed to be ultrametric with treePL (Smith and O'Meara 2012) (version 2.6.3) and the orthogroup gene counts were filtered to only retain gene families with gene copies in at least two species of the specified clades and split in two according to gene family size (small families with < 100 and big families > 100 gene copies in one or more species) with a custom R script. Results were visualized with CafePlotter (version 0.2.0, repository retrieved from https://github.com/moshi4/CafePlotter).

2.2.8 Molecular cloning

The gene of interest was amplified with attB flanking sites and cloned into the Gateway donor vector pDONR221 using BP Clonase II. Verified entry clones were then recombined with the destination vector pB8m34GW-FAST using LR Clonase II to generate expression constructs under the control of the AtUBQ10 promoter and in-frame with C-terminal fusion tag (mCherry or eGFP). All constructs were confirmed by sequencing.

2.2.9 Transient and stable transformation of plants

For transient transformation of *Nicotiana benthamiana*, *Agrobacterium tumefaciens* (strain AGL1 or GV3101) carrying the desired constructs were resuspended in infiltration buffer (10 mM MES, 10 mM $MgCl_2$, pH 5.5-5.6) supplemented with 100 µM acetosyringone. Bacteria were pelleted by centrifugation at 3000 x g for 3 min, washed once with infiltration buffer, and resuspended to a final OD_{600} of 0.2–0.4. The bacterial suspension was infiltrated into the abaxial side of fully expanded leaves of 6-8-week-old *N. benthamiana* plants using a needleless 1-mL syringe. Infiltrated plants were grown under standard conditions, and leaf samples were harvested at 2-3 days post-infiltration (dpi) for downstream microscopy, ROS, Western blot analyses.

Stable transgenic *Arabidopsis* lines were generated via *Agrobacterium*-mediated floral dip method (Zhang et al. 2006). *A. tumefaciens* carrying the binary construct was resuspended in 5% sucrose with 0.02% Silwet L-77 (OD_{600} = 0.6-0.8). Flowering plants were dipped for 2-3 s, covered overnight, and grown to seed set. Transformants were selected on antibiotic-containing ½ MS medium and confirmed by PCR.

2.2.10 ROS assay

Reactive oxygen species (ROS) burst assays were performed as reported (Hawkins et al. 2023). In brief, leaf discs were collected with a biopsy puncher (4 mm width), placed in a white 96-well multiplate (minimum 8 discs per treatment per assay), and incubated overnight in 200 µL of distilled water. The water was then replaced with 100 µL assay solution containing luminol (17 µg/mL), horseradish peroxidase (HRP, 10 µg/mL), PAMP either 100 µM flg22, 100 µM SCOOP12, 100 µM *Xf* PEPs, 1 mg/mL chitin, or no elicitor (mock). Luminescence was detected over time using a Photek camera system and software.

2.2.11 MAPK phosphorylation assay

Leaf tissues from *A. thaliana*, *N. benthamiana*, and *Olea europaea* were treated with bacterial extracts or elicitors for different time points. Proteins were extracted in buffer containing 10% glycerol, 25 mM Tris-HCl pH 7.5, 1 mM EDTA, 150 mM NaCl, 0.2% NP-40, 1 mM DTT, and protease inhibitor cocktails. Supernatants were collected after centrifugation, mixed with

Funded by the European Union

Lämmli buffer (1:1 ratio), boiled at 95°C for 5 min, separated by 10% SDS-PAGE, and transferred to PVDF membranes. Phosphorylated MAPKs were detected using α-pERK1/2 antibodies, with CBB staining as a loading control.

2.3. Genome Wide Association Study (GWAS) of olive cultivars and progeny

2.3.1 Probe design for single-primer enrichment technology

Single primer enrichment technology (SPET, United States Patent 9,650,628) is a customizable solution for targeted sequencing. SPET requires a priori genomic or transcriptomic information and identification of SNPs for probe design. Its application to plant materials is still largely unexplored, with one recent exception (Scaglione et al., 2019) assessing SPET application to *Zea mays* L. and to *Populus nigra* L. In the present study, SPET primers have been designed for the first time for genotyping of olive germplasm. To design SPET probes, 82 *Olea europaea* published genomes related to cultivars and wild types with high quality data have been selected, after global WGS coverage filter analyses, 13 genomes with low coverage have been removed.

Genetic relatedness analysis: Genetic relationships among samples were inferred by means of identity-by-state (IBS) analysis (Stevens et al. 2011). Filters were applied on the IBS-0 and IBS-2 values, i.e., the number of loci in which two individuals share 0 alleles or 2 alleles, respectively. For each couple in the population, a sample was excluded when either IBS0<0.05% or IBS2>90%. Following Variant filtration, from 921,550 putative regions, 176,661 regions have been selected. only the regions with length between 5 and 1000 bp and SNP density<10%, were chosen (**Figure 1**).

Gene annotation criteria:

- ~53,000 genes have been predicted in the *O. europaea* genome.
- The polymorphic regions obtained here could cover, ideally, up to 41,989 genes.
- To maximize the number of covered genes, lenient thresholds were applied inside genic regions.
- At least two regions per gene were included, of which one was exonic.

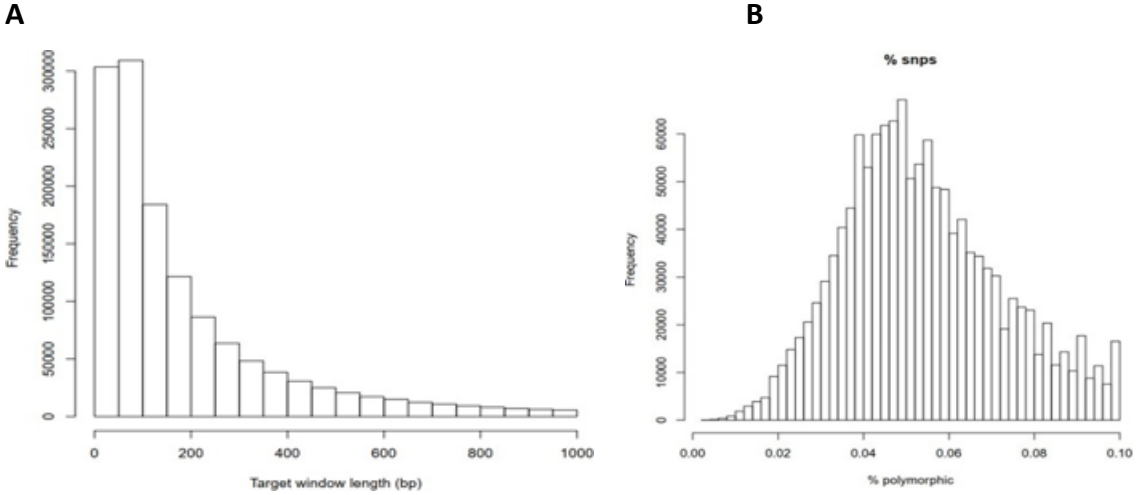
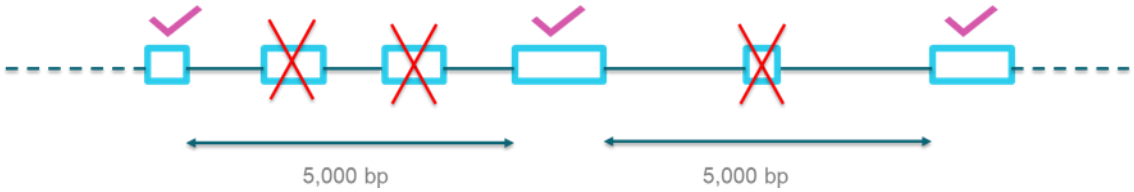


Figure 1. Selection of region (A) and SNP (B) with highest frequency.

Funded by the European Union

Spacing filter: A minimum gap of 5,000 bp between regions was defined to ensure uniform genome space distribution throughout the genome:



The presence of large (>100 kb) portions of the genome with the absence of regions was also checked. These gaps were filled by selecting the most suitable regions among those that had been previously discarded.

A set of 176,661 regions were carefully selected, which should allow obtaining an expected final number of ~90,000 probes. This SPET region set designed can target 41,595 genes in the *Olea europaea* 'Arbequina' reference genome. These probes are uniformly distributed across the olive genome and are theoretically designed to capture and sequence target regions of approximately 300 base pairs (bp).

To date, an initial batch of 1,200 samples of ongoing CNR projects, comprising 133 distinct cultivars and their associated progeny, sequenced via Single Primer Enrichment Technology (SPET) on the Illumina short-read platform has been processed.

2.3.2 DNA extraction, library preparation and sequencing

A total of 111 olive trees were sampled from CNR olive collections and 21 *Xf*-resistant 'Leccino' progenies (**Table 1**), were added to this list (La Notte et al., 2024).

Genomic DNA was extracted from leaf tissue using the Zymo Research Mini Plant/Seed DNA Extraction Kit, following the manufacturer's instructions. Tissue maceration was performed using a HOMEX XS homogenizer (Bioreba AG, Reinach, Switzerland) with its original extraction bags. Finally, DNA quantity and quality were assessed using a NanoPhotometer® NP80 (IMPLEN, DE).

Genomic DNA was quantified using a Qubit 2.0 Fluorometer (Invitrogen, Carlsbad, CA). Library preparation was carried out following the Allegro Targeted Genotyping protocol (Tecan Genomics, Männedorf, Zurich, Switzerland), starting from 100 ng of input DNA and adhering to the manufacturer's guidelines. The protocol included the incorporation of a 6-bp Unique Molecular Identifier (UMI) on each original DNA fragment. The resulting libraries were quantified again using the Qubit 2.0 Fluorometer, and fragment size distribution was assessed with the High Sensitivity DNA assay on a Bioanalyzer system (Agilent Technologies, Santa Clara, CA).

Sequencing was performed at IGA Technology Services (IGATech, Udine, Italy) using an Illumina NovaSeq 6000 platform (Illumina, San Diego, CA, USA) in paired-end configuration (2 × 150 bp). Raw BCL files generated by the instrument were converted into FASTQ format using the standard Illumina pipeline.

Funded by the European Union

Table 1. List of the selected cultivars and genotypes (with their synonymous if presents) and ''Leccino'' progeny to perform the SNP genotyping.

Arbequina	Carolea	Pendolino	Verdella 24g
Arbosana	Cerasa di Montenero	Picholine Languedoc	Grossane
Barnea	Chemlal de Kabilye	Racioppa/Lezze/Ogliastro	'Leccino'
Biancolilla	Chiquitita	Ravece	Lumiaro
Bosana	Cima di melfi	Calatina	Memecik
Cellina di nardò	Domat	Aitana	Myrtolia
Chetoui	Don carlo	Blanqueta	Lc x FS 27_287
Coratina	Forastera de tortosa	Canivano Negro/ Campanita	Lc x FS 1_293
Erbano	Grappuda	Dolce di Rossano	Lc x FS 10_286
Favarol	Kalamata	Giulia	Lc x FS 13_284
Gordal de granada	Koroneiki	Leccio del Corno	Lc x FS 14_291
Hojiblanca	Leucocarpa	Morisca	Lc x FS 17_276
Intosso	Manzanillera de huercal overa	Nocellara Messinese	Lc x FS 3_278
Itrana	Minuta	Oliva Nera di Colletorto	Lc x FS 30_285
Lechin de sevilla	Olivo San Lupo	Olivastra Seggianese	Lc x FS 31_281
Llumeta	Rossanel/Rossanello Veronese/Carbo	Palmareccia	Lc x FS 34_280
Manzanilla de sevilla	Zaituna	Pasola	Lc x FS 35_288
Meski	Abou kanani	Redondal	Lc x FS 46_283
Morrut	Albatro	Rossina	Lc x FS 47_282
Nociara	Barri	Toscanina	Lc x FS 51_277
Nolca	Bella di Cerignola	Uslu	Lc x FS 65_301
'Ogliarola salentina'	Castiglionese	Verdial de Huevar	Lc x FS 7_290
Olivastra	Cerasuola	Ascolana Tenera	S105-Lc x CP_272
Palomar	Dritta di Moscufo	Cassanese	FS x Lc_292
Passalunara	Empeltre	Changlot Real	Lc x FS 16_289
Picholine Marocaine	Frantoio	Cipressino	S218-Lc x CN_274
Picual	Gordal Sevillana	Cornilar	S234-Lc x OG_275
Picudo	Lastovka	Dolce d'Andria	
Pinonera	Maremmano	FS17	
Simone	Marina	Less	
Borgiona	Maurino	Maarri	
Bottone di gallo	Moraiolo	Rosciola Marche	
Brandofino	Nasitana	Sirole	
Canino	Nocellara Etnea	Toffahi 621	
Capolga er	Olivastra di Montenero	Uovo di Piccione	

Funded by the European Union

2.3.3 Short read mapping and SNP detection for SPET benchmark

Adapter sequences and low-quality bases at the 3' ends were trimmed from raw reads using cutadapt (Martin, 2011) and Fastp (Chen et al., 2018), applying default parameters. Reads shorter than 50 bp after trimming were discarded. The remaining high-quality reads were aligned to the reference genome of *Olea europaea* L. *subsp. europaea* cv. 'Arbequina' (Rao et al., 2021) using the BWA-MEM aligner with default settings (Li & Durbin, 2009).

PCR duplicates were subsequently removed using a custom Perl script exploiting UMI information introduced during library preparation. Variant calling was performed exclusively on uniquely mapped reads using the GATK toolkit (v4.5.0.0; McKenna et al., 2010). Initially, HaplotypeCaller was run in GVCF mode to identify candidate variants at the single-sample level within SPET target regions. Joint genotyping across all samples was then conducted using GenomicsDBImport followed by GenotypeGVCFs.

SNPs were extracted and filtered using GATK SelectVariants (--select-type-to-include SNP --ignore-non-ref-in-types) and VariantFiltration with the expression "QD < 2.0 || MQ < 40.0 || MQRankSum < -12.5". To eliminate SNPs potentially arising from ambiguous mapping in paralogous regions, the HDplot approach was applied (McKinney et al., 2017) with parameters Hmax = 0.6, RAFmin = 0.2, RAFmax = 0.8, Dmin = -10, and Dmax = 10.

Further genotype-level filtering was carried out using bcftools v1.21 (Danecek et al., 2021). Only biallelic SNPs were retained for downstream analyses. Additionally, loci were kept only if they met the following criteria: read depth (DP) ≥ 6, genotype quality (GQ) ≥ 20, at least 50% of samples with coverage greater than six reads, and a minimum of three reads supporting the minor allele.

2.3.4 SPET benchmark data analysis

Performance metrics indicated successful hybridization for ~60,000 probes, yielding an average sequencing depth of 40x within the target loci. Overall, 1,095,689 Single Nucleotide Polymorphisms (SNPs) were identified, with an average density of ~160,000 SNPs per individual sample. Preliminary genotyping analyses confirmed a high resolution, with ~150,000 high-quality SNPs resolved per genotype.

2.3.5 Genome-wide association study for *Xylella fastidiosa* phenotypes

Data in variant call format (VCF) were converted to PLINK binary format using PLINK v1.9 (Purcell et al., 2007), and quality control filtering was applied to retain SNPs with minor allele frequency (MAF) ≥ 0.05 and missing genotype rate ≤ 10%. Population structure was assessed by principal component analysis (PCA) on the filtered dataset, and the first two principal components were retained as covariates in the association analyses to account for genetic stratification.

Two phenotypic traits related to resistance to *Xf* were analyzed: (i) bacterial load, a quantitative continuous trait defined by the Cq value of quantitative-PCR, and (ii) an ordered categorical trait representing resistance classes, determined by combining symptom severity

Funded by the European Union

and bacterial load. GWAS for the quantitative trait was performed using a linear regression model implemented in PLINK, testing the additive effect of each SNP while including the first two principal components as fixed covariates. For the categorical trait, association analysis was conducted using an ordinal logistic regression model implemented in R (package ordinal), which is more appropriate for ordered phenotypic classes, including the same PCA covariates.

Significance of marker–trait associations was evaluated based on p-values, using a suggestive threshold of $P < 1 \times 10^{-4}$, and results were visualized through Manhattan plot generated with the qqman R package. Candidate loci were further investigated by intersecting SNP genomic positions with gene annotations and by identifying nearby genes within 50 kb windows using BEDTools. Functional effects of selected variants were predicted using the Ensembl Variant Effect Predictor (McLaren et al., 2016).

2.4 Characterization of the molecular response of resistant and susceptible olive cultivars to *Xylella fastidiosa* infection

2.4.1 Plant inoculations and RNA-Seq analysis

The molecular response of olive to *Xf* subsp. *pauca* ST53 (*Xfp*) was studied by RNA-seq and bioinformatic analysis of total RNAs purified from xylem tissues of twigs from artificially inoculated or naturally field infected olives. Libraries were generated across multiple independent projects over nearly a decade of research (2016–present). Artificially inoculation was performed by needle puncturing 1-year old twigs with 8-day-old *Xf*p suspensions in 1X PBS at $1x10^9$CFU/mL. Five twigs per plant were punctured after placing a 10 µL drop of bacterial culture suspension below the petioles. A minimum of three plants per experiment where inoculated while additional three plants were inoculated only with 1X PBS as control.

At each sampling date of artificial inoculations, twigs of 50–60 cm length, containing the inoculation point, were sampled and immediately processed for total RNA extraction. Similar sizes twigs were sampled from field infected olives. Twigs were debarked with a scalpel to expose woody xylem tissues. Total RNA was then extracted from 2 g of wood tissue that was powdered in liquid nitrogen as described in Giampetruzzi et al. (2016). RNA concentrations were quantified using NanoDrop measurements (Thermo Fisher Scientific, Waltham, USA) and their integrity was assessed by visualization on a 1% agarose gel. cDNA libraries were constructed using different Illumina sequencing modes in paired-end (2 x 50 and 2 x 150 bp) as they covered more than a decade period. Library preparations from shipped RNAs and sequencing was outsourced to private companies.

2.4.2 Bioinformatic analysis

Raw reads were quality trimmed with BBDuk, part of BBTools v38.90 (Joint Genome Institute, 2022; https://biogrids.org/software/titles/bbtools). Most of the read-mapping were performed on the *O. europaea* cv. 'Farga' as the reference genomes (Cruz et al. 2016; Julca et al. 2020) due to its overall higher mapping quality (i.e., higher ratio of uniquely mapped reads, and a lower lesser proportion of multimapped reads). Read mapping of the most recent libraries was made on a recent released 'Leccino' Genome (Lv et al. 2024). The data

Funded by the European Union

were then normalized using variance stabilizing transformation (VST) with DESeq2 v1.36.0 (Love at al. 2014) and first visualized by principal component analysis (PCA) using the R package ggplot2 v3.3.6 (Wickham et al. 2011). A differential gene expression analysis was done with DESeq2 to identify significant differentially expressed genes (DEGs) between the treatments for each time point, applying thresholds of a Benjamini-Hochberg (BH) adjusted p-value (padj) of less than 0.1 and a log2 fold change (LFC) of greater than 2.

Gene ontology (GO) enrichment analysis was carried out on all differentially expressed genes or separately up- and downregulated genes, using the ShinyGO platform (http://bioinformatics.sdstate.edu/goc/) where the cv. 'Farga' genome's annotations and GO terms description were previously uploaded.

2.5 Characterization of the mineral element concentrations (ionome) in susceptible and resistant almond and olive cultivars.

Leaf samples collected from several experiments described in Deliverable 1.3 were used for ionomic analysis to characterize mineral element concentrations in susceptible and resistant almond and olive cultivars. Specifically, the laminar part of leaf samples remaining after removing petiolar and midrib portion of leaves for DNA extraction, was used for ionome analysis by inductively coupled plasma-optical emission spectroscopy (ICP-OES) following a previously published protocol (De La Fuente et al. 2013).

The samples were prepared by drying overnight in the oven at 65°C. The dried tissue was grounded using mortar and pestle and was transferred to 2ml Eppendorf tube. From this stock, 10 mg of the sample was weighed and placed into a new 2 ml Eppendorf tube. After adding 200 µl of mineral-free concentrated nitric acid in the tubes containing samples, these were incubated on a heat block at 100 °C for one hour. After digestion, the samples were diluted with 800 µl of mineral free water and centrifuged to transfer the supernatant to a new Eppendorf tube. The diluted samples were analyzed for elemental composition using ICP-OES.

The analysis included susceptible and resistant almond and olive cultivars from the experiments described in Deliverable 1.3, as detailed in the corresponding Results sections.

Funded by the European Union

3. RESULTS

3.1 Transcriptomic analysis of resistant and susceptible almond cultivars in response to *Xylella fastidiosa* subsp. *fastidiosa* inoculation

The transcriptomic analysis revealed a substantial difference between 'UEF' and 'Lauranne' in their response to *Xff* inoculation. While 'UEF' exhibited a broad transcriptional response characterized by more than 2,000 differentially expressed genes (DEGs), most of which were upregulated, 'Lauranne' displayed a much more limited response, with only 249 DEGs, the majority of which were downregulated (**Figure 2**). Comparison of the basal, non-inoculated state between cultivars (Lc/Uc) revealed pronounced transcriptional differences, with 2,362 DEGs identified. Of these, 88% were upregulated in 'Lauranne' relative to 'UEF'. Conversely, comparison of the cultivars after inoculation (Li/Ui) identified 1,427 DEGs, of which approximately 80% were downregulated in 'Lauranne' relative to 'UEF' (**Figure 2**).

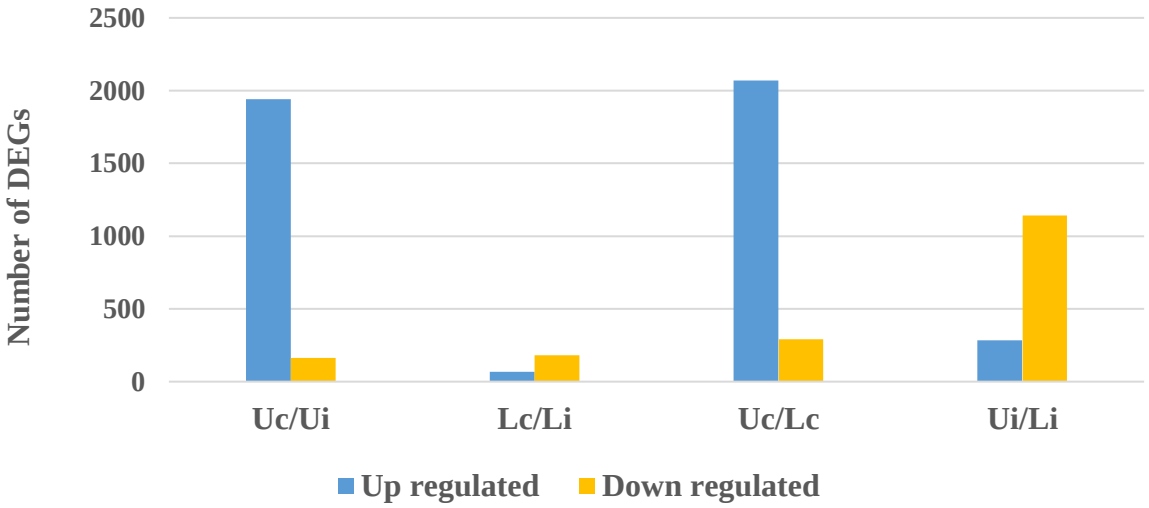


Figure 2. Number of significantly differentially expressed genes (DEGs; padj<0.05 & $|\log_2 FC| \geq 1$) in each comparison. The susceptible almond cultivar 'UEF' (U) and the resistant cultivar 'Lauranne' (L) were analyzed under control (c) and *Xylella fastidiosa* subsp. *fastidiosa* inoculation (i) conditions. Uc/Ui and Lc/Li represent transcriptional changes following inoculation within each cultivar. Uc/Lc reflects basal transcriptional differences between cultivars under control conditions. Ui/Li reflects transcriptional differences between cultivars following Xff inoculation.

To understand the biological significance of the large transcriptional response observed in 'UEF', functional enrichment analyses (GO and KEGG) were performed on the up-regulated DEGs. Following inoculation, 'UEF' showed increased expression of classical immune-related pathways, including hypersensitive response (HR), responses to fungal and oomycete pathogens, ABA-mediated signaling, and pathways involved in the biosynthesis of secondary metabolites, flavonoids, very long-chain fatty acid (VLCFA), and suberin (**Figure 3**). Secondary metabolites, particularly phenolic compounds and flavonoids, are known to possess

Funded by the European Union

antimicrobial properties and contribute to vascular occlusion. Their accumulation has been reported in response to *Xf* infection and plant-pathogen interactions in general (Lee et al., 2020; Maddox et al., 2009; Wallis & Chen, 2012). Similarly, VLCFA and suberin are associated with reinforcement of cell walls and structural defense mechanisms (Graça, 2015; Raffaele et al., 2008). Downregulated pathways in 'UEF' were mainly associated with cellular homeostasis, including chloroplast, nuclear, and cytoplasmic functions, protein folding and binding, and iron metabolism and transport.

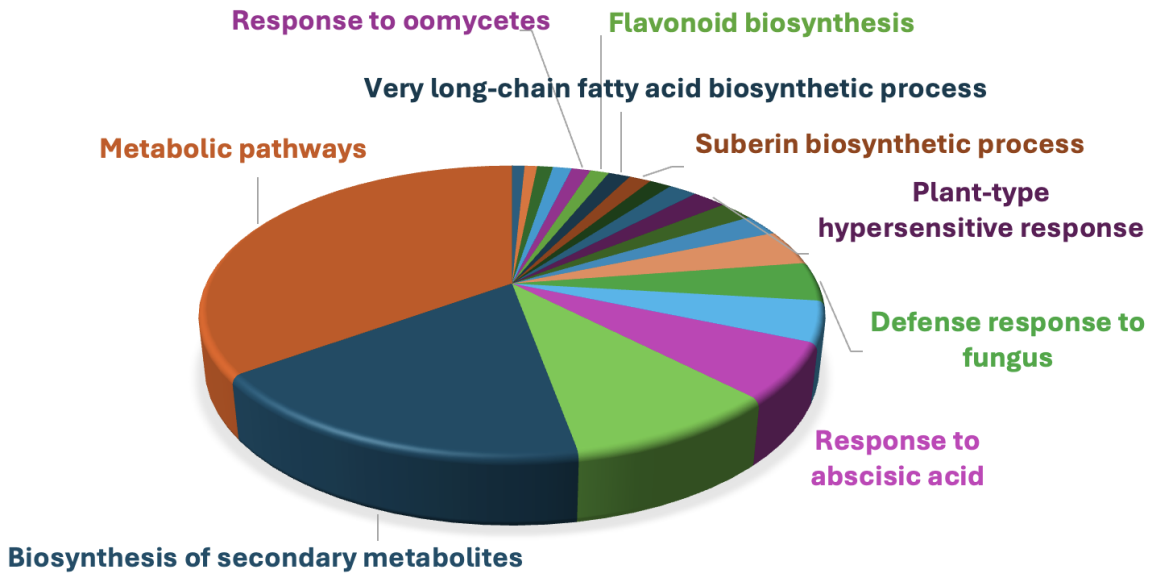


Figure 3. GO Biological Process (BP) and KEGG pathway enrichment analysis of up regulated genes in 'UEF' almond cultivar following *Xylella fastidiosa* subsp. *fastidiosa* inoculation (Ui/Uc). Selected pathways are highlighted.

In 'Lauranne', the relatively small number of DEGs resulted in enrichment of only three GO catagories: cytoplasm, Golgi apparatus, and protein binding. These categories suggest limited changes in general cellular functions rather than activation of extensive defense-specific pathways.

As noted above, substantial basal transcriptomic differences existed between the cultivars before inoculation (**Figure 2**). Functional enrichment analysis (GO and KEGG) of the up-regulated DEGs in the basal state revealed that non-inoculated 'Lauranne' exhibited elevated expression of numerous defense-related pathways compared with non-inoculated 'UEF' (**Figure 4**). Notably, 33.8% of these pathways overlapped with those induced in 'UEF' only after inoculation (**Figure 5**). Shared pathways included HR, ABA signaling, secondary metabolite biosynthesis, flavonoid production, and long-chain fatty acid oxidation, all of which are associated with *Xf* responses (**Figure 6**). Notably, other immune-related pathways that are up regulated in 'Lauranne' basal state, but not shared with inoculated UEF are: biosynthesis of lignin, flavonoids and fatty acids biosynthesis, responses to desiccation**,** salt stress, cold and wounding.

Funded by the European Union

These findings suggest that 'Lauranne' is pre-activated for the same pathways 'UEF' induces after infection.

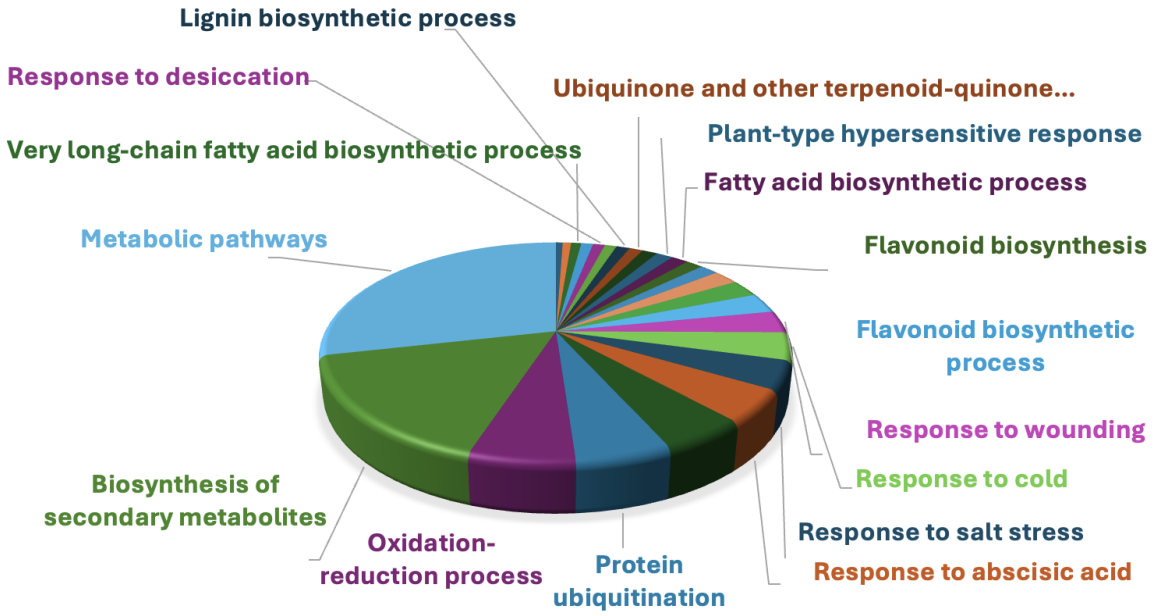


Figure 4. GO Biological Process (BP) and KEGG pathway enrichment analysis of up regulated genes in 'Lauranne' and UEF un-inoculated control (Lc/Uc). Selected pathways are highlighted.

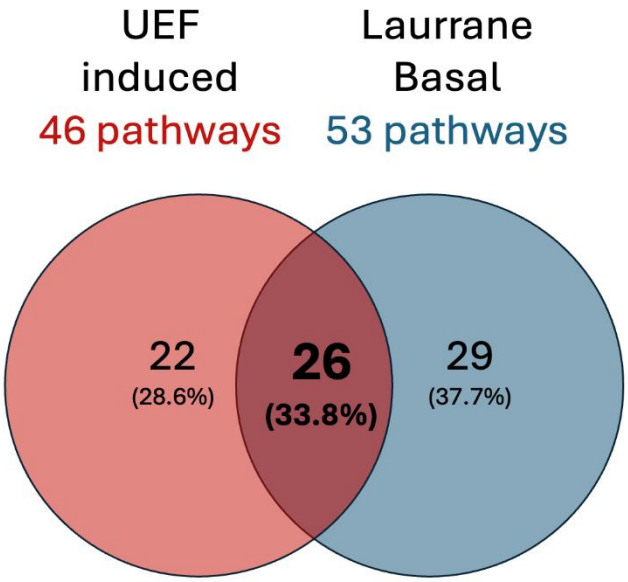


Figure 5. Venn diagram of the shared GO terms up regulated in 'UEF' susceptible almond cultivar following inoculation (left red circle) and in 'Lauranne' resistant almond cultivar compared with 'UEF' before inoculation (right blue circle).

Funded by the European Union

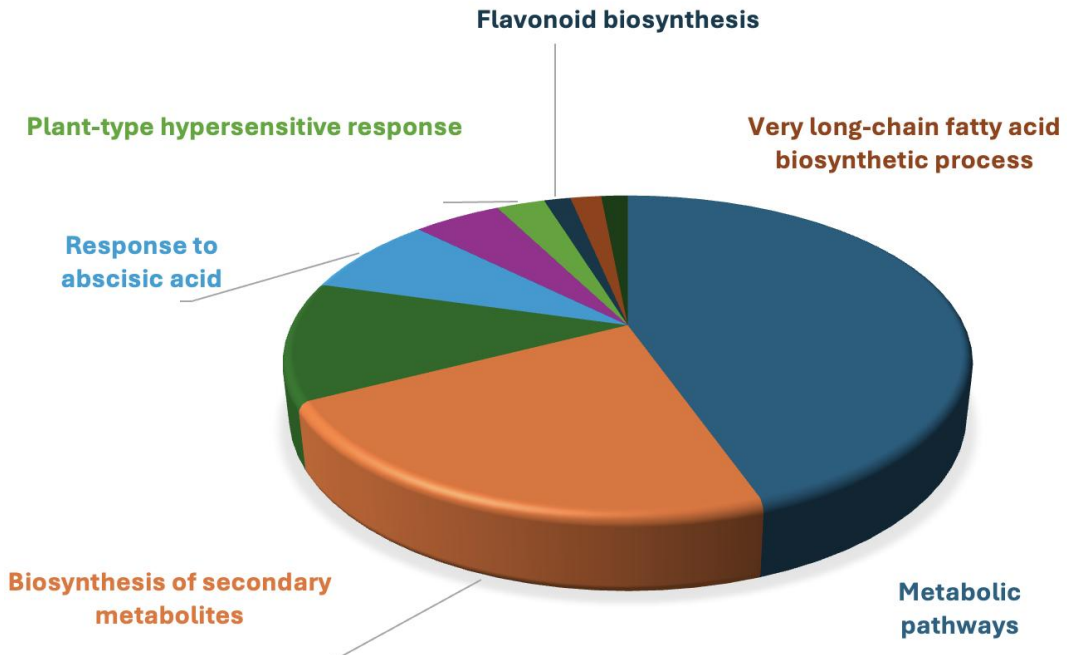


Figure 6. Shared enriched Gene Ontology (GO) Biological Process terms and KEGG pathways in susceptible and resistant almond cultivars. Enrichment analysis was performed using two gene sets: (i) differentially expressed genes (DEGs) upregulated in the susceptible cultivar UEF following *Xylella fastidiosa* subsp. *fastidiosa* (Xff) inoculation, and (ii) DEGs showing higher basal expression in the resistant cultivar 'Lauranne' than in uninoculated UEF (Ui/Lc). Shared enriched GO terms and KEGG pathways are shown, with selected pathways highlighted.

A focused analysis was performed on selected enriched pathways that have previously been implicated in plant responses to xylem-colonizing pathogens, including flavonoid biosynthesis, callose deposition, tylose formation, and the HR. Examination of the underlying gene sets revealed constitutive upregulation of several flavonoid- and phenylpropanoid-related genes in 'Lauranne', including CHS, FLS, F3H, C4H, 4CL, and OMT (**Table S1**). In addition, genes associated with callose synthesis, carbohydrate metabolism, sugar transport, and HR-related signaling were also overexpressed in 'Lauranne' relative to 'UEF' (**Tables S2–S4**). These pathways were selected for further examination due to their documented involvement in plant defense responses and their reported association with resistance mechanisms against vascular pathogens, including *Xf* (Maddox et al., 2009; Rapicavoli et al., n.d.; Sabella et al., 2019).

Funded by the European Union

3.2 Genome sequencing and immune profiling of the immune receptor landscape of olive

3.2.1 Genome assembly and gene model prediction of *Olea europaea* cultivars 'Leccino' and 'Ogliarola salentina'

Olea europaea is a globally cultivated crop increasingly threatened by a range of pathogens, including *Xf*, *Pseudomonas savastanoi*, and *Verticillium dahliae*, as well as insect pests such as the olive fruit fly (Saponari et al. 2019; Quesada et al. 2010; Grasso et al. 2017; Montes-Osuna and Mercado-Blanco 2020). The cultivars 'Leccino' and 'Ogliarola salentina' were selected for genome sequencing because they differ markedly in their susceptibility to *Xf*, *P. savastanoi*, and *V. dahliae* (**Supplementary Table S5**). Using PacBio HiFi and Illumina Hi-C sequencing, we generated de novo assemblies for both haplotypes of each cultivar (Table 2). The resulting four assemblies each comprise 23 chromosome-scale sequences and range in size from 1.16 to 1.41 Gb (**Table 2**), consistent with the recently published chromosome-level assembly of 'Leccino' (1.28 Gb) (Lv et al. 2024). Genome quality assessment using Merqury yielded k-mer-based quality values between 57.1 and 61.3 (Rhie et al. 2020), corresponding to approximately one substitution error per megabase (**Table 2**), a quality standard characteristic of near-finished genome assemblies (Rhie et al. 2021).

Gene models were annotated using the Helixer pipeline, integrating *ab initio* prediction, homology-based annotation, and transcriptomic evidence. After filtering low-confidence predictions, we identified between 40,798 and 41,285 protein-coding genes per haplotype (**Table 2**). Annotation completeness, assessed with BUSCO, ranged from 96.4% to 97.7% (including single-copy and duplicated orthologs), indicating a highly complete gene space. In addition, the monoexonic-to-multiexonic gene ratio ranged from 0.17 to 0.18 (Table 3), closely matching the expected value of ~0.2 for high-quality plant genome annotations (Vuruputoor et al. 2023).

Table 2. Summary of genome assembly and annotation for *Olea europaea* cultivars

Genome features	'Leccino' haplotype 1	'Leccino' haplotype 2	**'O. salentina' haplotype 1**	**'O. salentina' haplotype 2**
Estimated genome size	1,19	1,19	1,17	1,17
Total assembly (Gb)	1,41	1,16	1,21	1,41
Chromosomes	23	23	23	23
Gene models	40921	40991	41285	40798
BUSCO (% single + double)	96,4	97,7	96,8	96,7

Funded by the European Union

3.2.2 Genome features of *Olea europaea* cultivars

To investigate the evolutionary relationships among olive genomes, we clustered representative protein sequences from 11 assemblies, including the four haplotype-resolved genomes generated in this study, three additional *Olea europaea* cultivars, one *O. europaea* var. *sylvestris* genome, two *Fraxinus* species, and the outgroup *Populus trichocarpa* (black cottonwood). The resulting phylogeny showed that haplotype 1 of 'Leccino' is most closely related to haplotype 1 of 'Ogliarola salentina', while haplotype 2 of 'Leccino' clusters with haplotype 2 of 'Ogliarola salentina' (**Supplementary Figure S1**), indicating a shared evolutionary origin of the corresponding haplotypes. Molecular dating analyses suggest that the lineage containing 'Leccino' and 'Ogliarola salentina' diverged from the other cultivated olives and the *sylvestris* wild type approximately 4.45 million years ago (**Supplementary Figure S1**), consistent with previous phylogenetic studies based on plastid sequences (Besnard et al. 2002; Besnard et al. 2009; Mariotti et al. 2023).

The haplotype-resolved, reference-grade genome assemblies enabled a comprehensive analysis of chromosome-scale synteny and structural variation (SV) between olive cultivars. Across the four haplotypes, we identified a total of 3490367 large SVs, including insertions, deletions, duplications, inversions, and translocations, affecting approximately from 39.63 to 66.20 Mb of genomic sequence in each haplotype (**Supplementary Table S6**). The distribution and abundance of SVs among the four assemblies reflect the shared ancestry between 'Leccino' and 'Ogliarola salentina' (**Supplementary Figure S2**).

3.2.3 Defining the *Olea europaea* cultivar immune receptor repertoire

Plant PRRs are predominantly receptor-like kinases (RLKs) and receptor-like proteins (RLPs). RLKs possess extracellular ligand-binding domains coupled to intracellular kinase domains, whereas RLPs lack a cytoplasmic kinase domain. Based on their ectodomain architecture, RLKs can be further classified into families containing leucine-rich repeats (LRRs), lysin motifs (LysMs), and other domain types (Sun and Zhang 2020). Well-characterized members of the LRR-RLK-XII family, including EFR and FLAGELLIN SENSING 2 (FLS2), directly perceive PAMPs, whereas LRR-RLK-II proteins such as BAK1 function as co-receptors that facilitate immune signaling. LysM-containing receptors play key roles in the perception of microbial carbohydrates involved in both immunity and symbiosis (Zipfel et al. 2006; Gómez-Gómez and Boller 2000; Chinchilla et al. 2006; Heese et al. 2007; Miya et al. 2007; Madsen et al. 2003). Across the four olive haplotypes, we identified 316 LRR-RLK-XII receptors and 95 LysM-RLKs (**Table 3**). In addition, we annotated 445 LRR-RLPs and 83 LysM-RLPs (**Table 3**), receptor classes that are thought to represent the evolutionary predecessors of LRR-RLKs (Ngou et al. 2022).

PRRs and NLRs function as interconnected components of the plant immune system, and expansion of the NLR repertoire often parallels the diversification of PRRs across plant genomes (Ngou et al. 2022; Ngou et al. 2021; Yuan et al. 2021). NLRs are intracellular immune receptors characterized by a central NB-ARC domain, typically flanked by C-terminal leucine-rich repeats (LRRs) and variable N-terminal signaling domains. Based on their N-terminal architecture, NLRs are classified as coiled-coil NLRs (CNLs), Toll/interleukin-1 receptor NLRs (TNLs), or RPW8-like coiled-coil NLRs (RNLs). In addition, some NLRs contain integrated

Funded by the European Union

domains, such as Armadillo (ARM) repeats, that may function in effector recognition and are classified as ARM-NLRs (Förderer and Kourelis 2023). Across the four olive haplotypes, we identified 358 CNLs, 33 TNLs, 30 RNLs, and 66 ARM-NLRs, together with 615 NL proteins containing an NB-ARC domain but lacking a canonical N-terminal signaling domain (**Table 3**).

Table 3. Summary of PRR and NLR annotation for *Olea europaea* cultivars

	'Leccino' **haplotype 1**	'Leccino' **haplotype 2**	**O. salentina haplotype 1**	**O. salentina haplotype 2**
PRR type				
LRR-RLK-XII	90	85	69	72
LRR-RLP	101	129	99	116
LysM-RLK	21	25	25	24
LysM-RLP	20	24	21	18
NLR type				
CNL	91	77	89	101
TNL	6	10	8	9
RNL	4	10	6	10
ARM-NLRs	10	18	14	18
NL only	138	145	141	131

To prioritize candidate immune receptors for functional studies, we examined the expression profiles of *PRR* and *NLR* gene families in healthy and diseased olive trees. Notably, only ten *PRRs* per cultivar were among the top 20% most highly expressed genes in healthy field-grown trees, and even fewer *PRRs* reached this expression threshold in healthy greenhouse-grown plants (Supplementary Figure S3). By contrast, between 25 and 29 *NLRs* were among the top 20% most highly expressed genes in healthy field-grown trees of both cultivars. While these expression levels were largely maintained in greenhouse-grown 'Leccino' plants, only ten *NLRs* remained within the top expression percentile in 'Ogliarola salentina' (**Supplementary Figure S3**).

We next investigated immune receptor expression during disease. Across both cultivars, numerous *PRRs* were transcriptionally induced following infection, whereas most *NLRs* were downregulated (**Supplementary Figure S4**). This trend was observed in both naturally infected field-grown trees and artificially inoculated greenhouse-grown plants, suggesting that it reflects a conserved response to *Xf* rather than environmental differences. Given the xylem-restricted lifestyle and chronic nature of *Xf* infection (Sicard et al. 2018; Ramesh et al. 2026), the observed predominance of *PRR* induction may indicate a greater contribution of PTI than intracellular *NLR*-mediated responses during disease progression. Collectively, these expression patterns highlight a subset of *PRRs* and *NLRs* as promising candidates for further investigation of olive immune responses.

Funded by the European Union

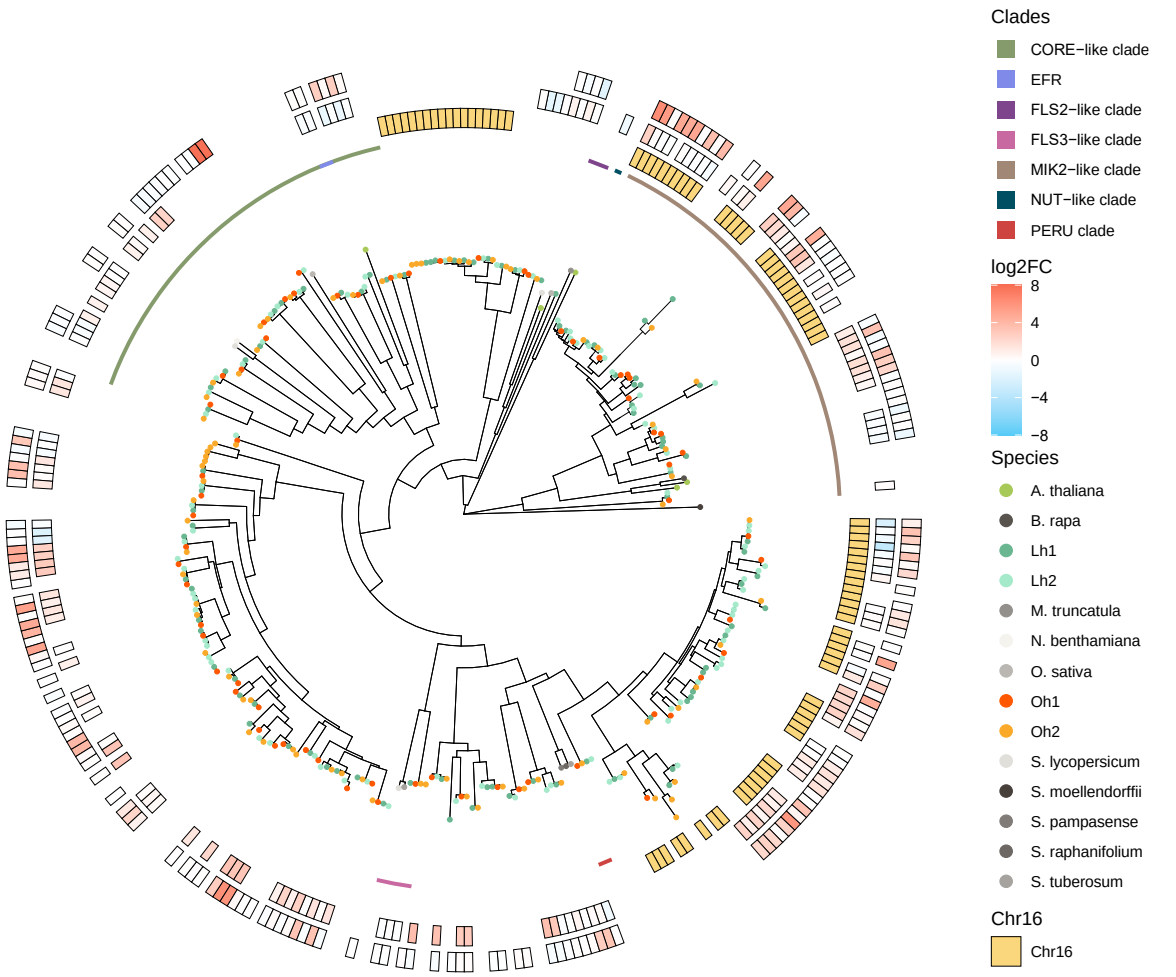


Figure 7. Phylogenetic tree of olive LRR-RLK-XII. The phylogenetic tree was constructed based on ectodomain protein sequence alignment of all identified *Olea europaea* 'Leccino' and 'Ogliarola salentina' LRR-RLK-XII and known LRR-RLK-XII receptors from other plant species. The branch tip circles indicate the species and haplotypes. The triangle sectors indicate the clade clustering with known LRR-RLK-XII receptors from other plant species supported by OrthoFinder (white sectors within a clade indicates that homologies of these olive receptors with known LRR-RLK-XII were not additionally supported by Orthofinder), the inner ring shows genes encoded on the chromosome 16, the middle and outer rings show their differential expression in *X. fastidiosa* infected trees in the field and glasshouse, respectively. Lh1 = 'Leccino' haplotype 1, Lh2 = 'Leccino' haplotype 2, Oh1 = 'Ogliarola salentina' haplotype 1, Oh2 = Ogliarola haplotype 2.

To investigate PRR diversity in olive, we reconstructed a phylogenetic tree using the ectodomains of LRR-RLK-XII proteins from the four olive haplotypes together with functionally characterized LRR-RLK-XII receptors from other plant species (**Figure 7**). LRR-RLK-XII receptors have undergone extensive lineage-specific expansion during land plant evolution, generating substantial diversity in receptor repertoires (Kileeg et al. 2023). Whereas the *A. thaliana* genome encodes only ten LRR-RLK-XII members, many plant species possess considerably larger families (Ngou et al. 2025).

Funded by the European Union

Within the olive genomes, we identified candidate orthologues of the well-characterized receptors FLS2, FLAGELLIN SENSING 3 (FLS3), COLD-SHOCK PROTEIN RECEPTOR (CORE), and MALE DISCOVERER1-INTERACTING RECEPTOR-LIKE KINASE 2 (MIK2). Notably, the CORE- and MIK2-related clades were markedly expanded, comprising 41 *OeCORE*-like and 39 *OeMIK2*-like genes, respectively (**Figure 7**). This expansion is particularly intriguing for the MIK2-like family, as MIK2 differs from most LRR-RLK-XII receptors by perceiving both self and non-self molecular patterns (Hou et al. 2021; Rhodes et al. 2021). In *A. thaliana*, MIK2 recognizes SERINE-rich ENDOGENOUS PEPTIDEs (SCOOPs), a family of Brassicaceae-specific phytocytokines, as well as pathogen-derived SCOOP-like molecules and additional, as yet unidentified, microbial elicitors (Hou et al. 2021; Rhodes et al. 2021; Snoeck et al. 2024; Maroschek et al. 2025).

To further characterize the olive PRRome, we reconstructed a phylogenetic tree of LysM-RLKs and LysM-RLPs using their extracellular domains, together with functionally characterized LysM receptors from *A. thaliana* and rice (**Supplementary Figure S5**). LysM receptors play central roles in the perception of oligosaccharide-derived molecular patterns, including bacterial PGN, fungal chitin and chitosan (Willmann et al. 2011; Shimizu et al. 2010; Petutschnig et al. 2010). Phylogenetic analysis identified candidate olive orthologues of the chitin receptors LYK4 and LYK5, as well as CHITIN ELICITOR RECEPTOR KINASE 1 (CERK1), a conserved LysM co-receptor required for chitin-induced immune signaling (Cao et al. 2014). OliveLysM-RLKs and LysM-RLPs comprise 95 and 83 members, respectively, across the four haplotypes (**Supplementary Figure S5**), suggesting diversification of oligosaccharide perception mechanisms in this species.

To investigate NLR diversity in olive, we reconstructed a phylogenetic tree using the conserved NB-ARC domains of all predicted NLR proteins from the four olive haplotypes (**Figure 8**). The resulting phylogeny revealed the expected CNL, TNL, and RNL clades, but also highlighted a substantial expansion of ARM-NLRs. This finding is notable because ARM-NLRs are generally not among the predominant NLR classes in most plant genomes (Förderer and Kourelis 2023). The integration of ARM repeat domains is thought to increase NLR functional diversity by providing protein–protein interaction scaffolds that may facilitate effector recognition or act as integrated decoys targeted by pathogen virulence factors (Sarris et al. 2016; Kroj et al. 2016). The abundance of ARM-NLRs in olive therefore suggests an expanded repertoire for intracellular pathogen surveillance. In addition, we observed a relatively large number of NL only genes across cultivars and haplotypes (**Figure 8**), which may reflect diversification of regulatory components within NLR signaling networks. These patterns are consistent with the rapid evolution that characterizes plant *NLR* loci and indicate that structural variation contributes to immune receptor diversity in olive.

Funded by the European Union

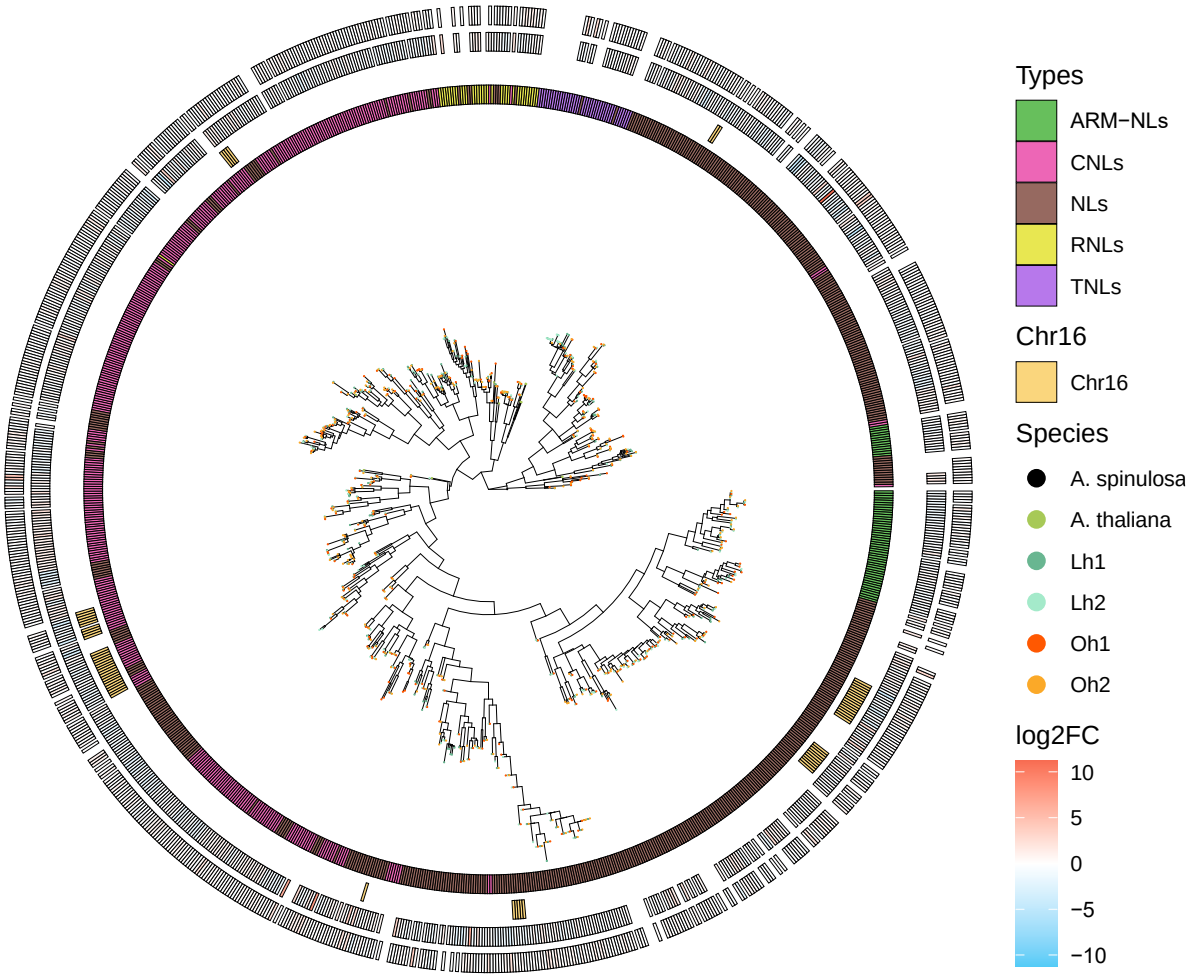


Figure 8. Phylogenetic tree of olive NLRs. The phylogenetic tree was constructed based on NB-ARC domain protein sequence alignment of all identified *Olea europaea* 'Leccino' and 'Ogliarola salentina' NLRs. The branch tip circles indicate the species and haplotypes. The inner ring indicates the types of NLRs according to their domain composition; the inner ring in yellow shows genes encoded on the chromosome 16, the next inner and outer rings show their differential expression in X. fastidiosa infected trees in the field and glasshouse, respectively. Lh1 = 'Leccino' haplotype 1, Lh2 = 'Leccino' haplotype 2, Oh1 = 'Ogliarola salentina' haplotype 1, Oh2 = Ogliarola haplotype 2.

A prominent region of structural variation was identified on Chromosome 16, distinguishing 'Leccino' and 'Ogliarola salentina' cultivars (**Figure 9a**). These structural rearrangements are associated with local expansion and contraction of *PRR* genes, highlighting the importance of haplotype-resolved, chromosome-scale genome assemblies for accurately capturing immune receptor diversity. Notably, the corresponding region (between 20 and 30 Mbp of the Chromosome 16) in 'Leccino' contains a larger repertoire of *PRR* genes than the homologous locus in 'Ogliarola salentina' (**Figure 9a**). This is supported by gene family expansion analysis of *PRRs* encoded in this genomic region, revealing a significant expansion of these receptor genes in 'Leccino' haplotypes 1 and 2 and a contraction in 'Ogliarola salentina' haplotype 1 and 2 (**Figure 9b**). Given the contrasting disease phenotypes of these cultivars

Funded by the European Union

(**Supplementary Table S5**), the expansion of *PRR* genes in 'Leccino' represents a compelling candidate region underlying differences in pathogen resistance.

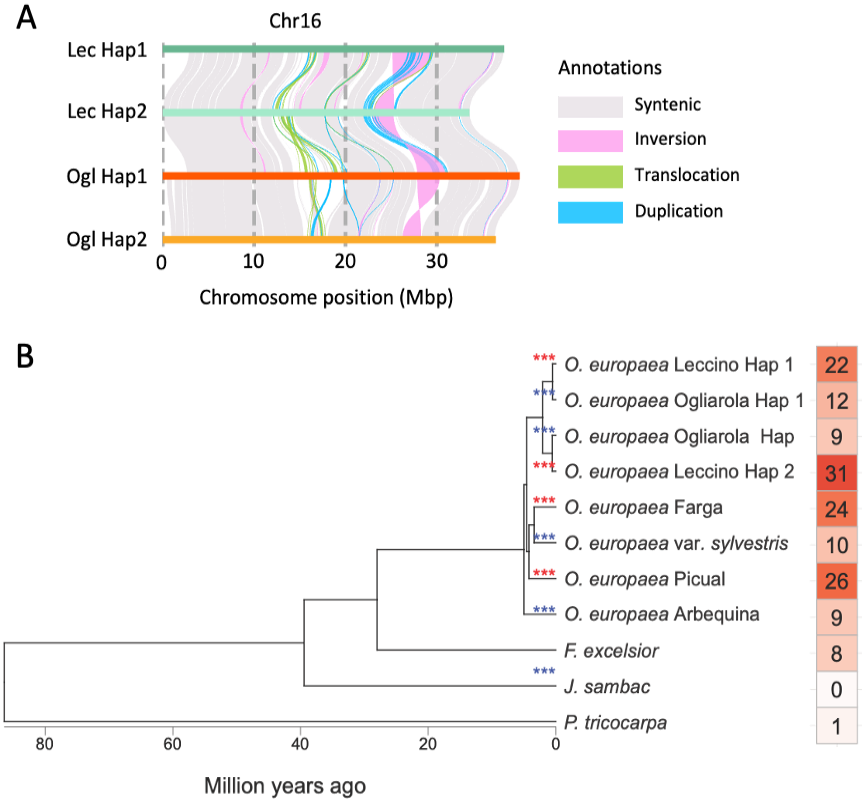


Figure 9: Structural variation between olive 'Leccino' and 'Ogliarola salentina' at Chromosome 16. **A.** Synteny analysis shows loci of chromosomal rearrangements on the Chromosome 16 of all haplotypes. **B.** Gene family expansion analysis of LRR-RLK-XII receptors encoded in the regions between 20 and 30 Mbp of Chromosome 16, reveals a significant expansion in 'Leccino' haplotypes 1 and 2 and a contraction in Ogliarola haplotype 1 and 2. Significance is marked by stars (* $p < 0.05$; ** $p < 0.01$; *** $p < 0.001$), expansion is marked in red and contraction in blue.

3.2.4 The PTI landscape of the *Olea europaea* cultivars and *Xylella fastidiosa* responses

Several PAMPs have been identified in *Xf*, including the EF-Tu-derived peptides elf18/26, LPS, and cold-shock protein-derived peptides csp20/22 (Mitre et al. 2021; Kunze et al. 2004; Wei et al. 2021; Rapicavoli et al. 2018). In addition, comparative analysis of the *Xff* Temecula-1 and *X. fastidiosa* subsp. *pauca* (*Xfp*) genomes predicts the presence of PGN oligosaccharide and a SCOOP-like peptide candidate as potential immune elicitors (Van Sluys et al. 2003; Simpson et al. 2000; Giampetruzzi et al. 2017). To assess the PTI landscape of the two olive cultivars, we screened for responses to five well-characterized microbial patterns (flg22, flgII-28, csp22, SCOOP12, and chitin) using mitogen-activated protein kinase (MAPK) phosphorylation as a prototypic PTI output (Jones and Dangl 2006; Zipfel 2014). We further

Funded by the European Union

tested bacterial extracts of the phytopathogenic strains *Xf*f Temecula-1, *Xf*p De Donno and *A. tumefaciens*.

Both cultivars exhibited MAPK activation in response to chitin (**Figure 10**). Yet, the magnitude of MAPK activation differed between cultivars, indicating quantitative rather than qualitative variation in PTI responsiveness. Similar differences were observed following treatments with *Xf*p and *A. tumefaciens* extracts (**Figure 10**). Notably, neither flg22 nor flgII-28 triggered detectable immune responses in olive (**Figure 10**), despite the presence of candidate *OeFLS2*-like genes in the genome. Similarly, csp22 and SCOOP12 failed to induce MAPK activation despite the presence of *OeCORE*- and *OeMIK2*-like genes, respectively. This is consistent with the restricted distribution of these perception systems, which are largely confined to the Solanaceae and Brassicaceae families, respectively (Rhodes et al. 2021). Together, these results provide a first functional overview of the PTI landscape in 'Leccino' and 'Ogliarola salentina', revealing conserved perception of chitin alongside cultivar-specific differences in responses to *Xfp* and *A. tumefaciens* and immune activation strength.

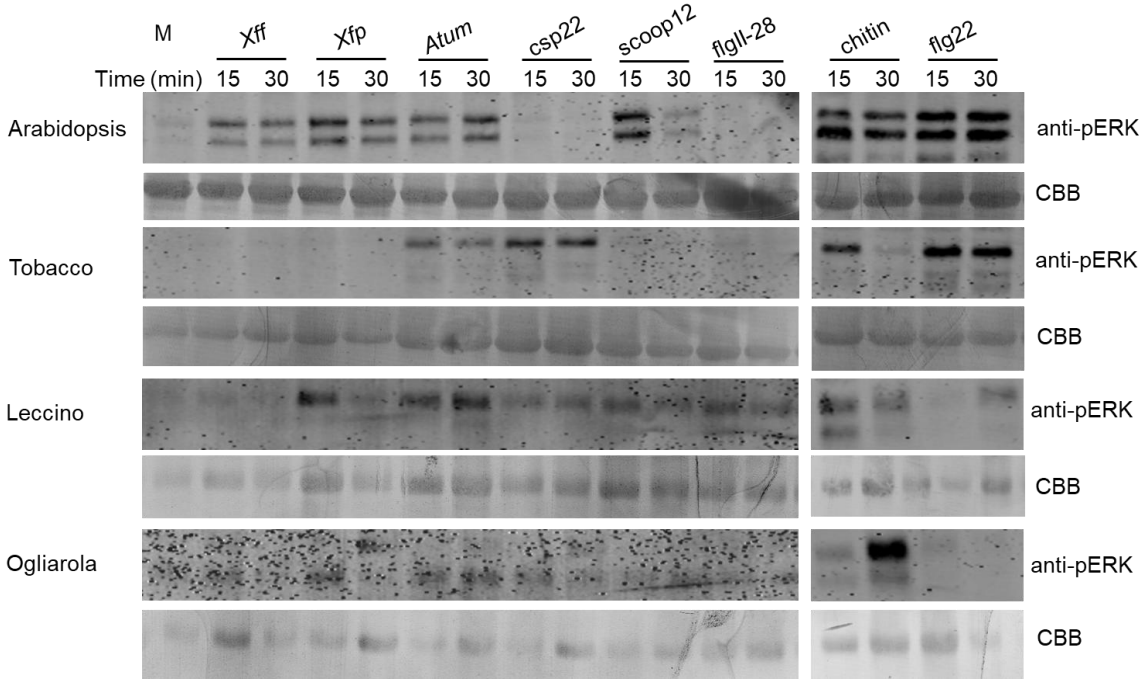


Figure 10. MAPK activation induced by common microbial patterns and bacterial extracts. Immunoblot analysis of protein extracts of leaves from the indicated plants and treated with the indicated elicitors at different time points was revealed with phospho-specific MAPK antibodies. Coomassie Brilliant Blue (CBB) is shown as loading control.

Across the four olive haplotypes, we identified a total of 939 *PRR* genes. To pinpoint receptors involved in the perception of known PAMPs and *Xf* -derived elicitors, we prioritized candidate genes for functional characterization through heterologous expression in the model plants *A. thaliana* and *N. benthamiana*. We initially focused on receptors predicted to mediate the recognition of the widely conserved microbial patterns flg22 and chitin. Although flg22 failed to induce detectable MAPK activation in either olive cultivar (**Figure 10**), phylogenetic analysis

Funded by the European Union

identified candidate one 'Leccino' *OeFLS2* ortholog within the LRR-RLK-XII family (**Figure 7**). Structural predictions revealed that the OeFLS2 ectodomain comprises 14 LRRs arranged in an architecture (**Supplementary Figure S6**), which differs from the canonical ectodomain configuration reported for *At*FLS2 (Sun et al. 2013). These structural differences may influence ligand recognition and/or co-receptor recruitment, potentially explaining the absence of detectable flg22-induced signaling in olive.

Upon ligand perception, PRRs typically undergo homodimerization or assemble into heteromeric complexes with receptor-like kinase co-receptors, most notably BAK1 (Sun et al. 2013; Schulze et al. 2010). These receptor complexes bring the intracellular kinase domains of PRRs and co-receptors into close proximity, thereby initiating downstream signaling events (Macho and Zipfel 2014). Across the olive genomes, we identified 29 SOMATIC EMBRYOGENESIS RECEPTOR KINASE (SERK) family members, including 13 candidate *OeBAK1* orthologues based on phylogenetic analysis (**Supplementary Figure S7**).

Structural modelling predicted that OeFLS2 retains the capacity to form a flg22-induced receptor complex with *OeBAK1* and trigger immune signalling (**Supplementary Figure S6**). To test this prediction experimentally, we generated expression constructs for candidate *OeBAK1* genes. All tested *OeBAK1* orthologs complemented the immune defects of the *A. thaliana bak1-4* null mutant (Kemmerling et al. 2007), demonstrating that OeBAK1 orthologues encode functional co-receptors (**Supplementary Figure S8**). These results suggest that the tested *OeBAK1* orthologs may engage as co-receptors in immune signalling complexes with other PRRs, including *OeCORE*- and *OeMIK2*-like orthologs, despite not mediating canonical flg22-induced immune signalling.

Although flg22 perception is widely conserved across flowering plants (Felix et al. 1999; Robatzek et al. 2007), losses of flg22 responsiveness have been reported in specific plant lineages (Winkelmüller et al. 2021; Vetter et al. 2012). To determine whether the absence of flg22 perception is a broader feature within the Oleaceae family, we examined reactive oxygen species (ROS) production following flg22 treatment in several family members, including *O. europaea* var. *sylvestris*, *Fraxinus*, *Jasminum*, and *Forsythia*. Remarkably, none of the tested species mounted a detectable ROS burst in response to flg22 (**Supplementary Figure S6**), indicating that flg22 insensitivity extends beyond olive and may be widespread within the Oleaceae. We also observed no response to flgII-28, the immunogenic flagellin epitope perceived by FLS3 in Solanaceae species (Clarke et al. 2013; Hind et al. 2016). These observations suggest that canonical flagellin recognition may not play a major role in immune activation in olive trees.

We next investigated candidate *OeCERK1*, *OeLYK4* and *OeLYK5* orthologs, which were identified through phylogenetic analysis of the olive LysM receptor family, revealing olive candidate LysM-RLKs highly similar to their *Arabidopsis* counterparts (**Supplementary Figure S5**). To assess their potential role in chitin perception, we transiently expressed selected *OeCERK1* receptor candidates in *N. benthamiana* and monitored chitin-induced ROS production (**Supplementary Figure S9**; **Figure 11**). Control *N. benthamiana* samples exhibited a prototypical ROS response to chitin. This was significantly enhanced in *N. benthamiana* samples expressing *OeCERK1-1* genes from 'Leccino' and 'Ogliarola salentina' (**Figure 11**), with the 'Ogliarola salentina' allele conferring a stronger response. These results indicate that

Funded by the European Union

OeCERK1-1 functions as a positive regulator of chitin-triggered immune signalling and supports its role as a conserved component of the olive chitin perception machinery.

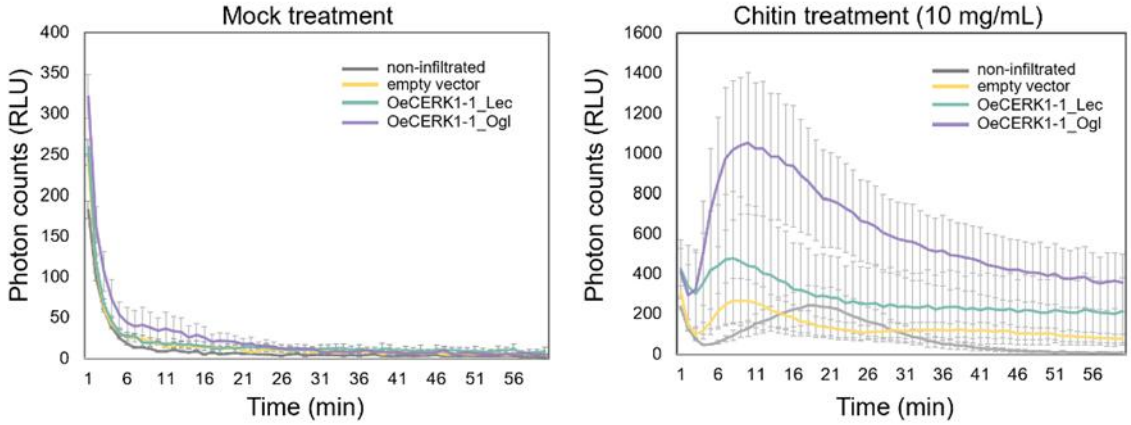


Figure 11. Identification and functional analysis of OeCERK1 co-receptors. ROS burst measured as relative luminescence units (RLU) over time in *Nicotiana benthamiana* leaves expressing OeCERK1-1 from olive cultivars 'Leccino' and 'Ogliarola salentina' treated with mock (distilled water, left panel) and chitin (right panel). Induced ROS burst in ROS production was measured over time.

Interestingly, treatment with *Xfp* De Donno and *A. tumefaciens* extracts elicited a markedly stronger MAPK activation in the resistant cultivar 'Leccino' than in the susceptible cultivar 'Ogliarola salentina' (**Figure 10**). This enhanced responsiveness suggests that 'Leccino' possesses a more robust capacity to perceive and respond to *Xf*p-derived elicitors. Cold shock protein-derived csp22 peptides from *A. tumefaciens* are known to activate immune responses through the CORE-related receptors SCOREs in plant species other than Soloanaceae (Ngou et al. 2025). Phylogenetic analysis revealed a substantial expansion of the *OeCORE*-like receptors in olive (**Figure 7**), raising the possibility that diversification of this receptor family may contribute to the perception of an *Xf*p-derived immunogenic csp20 variant (Burbank 2022).

Phylogenetic analysis of LRR-RLK-XII genes encoded within the structurally variable Chromosome 16 region revealed a 'Leccino'-specific expansion of closely related receptors within a OeMIK2-like clade (**Figure 7**). We therefore investigated the potential role of OeMIK2-like receptors. Phylogenetic analysis revealed candidate orthologs based on their clustering with AtMIK2 as well as their expansion on chromosome 16 (**Supplementary Figure S10**).

Candidate genes were selected for further investigation (**Supplementary Figure S10**). Transient expression in *N. benthamiana* revealed that none of the tested *OeMIK2*-like candidates conferred responsiveness to SCOOP12 or the predicted *Xf* SCOOP-like peptide (**Supplementary Figures S11 and S12**), whereas expression of *At*MIK2 enabled a robust response to SCOOP12 in *N. bethamiana*. Although SCOOP peptides have thus far only been identified in Brassicaceae species, MIK2-like receptors are widely distributed across angiosperms (Maroschek et al. 2025; Steidele et al. 2025), suggesting that their ancestral function may extend beyond SCOOP perception. Consistent with this possibility, recent

Funded by the European Union

evidence suggests that *At*MIK2 can perceive additional, as yet unidentified microbial patterns (Maroschek et al. 2025).

Taken together, our analyses provide a first functional framework for understanding PTI in olive. The data highlight a conserved role for chitin perception while revealing substantial diversification of *OeCORE*- and *OeMIK2*-like candidate receptor families, particularly within the expanded Chromosome 16 immune receptor locus associated with the resistant cultivar 'Leccino'.

Taken together, our analyses provide a first functional framework for understanding PTI in olive. The data highlight a conserved role for chitin perception while revealing substantial diversification of *OeCORE*- and *OeMIK2*-like candidate receptor families, particularly within the expanded Chromosome 16 immune receptor locus associated with the resistant cultivar 'Leccino'.

3.3 Genome wide association study (GWAS) of olive cultivars and progeny

3.3.1 SNP and phenotypic data merging for GWAS analysis

Phenotypic data from 111 cultivars and 21 resistant 'Leccino' progenies were integrated with SNP data to perform a GWAS. This analysis aimed to identify key genetic loci governing host plant responses to *Xfp*.

The GWAS was executed in two parallel trials targeting distinct phenotypic traits: 1. Bacterial load [Cq] (quantified via qPCR cycle threshold values); and 2. Resistance class. The latter trait was established by combining bacterial quantification data with symptom severity scores across individual replicates to categorize genotypes into three distinct phenotypic classes:

- Class 1: Susceptible traits
- Class 2: Intermediate tolerance
- Class 3: Resistant traits

3.3.2 Evaluation of quantitative bacterial load (Cq) associated loci

The Manhattan plot for the Cq trait revealed highly significant genomic clusters across multiple chromosomes. This distinct architecture of loci includes towering, major-effect peaks on Chromosomes 6, 8, 10, 18, and a highly critical pleiotropic locus on Chromosome 22. This pleiotropic cluster simultaneously influences both the Cq and the overall physical disease severity (Resistance category) and contains the cell-surface pattern recognition receptor Receptor-like protein kinase 2 (EVM0046669), alongside several structural components associated with the extracellular matrix.

- **Chromosome 10 (Peak Signal):** Demonstrated the most robust statistical association, with marker signals exceeding a -log10 (p-value) of 6 and approaching the stringent Bonferroni-corrected genome-wide significance threshold (**Figure 12**, red line). This

Funded by the European Union

highly significant region co-localizes with regulatory elements, specifically a gene encoding a transcription factor TCP5-like protein.

- **Chromosome 18:** Exhibited a sharp, prominent peak approaching a -log10 (p-value) of 6. This locus maps precisely to an ethylene-responsive transcription factor 1B-like gene, suggesting that allelic variation within this ethylene-signaling node plays a critical role in dictating the success of systemic bacterial colonization.
- **Chromosomes 6 and 8:** Both chromosomes displayed distinct, well-defined peaks rising significantly above the suggestive threshold line (*p*-value 5.5). These loci contain candidate genes involved in specialized plant defense metabolism:
  - **Chromosome 6:** Corresponds to a long-chain acyl-CoA synthetase 9 gene, implying a role in lipid-mediated or cuticular defense mechanisms.
  - **Chromosome 8:** Maps to a cytochrome P450 gene, likely involved in the biosynthesis of phytoalexins or antimicrobial secondary metabolites.
- **Chromosome 22 (Pleiotropic Locus):** This locus is of particular interest as it contains candidate genes exhibiting potential pleiotropic effects, such as a receptor-like protein kinase 2, which appear to simultaneously influence both Cq and overall phenotypic disease severity (resistance class).

The GWAS results visually confirm that the host plant's capacity to restrict *Xf* proliferation is a polygenic trait governed by prominent genomic regions on Chromosomes 6, 8, 10 and 18 (**Figure 12**).

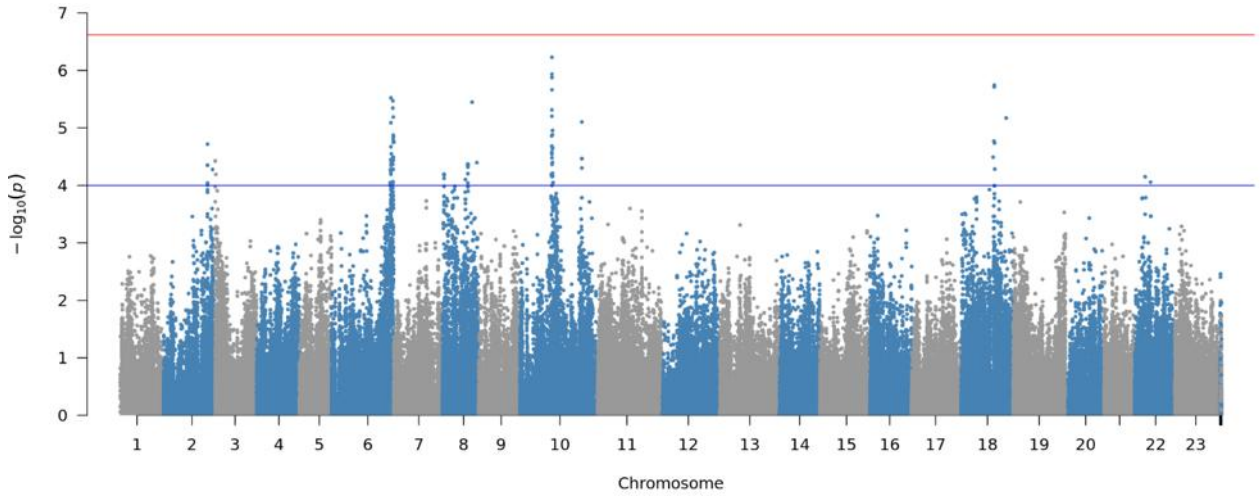


Figure 12. Manhattan plot of the Genome-Wide Association Study (GWAS) in olive for *Xylella fastidiosa* subsp. *pauca* bacterial load. The plot visualizes the statistical significance of SNPs associated with the plant's ability to restrict bacterial multiplication. The x-axis represents the physical distribution of SNPs across the 23 chromosomes, distinguished by alternating blue and grey clusters. The y-axis indicates the load score or statistical strength of the association, expressed as -log10(p). The horizontal blue line denotes a suggestive significance threshold p = 10^{-4}, while the red horizontal line represents the strict genome-wide significance threshold.

Funded by the European Union

Number of Identified Genes

The GWAS mapping within a 50kb genomic window for the Cq trait successfully isolated exactly 270 unique genes associated with the significant SNPs. This robust dataset encompasses both biologically annotated genes and numerous uncharacterized proteins.

Statistical Significance

The SNPs mapped across these genes exhibit strong statistical evidence of their association with the bacterial load (Cq) trait. The P-values for these significant SNPs range from an initial threshold of 9.95×10^{-5} down to distinct, major statistical peaks reaching as low as 5.90×10^{-7}. These lowest P-values, which indicate the absolute highest level of statistical confidence in the dataset, are densely clustered on Chromosome 10.

Functional Categories of the Identified Genes

The 270 annotated genes can be classified into several primary biological categories that dictate the plant's structural, sensory, and regulatory responses to *Xfp*:

- **Receptor Kinases & Early Pathogen Recognition:** A large category of the identified genes code for cell-surface sensors that detect bacterial presence. This includes various Leucine-Rich Repeat Receptor-like Kinases (LRR-RLKs) such as EVM0033063 and EVM0060094, as well as the pleiotropic Receptor-like protein kinase 2 (EVM0046669) mapped to the Chromosome 22 cluster.
- **Ubiquitination & Immune Regulation (E3 Ligases):** Confirming the secondary defense mechanisms, a significant subset of the genes encodes E3 ubiquitin-protein ligases. This critical regulatory category includes ATL23-like (EVM0059774), MARCH1-like (EVM0021107), DRIP2-like (EVM0022601), and CIP8-like (EVM0047074), which modulate downstream plant immunity pathways.
- **Transcription Factors & Gene Expression:** Dozens of identified loci act as transcription factors that reprogram the plant's internal networks during infection. This category spans multiple master regulatory gene families, including ethylene-responsive transcription factors (EVM0057883), MYB-family factors like MYB20 and MYB44 (EVM0027390, EVM0057614), and bHLH/TCP factors.
- **Structural Defenses (Lipids & Cell Walls):** The physical fortification of the plant is represented by genes linked to lipid and cuticular defenses. Key components in this category include Long-chain acyl-CoA synthetase 9 (EVM0061605), vegetative cell wall proteins (EVM0018106), and multiple GDSL esterase/lipases (e.g., EVM0045329).
- **Ion Transport and Osmotic Homeostasis:** Because *Xf* causes severe vascular blockage and subsequent drought stress, several highly significant genes encode membrane transporters. This includes the Sodium/hydrogen exchanger 1-like (EVM0026428) and various cation transport ATPases (EVM0006901) responsible for maintaining cellular pH and ion balance.

3.3.3 Evaluation of Plant Disease Severity Classification Associated Loci

GWAS mapping for plant disease severity classification revealed several highly significant loci. The most prominent and dense peak across the entire genome was localized to Chromosome

Funded by the European Union

22, with the leading SNPs reaching a -$\log_{10}$ (*p*-value) score of approximately 6.0. This specific genomic locus contains critical cell-surface PRRs, including *Receptor-like protein kinase S.2*. Notably, this region exhibits pleiotropic effects, simultaneously modulating both phenotypic disease severity classification and bacterial load (Cq).

Additional highly significant loci were identified on Chromosomes 12, 2 and 11:

- **Chromosome 12:** Characterized by a sharp, distinct peak extending well above the suggestive significance threshold -$\log_{10}$ (*p*) > 5.0. This peak maps to *Calmodulin-binding receptor-like cytoplasmic kinase 2*, a crucial downstream signaling molecule in early-phase immune responses activated by pathogen-induced cytosolic calcium (Ca^{2+}) influx.
- **Chromosome 2:** Displayed another highly significant peak exceeding a -$\log_{10}$ (*p*) value of 5.5. This locus corresponds to *NAC transcription factor 29-like*, a known master transcription regulator that coordinates downstream plant defense and stress-responsive gene networks.
- **Chromosome 11**: Even though the -log10 (4.5) reaches a lower value than the other two chromosomes described above, this chromosome presents the polymorphism closely related to resistance/susceptibility. The gene that possesses this polymorphism is the pentatricopeptide repeat-containing protein (see paragraph 3.3.5 on VEP analysis).

The Manhattan plot successfully demonstrates that the genetic architecture governing the host response to *Xfp* is oligogenic rather than highly polygenic or stochastic, driven primarily by a few major-effect loci. The towering genomic clusters on Chromosomes 22, 12, and 2 visually confirm that allelic variation within these specific loci serves as the primary determinant of plant resistance or susceptibility to disease severity (**Figure 13**).

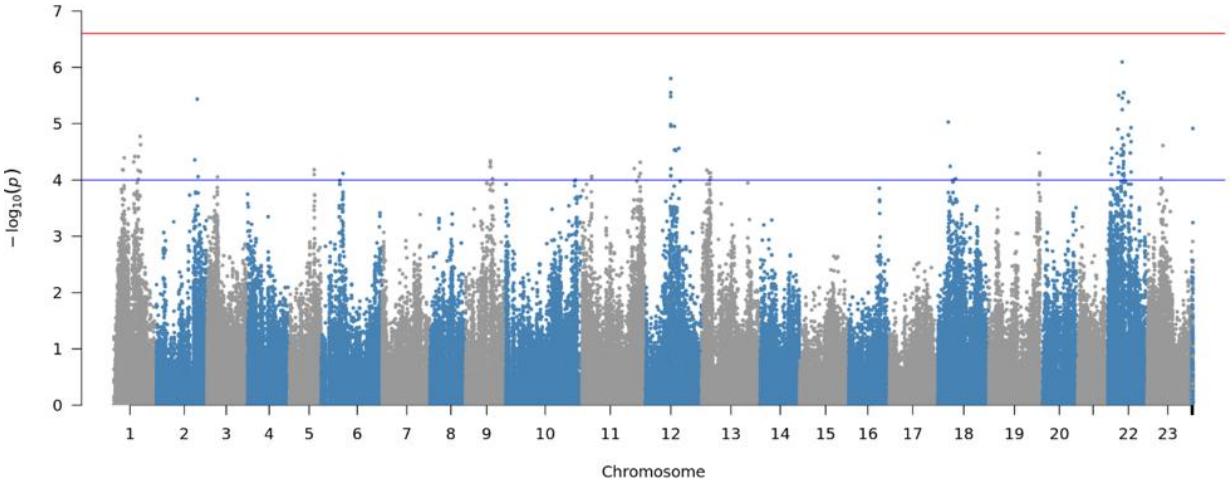


Figure 13. Manhattan plot of the Genome-Wide Association Study (GWAS) in olive for *Xylella fastidiosa* subsp. *pauca* disease response. The plot visualizes the statistical significance of SNPs associated with the plant's overall phenotypic disease severity classification. The x-axis represents the physical distribution of genetic variations across the 23 plant chromosomes, distinguished by alternating grey and blue clusters. The y-axis indicates the load score or statistical strength of the association, expressed as -log10(*p*). The horizontal blue line denotes a suggestive significance threshold $p = 10^{-4}$, while the red horizontal line represents the strict genome-wide significance threshold.

Funded by the European Union

The inclusion of highly susceptible genotypes (e.g., 'Ogliarola salentina' and 'Cellina di Nardò') alongside those with diverse resistance or tolerance profiles (such as 'Leccino') and its progeny allows for maximum statistical discrimination during genomic mapping.

Number of Identified Genes

The GWAS mapping within a 50kb genomic window for the disease severity class trait successfully isolated approximately 160 unique genes associated with the significant SNPs. Similar to the bacterial load (Cq) dataset, this includes both highly annotated structural and defense genes, as well as various uncharacterized loci.

Statistical Significance

The SNPs mapped to these genes exhibit strong statistical evidence of their association with the physical disease severity trait. Overall, the *P*-values for these significant SNPs begin at 9.98×10^{-5} and strengthen down into major statistical peaks. The most highly significant of these mutations reach exact P-values of 4.74×10^{-6} (for the locus found on Chromosome 12) and 4.91×10^{-6} (for the mutations located directly within the critical pleiotropic gene cluster on Chromosome 22).

Functional Categories of the Identified Genes

The identified genes governing physical disease resistance can be classified into several primary biological categories that dictate the plant's structural, sensory, and regulatory responses to *Xfp*:

- **Receptor Kinases & Signal Transduction:** A substantial portion of the genes encodes cell-surface sensors and downstream signaling kinases used to detect the pathogen. This prominently includes the pleiotropic Receptor-like protein kinase 2 (EVM0046669) on Chromosome 22, alongside other major sensors like probable LRR receptor-like serine/threonine-protein kinases, nodulation receptor kinases, and calmodulin-binding receptor-like cytoplasmic kinases.
- **Ubiquitination & Protein Degradation (E3 Ligases):** Mirroring the secondary defenses in the CQ trait analysis, a significant cluster of genes acts as master regulators of the plant's immune response via targeted protein degradation. This includes various E3 ubiquitin-protein ligases (such as PRT6-like and RHA4A), U-box domain-containing proteins, and ubiquitin carboxyl-terminal hydrolases.
- **Transcription Factors & Gene Expression:** The dataset contains numerous master regulators that reprogram the plant's internal defense networks during infection. This category spans NAC domain-containing proteins, ethylene-responsive transcription factors (RAP2-7-like, ERF104-like), MYB family factors (PHL8-like), and heat stress transcription factors.
- **Structural Defenses (Cell Wall & Lipid Metabolism):** Physical fortification against the bacteria's spread is represented by genes linked to cell wall remodeling and lipid synthesis. Key components include cellulose synthase-like proteins (D1 and G1), dirigent protein 16-like, xyloglucan 6-xylosyltransferase, and multiple 3-ketoacyl-CoA synthases.
- **Ion Transport and Osmotic Homeostasis:** To survive the severe vascular blockage and drought stress induced by *Xfp*, highly significant genes encode membrane transporters.

Funded by the European Union

This includes the critically important, pleiotropic Sodium/hydrogen exchanger 1-like (EVM0026428), along with potassium transporters, zinc transporters, and aquaporins (such as PIP2-1-like and TIP5-1).

- **Oxidative Stress & Detoxification:** The plant's response to cellular damage and toxicity is highlighted by genes dedicated to managing oxidative stress, such as superoxide dismutase [Cu-Zn] 2, putative nitric oxide synthase, and microsomal glutathione S-transferase 3.

3.3.4 Bioinformatic Integration and Literature Cross-Validation

The GWAS candidates identified in our data exhibit remarkable congruence with core transcriptomic networks validated across multiple plant species fighting *Xfp*:

- **Pattern Recognition Receptors (PRRs) and Kinases:** Our GWAS highlighted the critical role of LRR receptor-like kinases. Transcriptomic studies on the tolerant olive cv. ''Leccino'' confirm that these Leucine-Rich Repeat (LRR) proteins are heavily upregulated, acting as the first line of defense to perceive the pathogen and modulate cell wall architecture.
- **Cell Wall Remodeling and Integrity:** Our data flagged multiple cell wall restructuring genes (microfibrillar proteins, expansins, and cellulose synthases). Since *Xf* relies on cell-wall-degrading enzymes to enlarge pit membranes and move through the xylem, the plant's ability to structurally reinforce these barriers is paramount.
- **Transcription Factor Reprogramming:** The GWAS prominently flagged WRKY, ERF, and NAC transcription factors. Cross-species network analysis confirms that hubs like WRKY40 play an evolutionary-conserved role in *Xfp* resistance. Furthermore, ethylene-responsive transcription factors such as ERF071-like and ERF096-like are explicitly upregulated in *Xfp*-resistant genotypes to reprogram secondary metabolism and orchestrate systemic defense.

3.3.5 Variant Effect Prediction (VEP) and High-Impact Mutation Profiling

Following the identification of significant polymorphisms associated with bacterial load (Cq) and disease resistance class, a comprehensive Variant Effect Prediction (VEP) and genotype matrix analysis was conducted. By comparing highly resistant cultivars (such as the 'Leccino' progeny) against a cohort of 52 highly susceptible cultivars, several critical structural mutations were identified that dictate the host response to *Xfp*.

Identification of Primary Susceptibility (S) Factors.

The most crucial finding from the variant analysis is the identification of two HIGH-impact knockout mutations that act as the primary genetic differentiators between resistant and susceptible phenotypes. The first is a splice acceptor mutation located within the EVM0013689 (*uncharacterized protein LOC111379872*) gene on Chromosome 6, which governs the bacterial load (Cq) trait. The second is a high-impact mutation in EVM0017391 (*pentatricopeptide repeat-containing protein*), which acts as a primary determinant for physical disease severity (Class).

Funded by the European Union

- **Resistant Genotypes:** Highly resistant cultivars carry homozygous (1/1) knockout mutations that completely break both genes. By rendering these susceptibility factors non-functional, the plant effectively denies *Xfp* the specific pathways it exploits to multiply and cause structural deterioration.
- **Susceptible Genotypes:** Conversely, the genotype matrix revealed that the susceptible cohort (including specific samples such as 'Cima di Melfi', 'Kalamata', 'Cellina di Nardò', and 'Ogliarola salentina') predominantly carry the unbroken Wild-Type (0/0) or Heterozygous (0/1) genotypes. Because these plants lack complete knockouts, they produce functional susceptibility proteins, allowing the bacteria to rapidly multiply.

Moderate-Impact Missense Mutations Act Only as Secondary Defenses.

The bioinformatic pipeline also mapped over 20 MODERATE-impact missense variants, mutations that alter the 3D shape of proteins rather than breaking them. These included dense clusters on Chromosome 6 (affecting LRR-RLK bacterial sensors like EVM0033063), Chromosome 8 (EVM0029034), and Chromosome 10 (such as EVM0059368, which carries Threonine to Methionine and Leucine to Proline amino acid substitutions). However, cross-referencing these variants across the susceptible cohort revealed a highly mixed genotype distribution. For example, some highly susceptible cultivars (like sample 'Grappuda') carried fully modified (1/1) status for the EVM0033063 LRR-sensor but still suffered from severe disease. This demonstrates that while moderate-impact structural variations in secondary defenses are important, they are fundamentally insufficient to protect the plant on their own if the primary HIGH-impact susceptibility factors remain functional.

The statistical resolution and significance of GWAS are inherently constrained by the sample size of the evaluated cohort. Because the current phenotypic dataset is relatively small, the statistical power to resolve these specific causal variants is limited. To overcome this, ongoing research projects at CNR are strategically focused on expanding the phenotypic dataset. By significantly increasing the number of accurately-phenotyped olive cultivars, these ongoing projects aim to enhance the overall statistical power of the GWAS framework. Expanding the cohort is anticipated to elevate the LOD scores of true biological associations above the strict significance threshold, ultimately enabling the precise identification and subsequent validation of the exact causal genetic variants governing *Xfp* resistance.

3.3.6 Characterization of the water stress-responses

During the summer 2024 and 2025 field campaigns, assessments of cultivar responses to drought stress were replicated following the 2023 protocols. Physiological measurements included leaf relative water content (RWC), chlorophyll fluorescence (Φ_{PSII}), and stomatal conductance to water (g_{sw}). Phenotypic data spanning all three years are currently being analyzed to establish tolerance classifications and to perform genome-wide association studies.

Funded by the European Union

3.4 Characterization of the molecular response of resistant and susceptible olive cultivars to *Xylella fastidiosa* infection

A large dataset of 190 RNA-seq libraries has been produced by P5-CNR-IPSP since the start of the outbreak in Apulia, from 2016 to the present time. Libraries have been prepared using RNA collected from olives infected by *Xylella fastidiosa* subsp. *pauca* ST53 (*Xfp*) in natural conditions (field infections) or by artificial inoculations in potted plants maintained in greenhouse conditions. Olive cultivars include in these experiments include: 'Leccino' and FS17 (resistant); Arbequina, 'Ogliarola salentina', 'Cellina di Nardò' (susceptible); and spontaneous seedlings survived in the epidemic area (La Notte et al., 2024). Most of the artificially inoculated plants have been sampled at a minimum of 12 months post inoculation, when susceptible control cultivars started showing symptoms, thus corresponding to chronic infections. Some samples were collected as early as 48 hours or up to 10 days post inoculation to examine early responses to *Xfp* inoculation prior to establishment of chronic infection (**Figure 14**).

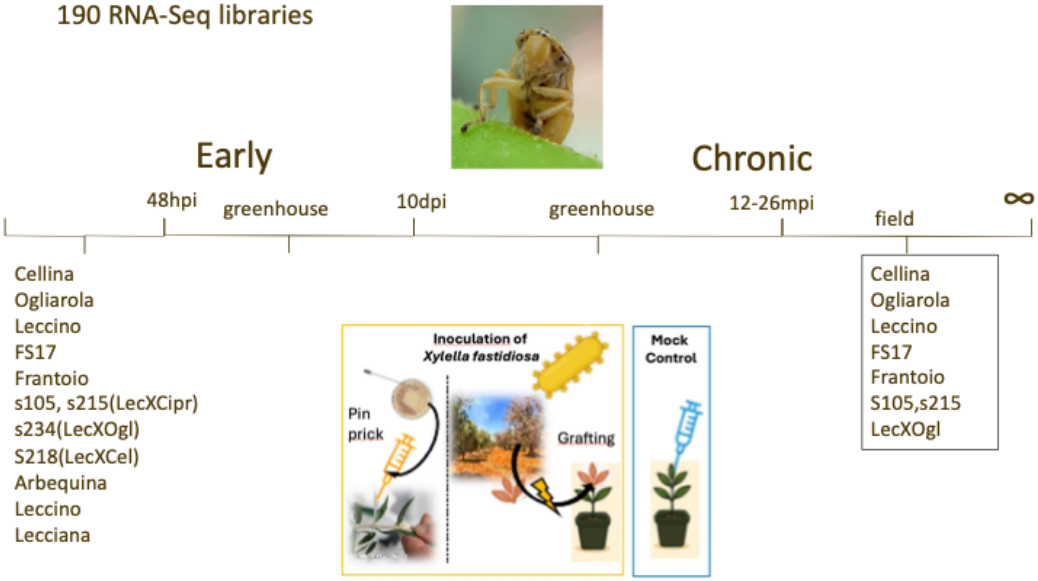


Figure 14. Composition of the database of 190 RNA-seq libraries from olives naturally or artificially infected by *Xylella fastidiosa* subsp. *pauca*, indicating time of infections and cultivars.

The meta-analysis of this extensive transcriptomic dataset provided insights into fundamental aspects of the *Xfp*–olive interaction, with particular emphasis on the molecular basis of susceptibility and resistance in selected olive cultivars. To illustrate the main findings of the meta-analysis, a selection of representative experiments that collectively summarize the overall results is presented below.

The first question we sought to address was: **"Does olive perceive *Xfp*, and if so, how early does this recognition occur?"**

The first selected dataset consisted of seven artificially inoculated clones of the cultivar 'Leccino' (Abou Kubaa et al. 2026). The analysis shows that as early as 48 hours post inoculation (hpi) 'Leccino' responds to *Xfp* DD infection by differentially expressing several genes, either up or downregulated (**Figure 15**).

Funded by the European Union

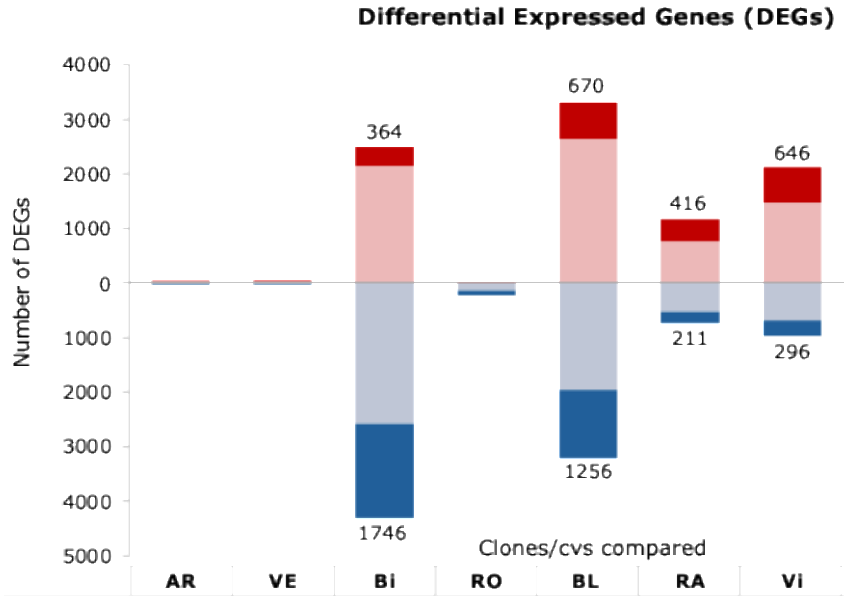


Figure 15. Differentially Expressed Genes (DEGs) at 48 hours post inoculation of seven 'Leccino' clones. The graph shows the numbers of up- and downregulated differentially expressed genes (DEGs) in artificially inoculated 'Leccino' clones compared with uninoculated control plants. DEGs are grouped according to fold-change intervals of 0 to +2 and 0 to −2 (red and blue, respectively), and >+2 and <−2 (dark red and dark blue, respectively).

Second evidence of olive sensing the presence of *Xfp* derives from the analysis of tissues from the susceptible cultivars 'Ogliarola salentina' sampled at 10 days post inoculation (dpi) (Giampetruzzi et al. 2026) (**Figure 16**). In these trials only 24 DEGs were altered in the expression.

Funded by
the European Union

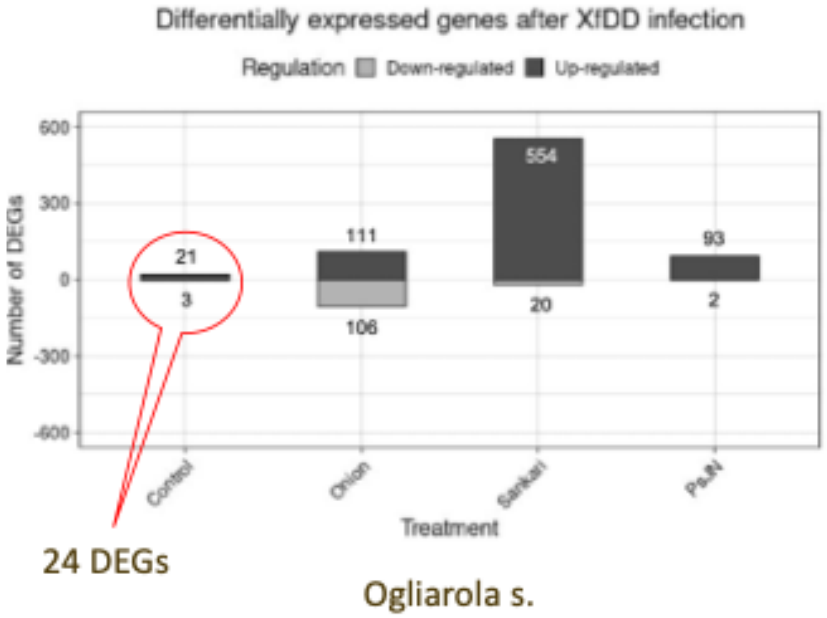


Figure 16. Differentially Expressed Genes (DEGs) at 10 dpi of plants of the cultivar 'Ogliarola salentina'**.** The graph reports the numbers of up- and downregulated DEGs distinct by respective fold changes in the 0 to +2 (dark grey) and 0 to −2 (light grey).

We further analyzed the database to look for conserved transcriptional responses to answer to the question "**are there recurrent pathways/DEGs occurring in these RNA-seq libraries?**".

To simplify the answer to this question we refer to the analysis of La Notte et al. (2024), where olives of the resistant cultivar 'Leccino' and susceptible 'Cellina di Nardò' were analyzed at 16 months post inoculation (mpi) (**Figure 17**).

Gene Ontology (GO) analysis identified 11 GO terms that were commonly enriched in both 'Leccino' and 'Cellina di Nardò', all of which were associated with 'plant immune responses to biotic stimuli' (**Figure 18**). In contrast, the 24 GO terms uniquely enriched in 'Leccino' were predominantly related to plant cell wall metabolism.

Funded by
the European Union

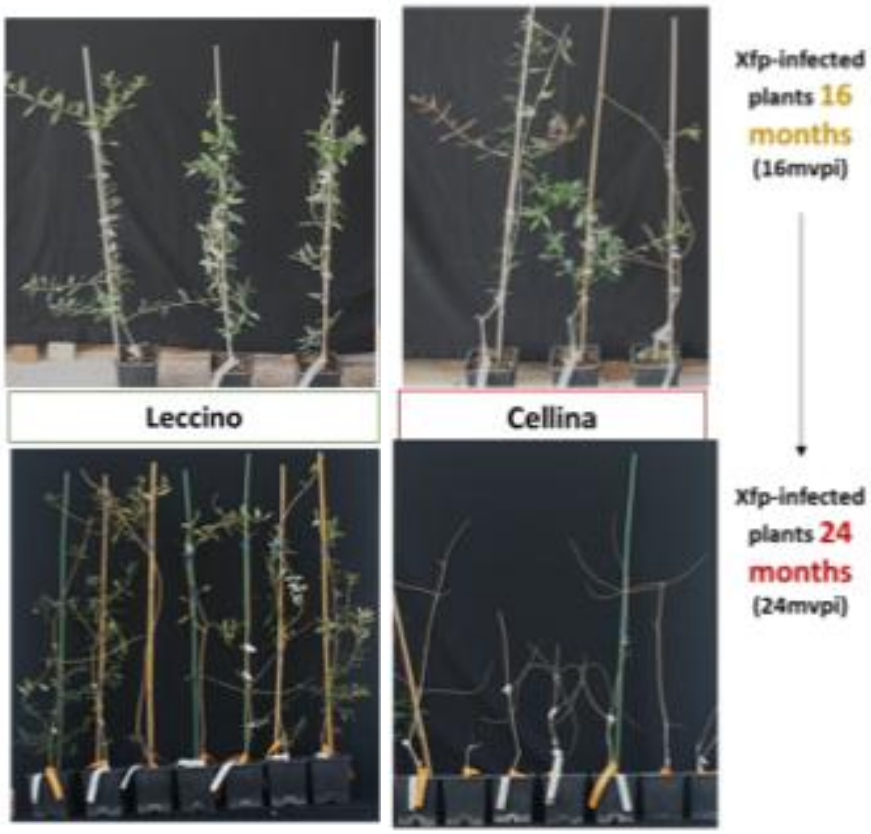


Figure 17. 'Leccino' and 'Cellina di Nardò' olive plants artificially inoculated with *Xylella fastidiosa* subsp. *pauca*. The upper panel shows plants at 16 months post-inoculation (mpi), when tissues were collected for RNA-seq analysis. The lower panel shows the complete desiccation of the susceptible 'Cellina di Nardò' plants at 24 mpi.

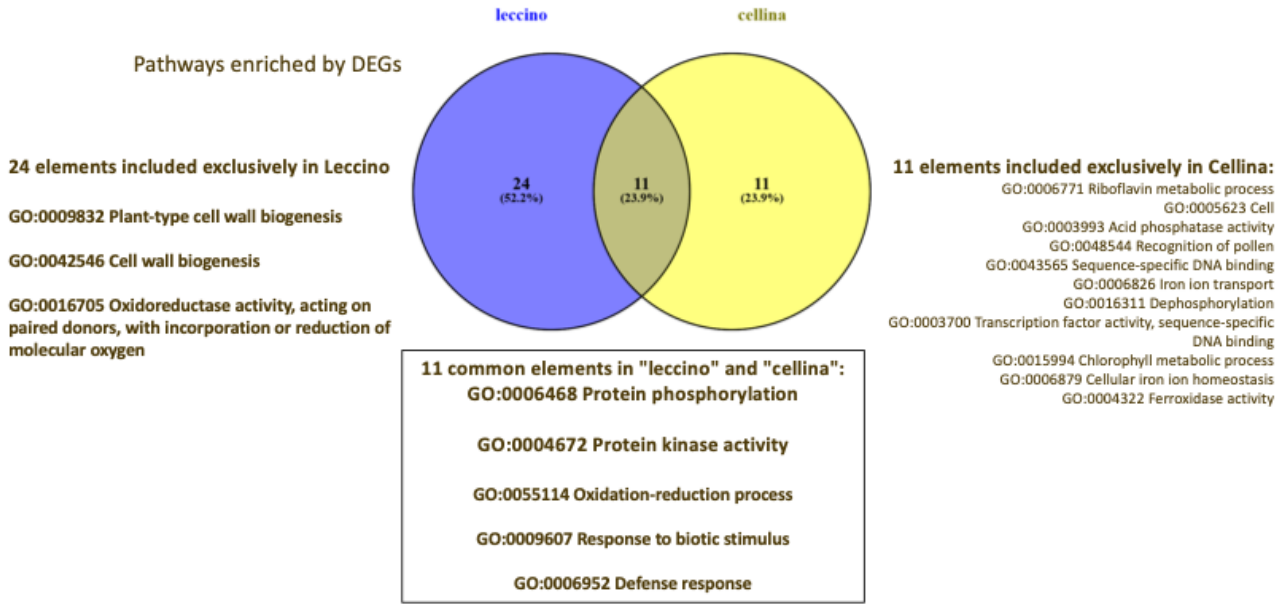


Figure 18. Differential and common GO terms enriched upon artificial inoculation of 'Leccino' and 'Cellina di Nardò' at 16 mpi.

Funded by the European Union

Besides several pathogenesis-related (PR) proteins, two genes were among the top nine upregulated DEGs that were consistently identified across multiple RNA-seq experiments (**Figure 19**). Downy Mildew Resistance 6 (DMR6) and several proteins containing a conserved EG45-like domain. In addition, a probable leucine-rich repeat (LRR) receptor-like serine/threonine kinase At3g47570 was also among the most highly upregulated genes.

1	OE9A029444	Putative EG45-like domain containing protein 1
2	OE9A117543	pathogenesis-related leaf 6-like
3	OE9A094670	Thaumatin
4	OE9A086946	pathogenesis-related STH-2-like
5	OE9A058974	Putative EG45-like domain containing protein
6	OE9A013998	probable LRR receptor-like serine threonine-kinase At3g47570
7	OE9A079697	DMR6
8	OE9A053389	probable nucleoredoxin 1
9	OE9A116998	probable WRKY transcription factor 70



Figure 19. Top DEGs in 'Leccino' and 'Cellina di Nardò' upon *Xylella fastidiosa* subsp. *pauca* inoculation at 16 months post inoculation. The graph shows the upregulation of two representative DEGs in infected plants.

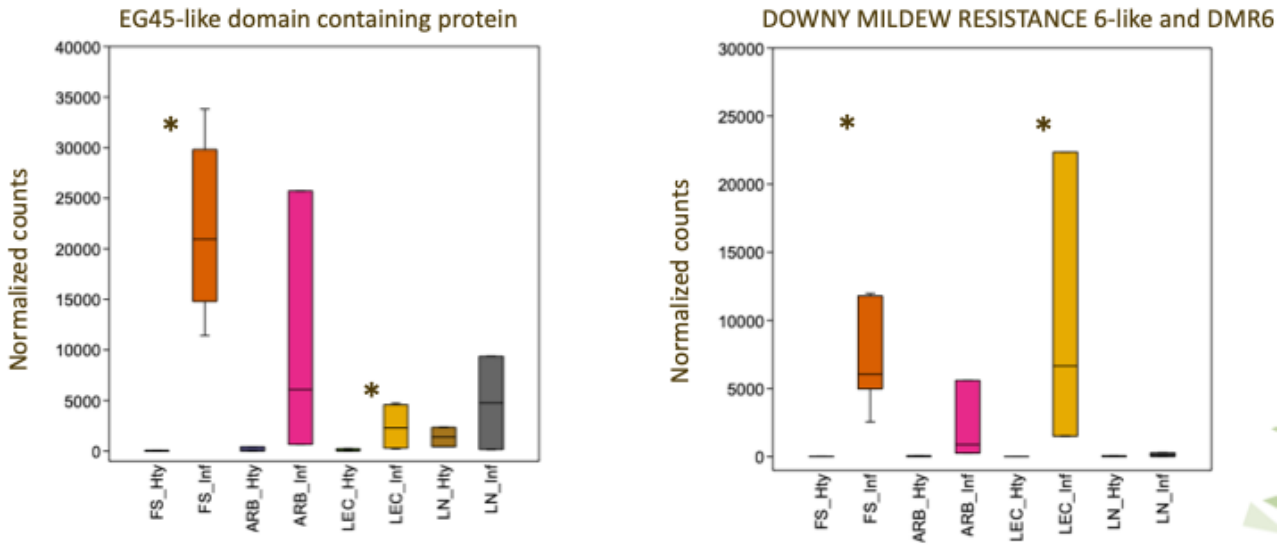


Figure 20. Upregulation of a EG45-like domain containing protein and DMR6 in response to *Xfp* inoculation. Expression level of EG45-like domain containing protein and DMR6 in inoculated and uninoculated olive cultivars at 12 months post inoculation. Asterisks indicate significant differences evaluated by t-test (Inf vs hty) at p=0.05. FS: 'FS17', ARB: 'Arbequina', LEC: 'Leccino', LN: 'Lecciana'.

The same two genes were also differentially upregulated in an independent experiment in which the susceptible cultivar Arbequina and the resistant cultivars 'FS17', 'Leccino', and 'Lecciana' were artificially inoculated with *Xfp*, and tissues were analyzed by RNA-seq at 12

Funded by the European Union

mpi. Both genes were upregulated in all four cultivars; however, this upregulation was statistically significant only in the resistant cultivars 'FS17' and 'Leccino' (**Figure 20**).

3.5 Characterization of the mineral element concentrations (ionome) in susceptible and resistant plants

To identify physiological traits associated with resistance to *Xf*, we compared the ionomic profiles of resistant and susceptible cultivars. Because mineral nutrient homeostasis can influence host-pathogen interactions, ionome analysis was used to identify elemental signatures associated with resistance.

3.5.1 Ionome analysis of susceptible and resistant almonds cultivars

The selection of almond cultivars for this experiment was based on cultivar screens for resistance to *Xf*, which were conducted by eihter P11-ARO-VOL in Israel or by P2-IVIA in Spain.

Almond samples from P11-ARO-VOL that included leaf tissue from the resistant almond cultivar 'Lauranne' and the susceptible cultivar 'UEF' ('Um El-Fahem') sampled from the same experiment described in section 2.1 were used. Linear models comparing the susceptible and resistant cultivars show that Magnesium (Mg) concentrations were significantly lower in susceptible plants compared to resistant plants (mean difference = –0.95 µg/mg; 95% CI: –1.51, –0.40; p = 0.001). Phosphorus (P) (mean difference = –0.50 µg/mg; 95% CI: –0.94, –0.07; p = 0.023) and manganese (Mn) (mean difference = –0.038 µg/mg; 95% CI: –0.070, –0.0056; p = 0.023) showed a similar pattern, with significantly lower concentrations in susceptible plants. Copper (Cu) was present at slightly higher concentrations in susceptible plants (mean difference = +0.00112 µg/mg; 95% CI: 0.00016, 0.00208; p = 0.024). For iron (Fe), susceptible plants had, on average, 0.00256 µg/mg lower concentration than resistant plants (95% CI: –0.0121, 0.0070; p = 0.592). No statistically significant differences were observed for calcium (Ca), potassium (K), Iron (Fe) and zinc (Zn) between the two groups (all $p > 0.05$). Data is summarized in **Figure 21** and **Table 4**.

The preliminary results for Mn (**Figure 21**, **Table 4**) showed the same tendency observed for previous experiments performed with olive, where also the resistant varieties accumulate higher concentrations of this element. More research is needed to determine if this is a signature of resistance to infection by *Xf* (data not shown).

Funded by the European Union

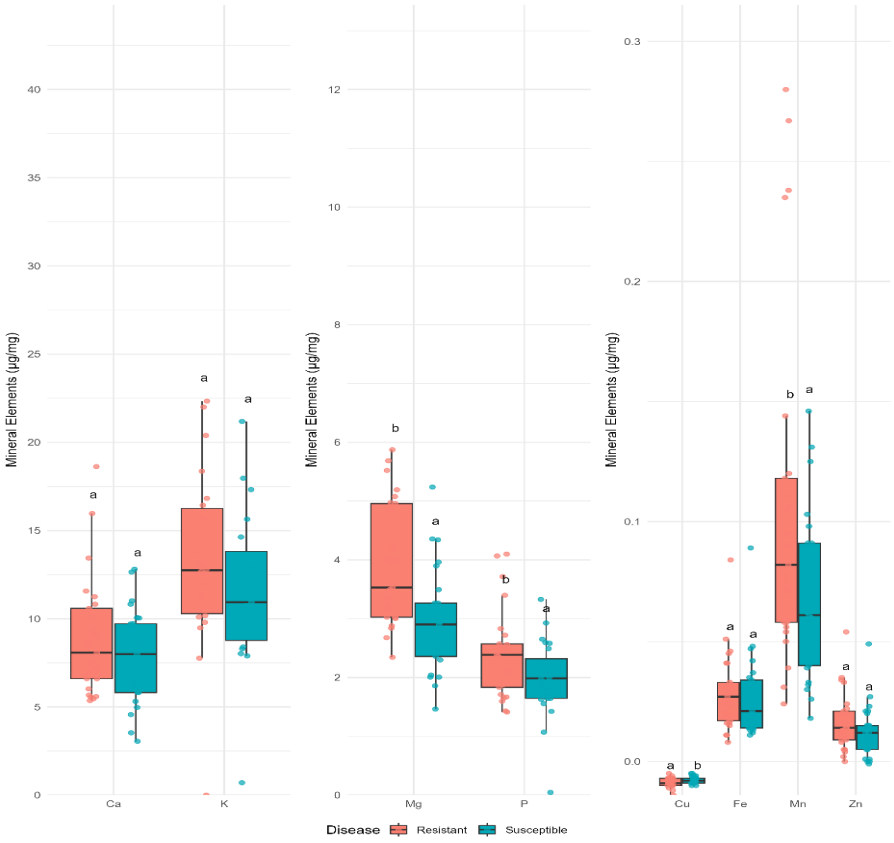


Figure 21. The ionome profile of almond leaves from resistant and susceptible cultivars. Boxplots show the distribution of calcium (Ca), potassium (K), magnesium (Mg), phosphorus (P), copper (Cu), iron (Fe), manganese (Mn), and zinc (Zn) concentrations (µg/mg dry weight) in leaf tissues of resistant (salmon) and susceptible (blue) cultivars. Points represent individual samples; box limits indicate the interquartile range, bold lines denote medians, and whiskers extend to 1.5× IQR or the most extreme data points within this range. Different letters above boxes denote statistically significant differences between disease groups for each element, as determined by linear models ($p < 0.05$, Compact Letter Display method). Notably, Mg, P, Mn, and Cu concentrations differed significantly between groups, while Ca, K, Fe, and Zn did not.

Table 4. Estimated differences in mineral element concentrations between susceptible and resistant almond cultivars.

Element	Estimated Mean Difference (µg/mg)*	95% CI**	p-value
Ca	–1.04	(–2.77, 0.70)	0.236
K	–1.74	(–4.80, 1.31)	0.255
Mg	–0.95	(–1.51, –0.40)	0.001*
P	–0.50	(–0.94, –0.07)	0.023*
Cu	+0.00112	(0.00016, 0.00208)	0.024*
Mn	–0.038	(–0.070, –0.0056)	0.023*
Zn	–0.00452	(–0.0112, 0.00212)	0.177
Fe	–0.00256	(–0.0121, 0.0070)	0.592

* Negative values indicate lower concentrations in susceptible plants compared to resistant plants.
**Values in parentheses represent the 95% confidence interval for each estimate.

Funded by the European Union

The samples from P2-IVIA consisted of the susceptible cultivar 'Marcona' and a less susceptible cultivar 'Belona' (**Figure 22, Table 5**), either infected or not infected with *Xfm* strains IVIA 5901 or ESVL (**Figures 23, 24**, **Table 5**).

Linear models show that 'Marcona' (susceptible) has significantly lower concentrations of phosphorus (P), manganese (Mn), copper (Cu), zinc (Zn), and potassium (K) than the 'Belona' (less susceptible) cultivar (**Figure 22**). Specifically, differences in P, Mn, and Cu were highly significant ($p < 0.001$). No statistically significant differences were found for calcium (Ca), magnesium (Mg), or iron (Fe) ($p > 0.05$) (**Table 5**). For this analysis, we combined strains and positions for each cultivar, but we also separated the results and statistical analysis by strains. We could not run the analysis by sample position since there was no uniformity across treatments.

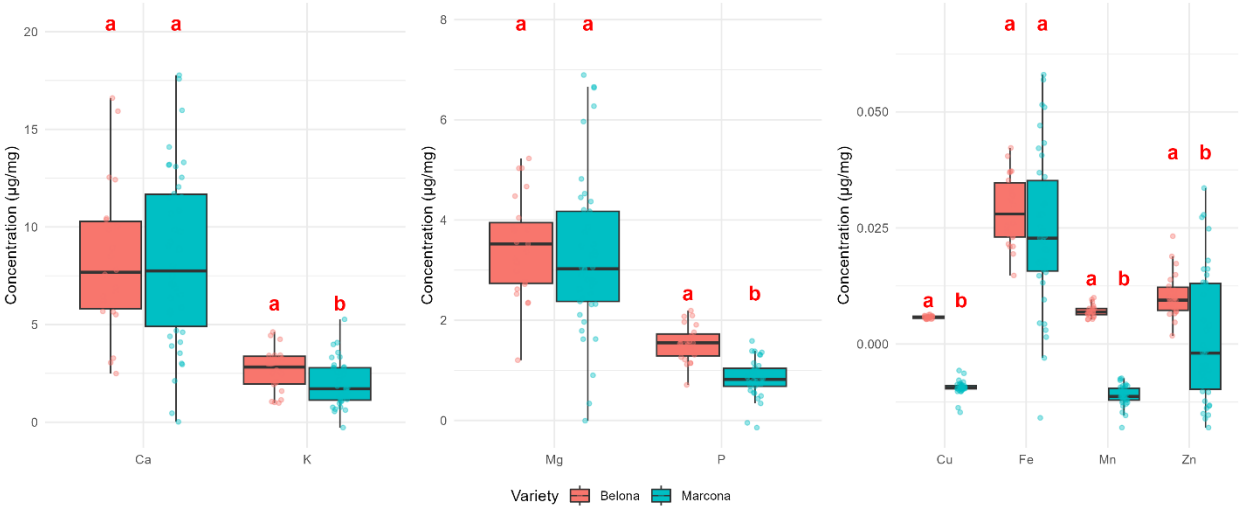


Figure 22. Differences in the ionome profile of two almond cultivars infected with *Xylella fastidiosa* subsp. *multiplex* (*Xfm*). Boxplots show the distribution of calcium (Ca), potassium (K), magnesium (Mg), phosphorus (P), copper (Cu), iron (Fe), manganese (Mn), and zinc (Zn) concentrations (µg/mg dry weight) in leaf tissues of 'Marcona' (highly susceptible to Almond Leaf Scorch) and 'Belona' (less susceptible) cultivars, infected with *Xfm*. Points represent individual samples after outlier's removal. Red letters above the boxes denote statistically significant differences ($p < 0.05$) derived from a linear model (Element ~ Cultivar). Notably, Zn, Mn, Cu, K, and P concentrations differed significantly between cultivars, whereas Ca, Mg, and Fe showed no significant variation. The Y-axis for the low-concentration element is scaled to include negative values to accurately represent the data range. Both strains and all sample positions were considered together for each one of the cultivars.

Table 5. Estimated differences in mineral element concentrations between 'Marcona' and 'Belona' almond cultivars.

Element	Mean_Belona*	Mean_Marcona*	Difference **	P_Value	Significance***
Ca	8.313144149	8.405262757	0.092118608	0.934230851	ns
Cu	0.005778155	-0.009411526	-0.015189681	1.11E-42	***
Fe	0.028699142	0.024279897	-0.004419245	0.245848319	ns
K	2.677187026	1.980157198	-0.697029828	0.029496392	*

Funded by the European Union

Mg	3.480996902	3.283185419	-0.197811483	0.593985595	ns
Mn	0.007076103	-0.011135582	-0.018211685	4.28E-37	***
P	1.545197063	0.833261847	-0.711935216	2.67E-09	***
Zn	0.010375757	0.001596455	-0.008779302	0.006541306	**

*Linear model estimates for the mean differences in elements between 'Marcona' and 'Belona', with 'Belona' as the reference group. Mean values for each cultivar were calculated after removing outliers using the 1.5 × Interquartile Range (IQR) method.
**The "Difference" column represents the estimated effect size ('Marcona' – 'Belona'); negative values indicate a lower concentration in the 'Marcona' cultivar relative to 'Belona'.
***Statistical significance is determined by the p-value from the linear model and is denoted as follows: * p <0.05, **p <0.01, *** p <0.01 and "ns" indicates no significant difference.

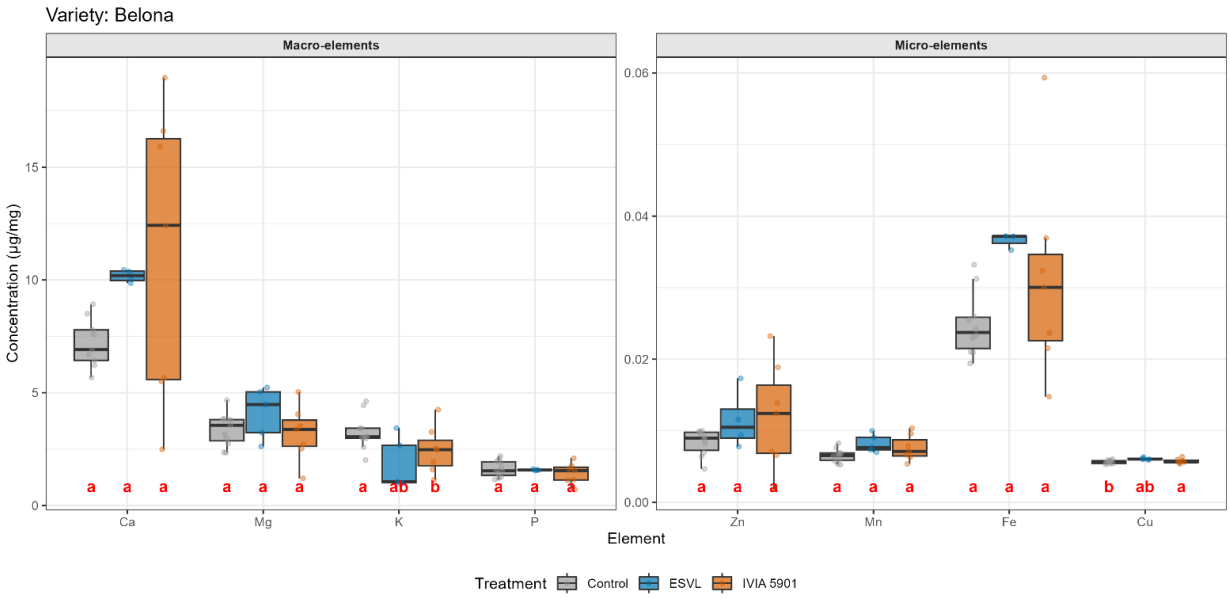


Figure 23. Effect of *Xylella fastidiosa* subsp. *multiplex* infection on the ionome profile of almond leaves in the 'Belona' cultivar. Boxplots show the concentration (µg/mg dry weight) of macro elements calcium (Ca), potassium (K), magnesium (Mg), phosphorus (P) on the left and micro elements copper (Cu), iron (Fe), manganese (Mn), and zinc (Zn) in the "less susceptible" 'Belona' cultivar under inoculation of different strains. ESVL (blue), IVIA5901(orange), and control (gray) to evaluate the change in the ionome profile. Points represent individual samples after outlier removal. Red letters below the boxes denote statistically significant differences ($p < 0.05$) derived from EMMeans.

Funded by the European Union

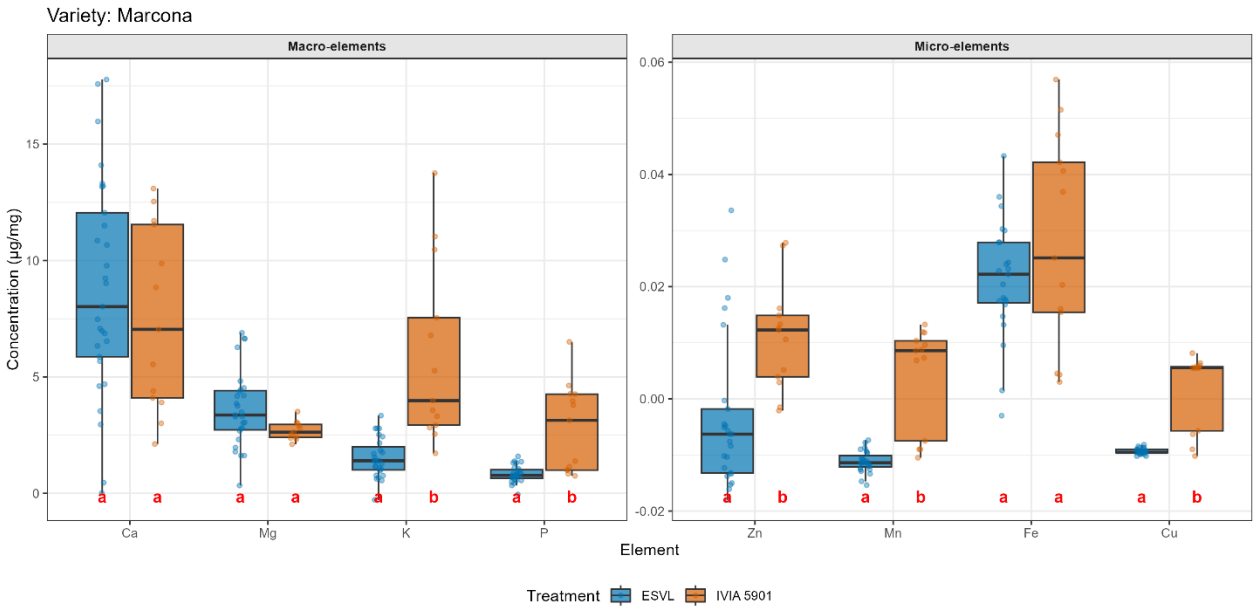


Figure 24. Effect of *Xylella fastidiosa subsp.* multiplex strains on the ionome profile of almond leaves in the 'Marcona' cultivar. Boxplots show the concentration (µg/mg dry weight) of macro elements calcium (Ca), potassium (K), magnesium (Mg), phosphorus (P) on the left and micro elements copper (Cu), iron (Fe), manganese (Mn), and zinc (Zn) in the highly susceptible 'Marcona' cultivar under inoculation of different strains. ESVL (blue) and IVIA5901 (orange) to evaluate the change in the ionome profile. Points represent individual samples after outlier removal. Red letters below the boxes denote statistically significant differences ($p < 0.05$) derived from EMMeans.

To determine if *Xfm* infection influences the ionome of almond leaves, two *Xf*m strains (IVIA5901 and ESVL) were used to inoculate two almond cultivars: 'Marcona' (susceptible) and 'Belona' (less susceptible). Comparisons were made between both strains and with non-inoculated control (except for 'Marcona' for which a non-treated control was absent). Data were analyzed using a linear model for each cultivar-element combination to assess treatment effects. A post-hoc test was performed using Estimated Marginal Means (EMMeans). The elements were grouped into macro- and micro-elements to enable clear visualization across different concentration scales.

Funded by the European Union

Table 6. Estimated pairwise treatment contrasts for 'Marcona' and 'Belona' almond cultivars.

Cultivar	Element	contrast	estimate	SE	p.value
Marcona	Ca	ESVL - IVIA 5901	1.287866055	1.486411	0.391424
	Mg	ESVL - IVIA 5901	0.932226913	0.505031	0.073146
	K	ESVL - IVIA 5901	-4.305957649	0.762819	1.75E-06
	P	ESVL - IVIA 5901	-1.993343909	0.373313	4.58E-06
	Zn	ESVL - IVIA 5901	-0.014328484	0.004253	0.001811
	Mn	ESVL - IVIA 5901	-0.015234522	0.001829	4.24E-10
	Fe	ESVL - IVIA 5901	-0.006692089	0.004885	0.17973
	Cu	ESVL - IVIA 5901	-0.011093454	0.00134	7.41E-10
Belona	Ca	Control - ESVL	-2.982777702	2.35856	0.446112
	Ca	Control - IVIA 5901	-3.890345942	1.977954	0.197226
	Ca	ESVL - IVIA 5901	-0.90756824	2.460049	0.71674
	Mg	Control - ESVL	-0.74966438	0.52986	0.379589
	Mg	Control - IVIA 5901	0.167473011	0.474978	0.728084
	Mg	ESVL - IVIA 5901	0.917137391	0.575227	0.379589
	K	Control - ESVL	1.42630397	0.524357	0.04076
	K	Control - IVIA 5901	0.802158913	0.471783	0.210783
	K	ESVL - IVIA 5901	-0.624145057	0.560562	0.279413
	P	Control - ESVL	0.051840405	0.216802	1
	P	Control - IVIA 5901	0.199937887	0.179529	0.837923
	P	ESVL - IVIA 5901	0.148097481	0.232735	1
	Zn	Control - ESVL	-0.003167253	0.002843	0.559747
	Zn	Control - IVIA 5901	-0.003628946	0.002368	0.428367
	Zn	ESVL - IVIA 5901	-0.000461693	0.003012	0.879871
	Mn	Control - ESVL	-0.00167828	0.000707	0.083361
	Mn	Control - IVIA 5901	-0.001074758	0.000634	0.211116
	Mn	ESVL - IVIA 5901	0.000603521	0.000768	0.441075
	Fe	Control - ESVL	-0.011771672	0.006034	0.203254
	Fe	Control - IVIA 5901	-0.00645685	0.004517	0.342022
	Fe	ESVL - IVIA 5901	0.005314822	0.006325	0.412434
	Cu	Control - ESVL	-0.000432988	0.000143	0.020844
	Cu	Control - IVIA 5901	-0.000119653	0.000129	0.364325
	Cu	ESVL - IVIA 5901	0.000313335	0.000153	0.10918

This preliminary result shows that from the eight elements measured, only five showed significant differences in the tested treatments. When cultivars were considered, 'Belona' (less susceptible) had higher concentrations than 'Marcona' (susceptible) for K, P, Zn, Mn and Cu. When strains were considered separately, almond plats inoculated with IVIA5901 strain had higher concentrations than those inoculated with ESVL strain in all the same elements

Funded by the European Union

only in 'Marcona' (susceptible), while no significant differences were found in 'Belona' (less susceptible). Preliminary results indicate that in 'Marcona', strain IVIA 5901 is more virulent than ESVL, which can explain the differences observed in the ionomes. On the other hand, both strains showed low infection at similar levels in 'Belona' (P2-IVIA preliminary results), but these observations need to be further studied.

3.5.2 Ionome analysis of susceptible and resistant olive cultivars

The ionome analysis of olive leaf samples was conducted with a pathogenicity experiment performed by P1-CSIC using four olive cultivars: 'Arbequina' and 'Ogliarola' as susceptible olive cultivars; 'FS17' and 'Leccino' as resistant olive cultivars. We compared two treatment conditions to observe how the ionome changes when olives were inoculated with *Xfp* strain XYL1961/18 of ST80 (**Figure 25**, **Table 7**).

No significant changes were observed in potassium (K), calcium (Ca), or magnesium (Mg) concentrations following inoculation in any of the four olive cultivars ($p > 0.05$), indicating that overall macronutrient homeostasis remained largely unaffected during the study period. In contrast, phosphorus (P) concentrations changed significantly in all cultivars. P levels decreased significantly in the susceptible cultivar 'Ogliarola' (estimate = −0.55, $p = 0.032$), whereas they increased significantly in the resistant cultivars 'Leccino' (estimate = 1.22, $p < 0.001$) and FS17 (estimate = 0.64, $p = 0.010$), as well as in the susceptible cultivar 'Arbequina' (estimate = 0.96, $p = 0.004$).

Zinc (Zn) concentrations exhibited a pattern similar to that observed for phosphorus. The susceptible cultivar 'Ogliarola' showed a significant decrease in Zn levels (estimate = −0.006, $p = 0.030$), whereas significant increases were detected in Arbequina, FS17, and 'Leccino' ($p < 0.001$). Likewise, manganese (Mn), iron (Fe), and copper (Cu) accumulated significantly in Arbequina, FS17, and 'Leccino' following inoculation ($p < 0.001$). In contrast, no significant changes in Mn, Fe, or Cu concentrations were observed in the susceptible cultivar 'Ogliarola', which remained statistically similar to the non-inoculated control.

Funded by the European Union

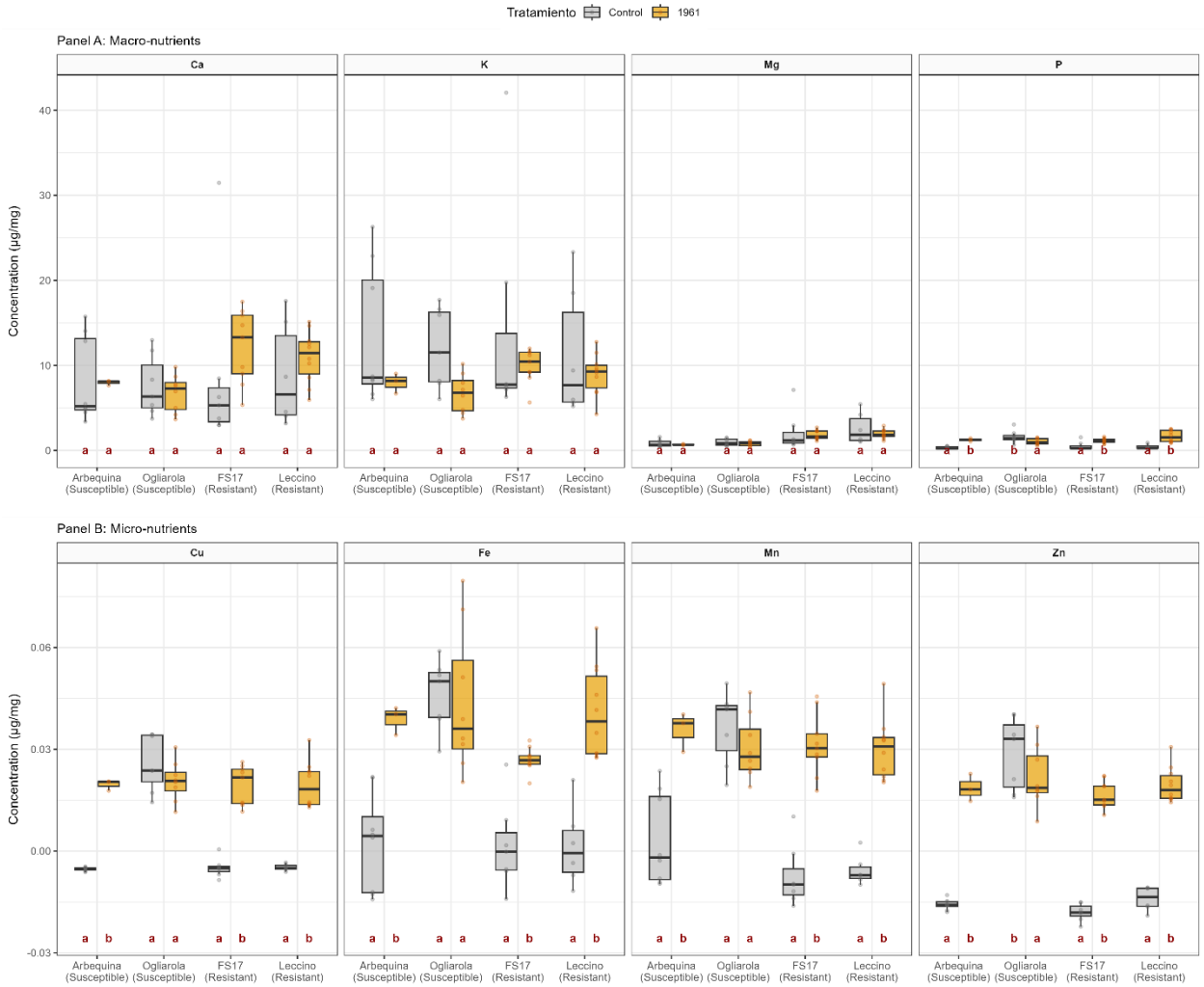


Figure 25. Comparative leaf ionome profile of four olive cultivars with and without *Xylella fastidiosa* subsp. *pauca* (*Xfp*) strain XYL1961/18 inoculation. Panel (**A**) displays the concentration (µg/mg) of macro-elements (K, Ca, Mg, and P), and Panel (**B**) displays micro-element concentrations (Zn, Mn, Fe, and Cu). Data are presented as boxplots showing the median and interquartile range (IQR), with individual sample replicates superimposed as jittered points (n = 10). Different lowercase letters at the base of each facet denote statistically significant differences between uninoculated control (grey) and inoculated (orange, *Xfp* strain XYL 1961/18) treatments within each cultivar at an alpha level of $p < 0.05$.

Funded by the European Union

Table 7. Estimated differences in leaf mineral element concentrations between Control and inoculated (XYL1961/18) olive cultivars

Cultivar	Estimate *	SE**	p value***	Element
Arbequina (Susceptible)	-5.309670029	4.354535	0.228435	K
Ogliarola (Susceptible)	-5.274754974	3.328915	0.119379	
FS17 (Resistant)	-4.109672375	3.241461	0.210725	
'Leccino' (Resistant)	-2.403497115	3.321509	0.472673	
Arbequina (Susceptible)	-0.2409082	3.502315	0.945435	Ca
Ogliarola (Susceptible)	-0.877377913	2.677418	0.74451	
FS17 (Resistant)	3.439152285	2.607079	0.193125	
'Leccino' (Resistant)	2.143204665	2.671461	0.4262	
Arbequina (Susceptible)	-0.142771742	0.722737	0.844204	Mg
Ogliarola (Susceptible)	-0.156814188	0.552512	0.77772	
FS17 (Resistant)	-0.289670574	0.537997	0.592673	
'Leccino' (Resistant)	-0.643528923	0.551282	0.248614	
Arbequina (Susceptible)	0.966828794	0.328289	0.00489	P
Ogliarola (Susceptible)	-0.552982295	0.250968	0.032201	
FS17 (Resistant)	0.649739855	0.244374	0.010506	
'Leccino' (Resistant)	1.226569826	0.250409	1.06E-05	
Arbequina (Susceptible)	0.034305028	0.004062	3.43E-11	Zn
Ogliarola (Susceptible)	-0.006933543	0.003105	0.030067	
FS17 (Resistant)	0.0347096	0.003024	1.27E-15	
'Leccino' (Resistant)	0.033561801	0.003098	1.02E-14	
Arbequina (Susceptible)	0.032434676	0.006562	9.05E-06	Mn
Ogliarola (Susceptible)	-0.00600916	0.005016	0.23659	
FS17 (Resistant)	0.038718131	0.004884	2.16E-10	
'Leccino' (Resistant)	0.035711266	0.005005	3.69E-09	
Arbequina (Susceptible)	0.036448438	0.009006	0.00018	Fe
Ogliarola (Susceptible)	-0.002070131	0.006885	0.764906	
FS17 (Resistant)	0.02542932	0.006704	0.000402	
'Leccino' (Resistant)	0.039517309	0.00687	5.29E-07	
Arbequina (Susceptible)	0.024869729	0.003605	8.63E-09	Cu
Ogliarola (Susceptible)	-0.005360136	0.002756	0.057399	
FS17 (Resistant)	0.024231276	0.002683	4.43E-12	
'Leccino' (Resistant)	0.024299063	0.00275	8.67E-12	

*The regression coefficient representing the predicted change in mineral concentration relative to the non-inoculated Control

**Standard error of the Estimate

***p-value generated from the linear model at alpha level of $p < 0.05$.

Funded by the European Union

4. DISCUSSION

The results presented in this deliverable provide a multifaceted view of the molecular and physiological mechanisms associated with resistance to *Xf* in almond and olive. By integrating transcriptomic analyses, haplotype-resolved genome sequencing, immune receptor profiling, genome-wide association studies and ionomic characterization, the work identifies complementary layers of host defence operating from pathogen perception and transcriptional regulation to structural reinforcement, systemic signalling and mineral homeostasis. Although the mechanisms differed among crops, cultivars and experimental systems, several recurrent themes emerged, including the contribution of constitutive or primed defence responses, diversification of immune receptor repertoires, regulation of salicylic acid-associated pathways, cell wall remodelling and the maintenance of physiological homeostasis during infection. Together, these findings support the view that resistance to *Xf* is a complex quantitative trait resulting from the coordinated action of multiple genetic, molecular and physiological processes rather than from a single resistance mechanism.

4.1 Transcriptomic analysis of resistant and susceptible almond cultivars in response to *Xylella fastidiosa* infection

Overall, the transcriptomic analysis highlights fundamental differences between the susceptible cultivar UEF and the resistant cultivar 'Lauranne' in their responses to *Xff*. UEF responds to infection through extensive transcriptional reprogramming and activation of multiple defense pathways, whereas 'Lauranne' exhibits only a limited transcriptional response following inoculation. However, 'Lauranne' already displays elevated basal expression of numerous defense-related pathways, many of which overlap with those activated in UEF only after infection.

These results support a model in which 'Lauranne' may maintain a primed or pre-activated defensive state that enables a faster and more efficient response to pathogen invasion. Nevertheless, 'Lauranne' does not appear to possess broad-spectrum resistance. Previous studies (Beluzan et al., 2022; Lucchese et al., 2026) have shown that this cultivar remains susceptible to several other almond diseases, suggesting that its resistance is likely specific, or at least particularly effective, against *Xff* rather than representing a general enhancement of disease resistance.

One of the most prominent pathways enriched both in non-inoculated 'Lauranne' and in inoculated UEF was the plant-like HR pathway, a hallmark of plant immune responses against pathogens (Balint-Kurti, 2019). This pathway included genes involved in immune signaling and programmed cell death, such as NB-ARC disease resistance proteins, components of the ubiquitin-mediated protein degradation system (including U-box and F-box proteins), and MYB transcription factors (**Supplementary Table S4**). These genes are known regulators of plant defense signaling (Rodrigues et al., 2013) and have previously been reported in almond responses to *Xf* infection (Moll et al., 2022).

Funded by the European Union

Together, these results suggest that 'Lauranne' resistance is associated with elevated basal expression of defense-related pathways, allowing a more limited transcriptional shift after *Xff* inoculation.

4.2 Haplotype-resolved genomes and immune profiling of the immune receptor landscape of olive

Olea europaea is an economically, ecologically, and culturally important crop species within the Oleaceae, a family composed predominantly of woody trees and shrubs that also includes genera such as *Fraxinus*, *Jasminum*, and *Forsythia (Besnard et al. 2009; Wallander and Albert 2000)*. Olive cultivars harbor substantial genetic diversity that underpins variation in resistance to major diseases, including OQDS, olive knot disease, and Verticillium wilt (Montes-Osuna and Mercado-Blanco 2020; Pavan et al. 2021; Salman et al. 2020; Valverde et al. 2023). In this study, we generated four haplotype-resolved genome assemblies representing the resistant cultivar 'Leccino' and the susceptible cultivar 'Ogliarola salentina'. These genomic resources enabled the construction of a comprehensive olive PRRome and NLRome, providing a framework for investigating the diversity and function of immune receptors in olive.

OQDS, caused by *X. fastidiosa*, remains one of the most serious threats to olive production since its emergence in Europe in 2013 (Saponari et al. 2019; Saponari et al. 2013). To gain insight into PTI in olive, we profiled immune responses to a range of microbial patterns and bacterial elicitors, and investigated the function of selected olive PRR candidates. Our results revealed that chitin perception is present in the two olive cultivars (**Figure 10**), supporting an important role for *OeLYK4/5* and *OeCERK1*-mediated signaling in antifungal immunity (**Figure 11b**). Chitin-induced MAPK activation was stronger in 'Ogliarola salentina' than in 'Leccino', mirroring the enhanced chitin-induced ROS burst mediated by OeCERK1-1 from 'Ogliarola salentina' relative to its 'Leccino' ortholog (**Figure 11b**). These differences may contribute to the relatively lower susceptibility of 'Ogliarola salentina' to Verticillium wilt (Supplementary Table S5). More broadly, these findings align with the widespread conservation of chitin perception across land plants (Miya et al. 2007; Shinya et al. 2015).

By contrast, neither 'Leccino' nor 'Ogliarola salentina' responded to flg22, and a lack of flg22 responsiveness was also observed in *Olea europaea* var. *sylvestris* and other Oleaceae species (**Supplementary Figure S6**). The apparent loss of canonical flg22 perception is particularly striking given the widespread conservation of FLS2-mediated flagellin recognition across land plants (Gómez-Gómez and Boller 2000; Snoeck et al. 2025; Xiao et al. 2026; Li et al. 2025). Moreover, long-lived species like olive trees require effective defence against pathogens over extended periods, and recent studies have highlighted expansions of PRR and NLR gene families that may broaden immune recognition capacities (Ngou et al. 2022). At the same time, immune activation imposes fitness costs, often through growth suppression (Huot et al. 2014). For example, perception of flg22 triggers signalling pathways that negatively impact plant growth (Gómez-Gómez and Boller 2000). One possible explanation for the loss of flg22 responsiveness in olive is that it reduces the costs associated with chronic flagellin perception in environments where flagellated pathogens exert relatively low selective pressure.

Funded by the European Union

However, the olive cultivar 'Leccino' retained responsiveness to bacterial suspensions, including *Xfp* and *A. tumefaciens* (**Figure 10**). This indicates that bacterial perception remains active and may contribute to 'Leccino''s tolerance to bacterial diseases (Supplementary Table S5). Such responses are likely mediated by other PRR complexes that utilize functional OeBAK1 co-receptors (**Supplementary Figure S8**). To this end, we focussed on the BAK1-dependent receptor kinases CORE and MIK2 (Ngou et al. 2025; Rhodes et al. 2021). We identified distinct OeCORE-like and OeMIK2-like clades, each displaying considerable sequence diversification (**Figure 7**), raising the hypothesis that 'Leccino'-specific receptor variants may mediate recognition of csp15/20/22 from *Xfp* De Donno and *A. tumefaciens*. To balance defence and growth, the expression of these *PRRs* might be tightly regulated (**Supplementary Figure S4**).

In summary, our study provides valuable genomic and functional resources for investigating immune receptor diversity and function in olive and will accelerate efforts to understand resistance and susceptibility to OQDS and other major olive diseases.

4.3 Genome Wide Association Study (GWAS) of olive cultivars and progeny

The current genomic evaluation provides compelling evidence that olive host resistance to *Xf*p, the causal agent of the devastating Olive Quick Decline Syndrome (OQDS) (Saponari et al., 2019), is governed by oligogenic architecture rather than a diffuse polygenic background. The foundational layer of this resistance paradigm relies on the loss-of-function in primary susceptibility (S) factors. Specifically, HIGH-impact knockout mutations in EVM0013689 and EVM0017391 are prerequisites to deny the bacterium the biological pathways necessary for rapid multiplication and systemic structural deterioration. The observation that fully modified secondary defense sensors cannot independently save susceptible cultivars perfectly aligns with modern crop immunity paradigms, establishing S-gene knockouts as the primary determinant of broad-spectrum resistance (La Notte et al., 2024; Balan et al., 2025).

Beyond these primary knockouts, successful disease mitigation requires a highly coordinated secondary defense network, orchestrated by the pleiotropic locus on Chromosome 22. The identification of *Receptor-like protein kinase 2* at this cluster confirms that pathogen perception at the cell surface directly bridges the restriction of bacterial load and the mitigation of physical symptom severity. This corroborates cross-species transcriptomic profiling demonstrating that the upregulation of Leucine-Rich Repeat Receptor-Like Kinases (LRR-RLKs) acts as a universal topological hub for initiating pathogen-triggered immunity against xylem-invading bacteria (Giampetruzzi et al., 2016; Balan et al., 2025). Once perceived, the immune response is dynamically regulated by E3 ubiquitin ligases and major transcription factors (e.g., NAC and ERF families), which manage hormonal crosstalk and clear stress-damaged proteins (Balan et al., 2025).

Finally, surviving chronic *X. fastidiosa* infection mandates, structural fortification and the management of severe physiological drought caused by bacterial vascular blockages (Saponari et al., 2019; Pierry et al., 2025). The mapping of *Long-chain acyl-CoA synthetase 9* underscores the evolutionary-conserved strategy of utilizing lipid metabolism and cuticular waxes to reinforce pit membranes against the pathogen's cell-wall-degrading enzymes (Balan et al., 2025). Concurrently, the tight linkage of the *Sodium/hydrogen exchanger 1-like* gene

Funded by the European Union

within the Chromosome 22 pleiotropic cluster highlights the plant's absolute requirement to actively maintain osmotic homeostasis and cellular pH to tolerate the physiological drought imposed by the pathogen's systemic colonization (Giampetruzzi et al., 2016; La Notte et al., 2024).

4.4 Characterization of the molecular response of resistant and susceptible olive cultivars to *Xylella fastidiosa* infection.

The integrated analysis of the olive transcriptomic datasets revealed a recurrent set of defence-related responses that provide insight into both the general molecular response to *X. fastidiosa* infection and the mechanisms potentially contributing to the enhanced resistance of 'Leccino'.

DMR6 encodes a salicylic acid (SA) 5-hydroxylase that converts SA into 2,5-dihydroxybenzoic acid (2,5-DHBA), thereby contributing to SA homeostasis. Although SA is a central regulator of plant immunity, promoting the production of antimicrobial secondary metabolites, lignin deposition, and other defense responses, excessive SA accumulation can be detrimental, leading to overproduction of reactive oxygen species (ROS), leaf chlorosis, growth inhibition, and a shift in resource allocation from growth to defense (the growth–defense trade-off). Consequently, SA levels are tightly regulated by catabolic enzymes such as DMR6.

A potentially related role may also be played by the EG45-like domain-containing proteins, which share similarity with Plant Natriuretic Peptide A (PNP-A). In *A. thaliana*, PNP-A has been shown to antagonize SA-mediated responses (Lee et al., 2020). PNP-A interacts with the cell surface receptor PNP-R2, which is distantly related to several leucine-rich repeat receptor-like serine/threonine kinases (LRR-RLKs), including GS01, the probable LRR receptor kinase At3g35710, and the probable LRR receptor-like serine/threonine kinase At3g47570, all of which were consistently upregulated in our RNA-seq analyses. Together, these findings suggest that modulation of SA signaling may represent a conserved component of the olive response to *Xylella fastidiosa* subsp. *pauca* (*Xfp*).

Additional support for this hypothesis comes from our proteomic analysis of *Xfp*-infected 'Arbequina' olive plants (unpublished data), in which we also detected increased accumulation of pathogenesis-related proteins and EG45-like domain-containing proteins.
We also sought to identify the molecular mechanisms that may underlie the resistance of 'Leccino' to *Xfp*. Among the genes exclusively differentially expressed in 'Leccino', we consistently observed differential regulation of genes associated with cell wall metabolism. Together with the SA-induced lignin deposition described above, these transcriptional changes suggest extensive cell wall remodeling and reinforcement, a well-established defense mechanism against vascular pathogens. This hypothesis is further supported by the upregulation of several multicopper oxidases (laccases), which are involved in lignin polymerization, in 'Leccino'. Similar cell wall modifications have previously been reported in 'Leccino' by Sabella et al. (2018).

In addition, our results suggest that 'Leccino' may exhibit tighter regulation of systemic acquired resistance (SAR). In the study by La Notte et al. (2024), two key regulators of the SAR pathway, salicylate carboxymethyltransferase-like (SAMT) and salicylic acid-binding protein 2 (SABP2), showed distinct expression patterns in 'Leccino' compared with the susceptible

Funded by the European Union

cultivar 'Cellina di Nardò' (**Figure 26**), indicating that fine-tuning of SA-mediated systemic signaling may contribute to the resistant phenotype.

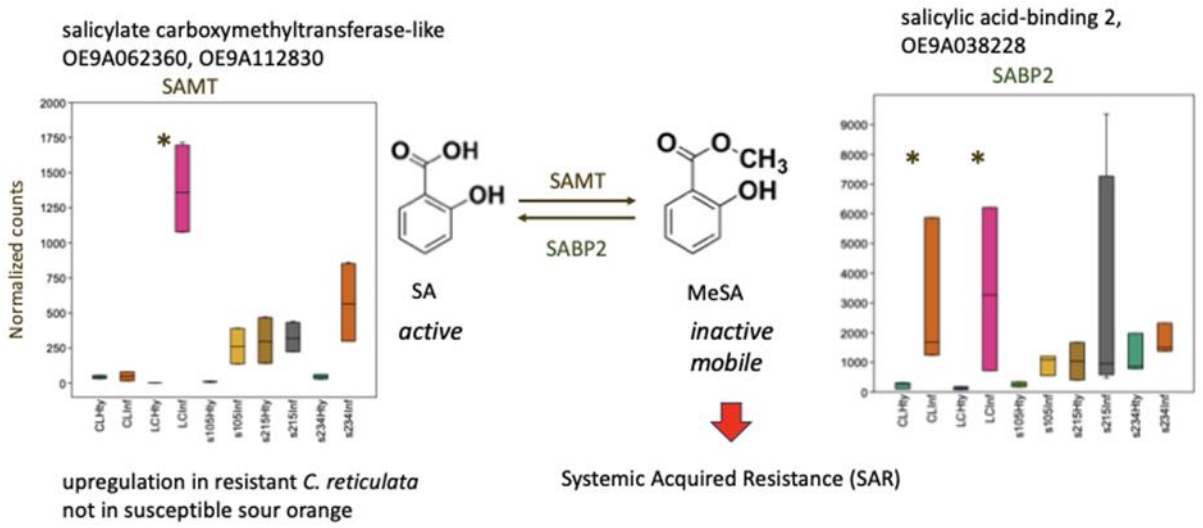


Figure 26. Graphs showing the differential expression of SAMT and SABP2 in 'Cellina di Nardò' (CL), 'Leccino' (LC) and three resistant spontaneous seedlings described in La Notte et al. (2024). Hty (Healthy plants); Inf (Infected plants). Asterisks indicate significant differences evaluated by T-test (Inf vs hty) at p=0.05.

SAMT and SABP2 catalyze two opposing reactions in the systemic acquired resistance (SAR) pathway. SAMT methylates salicylic acid (SA) to produce methyl salicylate (MeSA), thereby temporarily inactivating SA. Although MeSA is metabolically inactive, it is volatile and serves as a mobile SAR signal that is transported to distal tissues, where it is converted back to biologically active SA by SABP2, thereby activating systemic defense responses.

Based on these observations, we propose a working model for the resistance of 'Leccino' to *Xf*p infection. Following pathogen recognition, 'Leccino' may more efficiently convert SA into MeSA, limiting excessive local SA accumulation while simultaneously increasing the production of the mobile SAR signal. The resulting increase in MeSA availability would facilitate its transport to distal tissues, where it could be converted back to active SA by SABP2. Since both resistant and susceptible cultivars appear capable of expressing SABP2, the distinguishing feature of 'Leccino' may be its greater capacity to generate and mobilize MeSA, ultimately resulting in a stronger and more effective systemic acquired resistance response.

At present, this model should be regarded as a working hypothesis supported by the transcriptomic and proteomic datasets presented here. Preliminary quantitative gene expression analyses further support the involvement of several key components of this pathway, including DMR6, PNP-A-like proteins, and LRR receptor-like kinases. However, additional validation, particularly through detailed time-course expression analyses and functional characterization of these candidate genes, is currently underway and will be required to confirm this proposed mechanism.

Funded by the European Union

4.5 Characterization of the mineral element concentrations (ionome) in susceptible and resistant plants

The change in ionome levels in response to inoculation with *Xfp* strain XYL1961/18 highlights a clear physiological divergence between susceptible and resistant olive cultivars. The most striking differences were observed for phosphorus (P) and Zinc (Zn), which were significantly different in both resistant and susceptible cultivars.

The susceptible cultivar 'Ogliarola' showed decreases in P and Zn after inoculation with XYL1961/18, indicating nutrient depletion due to clogging of xylem vessels following infection. Although 'Arbequina' is classified as susceptible, its ionomic profile in this study more closely resembled that of resistant cultivars than that of 'Ogliarola', especially in terms of increased P and micronutrient concentrations. This suggests that 'Arbequina' possesses a degree of physiological resilience that 'Ogliarola' lacks, but this needs to be further studied.

In contrast, the resistant cultivars ('FS17' and 'Leccino') showed a significant accumulation of P and several micro-elements (Mn, Fe, Cu, and Zn). This enrichment profile may indicate an active physiological defense mechanism.

Potassium (K), Calcium (Ca), and Magnesium (Mg) remained relatively stable across all cultivars, but significant accumulation of trace metals like Copper (Cu), Iron (Fe), Manganese (Mn), and Zinc (Zn) expect the susceptible cultivar 'Ogliarola'.

The analysis revealed that 'Ogliarola' is uniquely characterized by a significant depletion of P and Zn, suggesting advanced xylem blockage and nutrient starvation. In contrast, the resistant cultivars 'FS17' and 'Leccino' showed an enrichment profile, significantly accumulating phosphorus and antimicrobial trace metals (Cu, Zn, Mn). These findings suggest that resistant cultivars maintain or even improve nutrient transport as part of a defensive strategy, while highly susceptible cultivars undergo a systemic collapse in mineral supply.

Considering all three types of samples analyzed, there was a consistent tendency of increased concentrations of P and Mn in resistant cultivars as compared to susceptible ones. This needs to be further studied to determine if there is any relationship with the plant mechanisms of defense.

Funded by the European Union

5. CONCLUSIONS

- The transcriptomic analysis revealed that the resistant almond cultivar ‘Lauranne’ exhibits a limited transcriptional response to *Xff* infection because it constitutively maintains elevated basal expression of multiple defense-related pathways, whereas the susceptible cultivar, 'UEF,' activates similar pathways only after infection. These findings suggest that ‘Lauranne’ resistance is associated with a primed immune state, enabling a faster and more effective defense against *Xff*.
- Taken together, results from the haplotype-resolved genomes and immune profiling of the immune receptor landscape of olive provided a first functional framework for understanding PTI in olive. The data highlight a conserved role for chitin perception while revealing substantial diversification of OeCORE- and OeMIK2-like candidate receptor families, particularly within the expanded Chromosome 16 immune receptor locus associated with the resistant cultivar ‘Leccino’."
- GWAS identified candidate loci associated with bacterial load and disease severity, including a pleiotropic region on chromosome 22 and putative high-impact variants in EVM0013689 **and** EVM0017391, implicating pathogen perception, defence signalling, structural reinforcement, and osmotic homeostasis in the olive response to *Xfp*; these associations require validation in larger, independent populations.
- Olive plants perceive *Xfp* rapidly after artificial inoculation, triggering a conserved immune response in both ‘Leccino’ and ‘Cellina di Nardò’ that includes induction of LRR-RLKs, pathogenesis-related proteins, and genes involved in salicylic acid regulation.
- The greater resistance of ‘Leccino’ appears to be associated with stronger systemic acquired resistance and extensive cell-wall reinforcement, including cell-wall remodelling and lignin deposition.
- Resistance to *Xf* in olive was associated with maintenance or accumulation of P and several micronutrients, particularly Mn, whereas the highly susceptible cultivar ‘Ogliarola salentina’ showed marked P and Zn depletion. These contrasting ionomic responses suggest that mineral homeostasis may contribute to cultivar-dependent physiological resilience, although its mechanistic relationship with disease resistance requires further investigation.

Funded by the European Union

6. REFERENCES

Abou Kubaa R, Giampetruzzi A, Del Grosso C, Amoia SS, Caruso G, Bartolini S, Altamura G, Surano A, Saldarelli P. Phenotyping and expression profile of clones of the olive cultivar 'Leccino' for the resistance to *Xylella fastidiosa*. Physiological and Molecular Plant Pathology 141, 103018 (2026).

Andolfo, G., Dohm, J. C. & Himmelbauer, H. Prediction of NB-LRR resistance genes based on full-length sequence homology. Plant J. 110, 1592–1602 (2022).

Balan, A.S., Tranchina, G., Bonanno, F., Caruso, T., Marra, F.P., Di Vaio, C. and Marchese, A. A systems biology framework integrating cross-species transcriptomics and PPI networks for *Xylella fastidiosa* resistance gene identification. BMC Plant Biology 25(1), p.1062. (2025).

Balint-Kurti, P. The plant hypersensitive response: concepts, control and consequences. Molecular Plant Pathology 20(8), 1163 (2019).

Beluzan, F., Miarnau, X., Torguet, L., Zazurca, L., Abad-Campo, P., Luque, J., & Armengol, J. Susceptibility of Almond (*Prunus dulcis*) Cultivars to Twig Canker and Shoot Blight Caused by *Diaporthe amygdali*. Plant Disease 106, 1890–1897 (2022).

Benedetti, M. et al. Plant immunity triggered by engineered in vivo release of oligogalacturonides, damage-associated molecular patterns. Proc. Natl. Acad. Sci. 112, 5533–5538 (2015).

Besnard, G., Khadari, B., Baradat, P. & Bervillé, A. *Olea europaea* (Oleaceae) phylogeography based on chloroplast DNA polymorphism. Theor. Appl. Genet. 104, 1353–1361 (2002).

Besnard, G., Rubio De Casas, R., Christin, P.-A. & Vargas, P. Phylogenetics of *Olea* (Oleaceae) based on plastid and nuclear ribosomal DNA sequences: Tertiary climatic shifts and lineage differentiation times. Ann. Bot. 104, 143–160 (2009).

Burbank, L. P. Threat of *Xylella fastidiosa* and options for mitigation in infected plants. CABI Rev. cabireviews 202217021 (2022).

Caballero, M. & Wegrzyn, J. gFACs: Gene Filtering, Analysis, and Conversion to Unify Genome Annotations Across Alignment and Gene Prediction Frameworks. Genomics Proteomics Bioinformatics 17, 305–310 (2019).

Cao, Y. et al. The kinase LYK5 is a major chitin receptor in *Arabidopsis* and forms a chitin-induced complex with related kinase CERK1. eLife 3, e03766 (2014).

Capella-Gutiérrez, S., Silla-Martínez, J. M. & Gabaldón, T. trimAl: a tool for automated alignment trimming in large-scale phylogenetic analyses. Bioinformatics 25, 1972–1973 (2009).

Castro, C. et al. *Xylella fastidiosa* modulates exopolysaccharide polymer length and the dynamics of biofilm development with a β-1,4-endoglucanase. mBio 14, e01395-23 (2023).

Chen, S., Zhou, Y., Chen, Y. and Gu, J. fastp: an ultra-fast all-in-one FASTQ preprocessor. Bioinformatics, 34(17), pp.i884-i890 (2018).

Cheng, H., Concepcion, G. T., Feng, X., Zhang, H. & Li, H. Haplotype-resolved de novo assembly using phased assembly graphs with hifiasm. Nat. Methods 18, 170–175 (2021).

Funded by the European Union

Chinchilla, D., Bauer, Z., Regenass, M., Boller, T. & Felix, G. The Arabidopsis Receptor Kinase FLS2 Binds flg22 and Determines the Specificity of Flagellin Perception. Plant Cell 18, 465–476 (2006).

Clarke, C. R. et al. Allelic variation in two distinct *Pseudomonas syringae* flagellin epitopes modulates the strength of plant immune responses but not bacterial motility. New Phytol. 200, 847–860 (2013).

Cruz, F. et al. Genome sequence of the olive tree, *Olea europaea*. Gigascience 5, s13742-016-0134–5 (2016).

Danecek, P., Bonfield, J.K., Liddle, J., Marshall, J., Ohan, V., Pollard, M.O., Whitwham, A., Keane, T., McCarthy, S.A., Davies, R.M. and Li, H. Twelve years of SAMtools and BCFtools. Gigascience 10(2), p.giab008 (2021).

De la Fuente, L., Parker, J.K., Oliver, J.E., Granger, S., Brannen, P.M., Santen, E. van, et al. The Bacterial Pathogen *Xylella fastidiosa* Affects the Leaf Ionome of Plant Hosts during Infection. *PLoS ONE* 8, 1–9 (2013).

Danecek, P. et al. Twelve years of SAMtools and BCFtools. GigaScience 10, giab008 (2021).

Dudchenko, O. et al. The Juicebox Assembly Tools module facilitates de novo assembly of mammalian genomes with chromosome-length scaffolds for under $1000. Preprint at bioRxiv 254797; doi: https://doi.org/10.1101/254797 (2018).

Emms, D. M. & Kelly, S. OrthoFinder: phylogenetic orthology inference for comparative genomics. Genome Biol. 20, 238 (2019).

Emms, D. M. & Kelly, S. OrthoFinder: solving fundamental biases in whole genome comparisons dramatically improves orthogroup inference accuracy. Genome Biol. 16, 157 (2015).

Felix, G., Duran, J. D., Volko, S. & Boller, T. Plants have a sensitive perception system for the most conserved domain of bacterial flagellin. Plant J. 18, 265–276 (1999).

Fernández-Escobar R., M., M. Evolution and sustainability of the olive production systems. in Present and future of the Mediterranean olive sector 11–42 (CIHEAM/IOC, Zaragoza) (2013).

Fritz-Laylin, L. K., Krishnamurthy, N., Tör, M., Sjölander, K. V. & Jones, J. D. G. Phylogenomic Analysis of the Receptor-Like Proteins of Rice and Arabidopsis. Plant Physiol. 138, 611–623 (2005).

Förderer, A. & Kourelis, J. NLR immune receptors: structure and function in plant disease resistance. Biochem. Soc. Trans. 51, 1473–1483 (2023).

Ghurye, J. et al. Integrating Hi-C links with assembly graphs for chromosome-scale assembly. PLOS Comput. Biol. 15, e1007273 (2019).

Giampetruzzi, A. et al. Complete Genome Sequence of the Olive-Infecting Strain *Xylella fastidiosa* subsp. *pauca* De Donno. Genome Announc. 5, e00569-17 (2017).

Giampetruzzi, A. et al. Transcriptome profiling of two olive cultivars in response to infection by the CoDiRO strain of *Xylella fastidiosa* subsp. *pauca*. BMC Genomics 17, 475 (2016).

Giampetruzzi A, Molin EM, Falcón-Piñeiro A, García-Madero JM, Abou Kubaa R, Kogej T, Zwarts L, Del Grosso C, Contaldo N, Dongiovanni C, Compant S, Saldarelli P. 2026.

Funded by the European Union

Comparative transcriptomics of biopesticide-treated olives subjected to *Xylella* infection. Preprint https://doi.org/10.21203/rs.3.rs-8603179/v1. Accepted for publication on BMC Plant Biology (2026).

Godena, S., Ivić, D., Ban, D. & Goreta Ban, S. Characterization of *Verticillium dahliae* isolates from olive and susceptibility of local olive cultivars to Verticillium wilt in Istria, Croatia. Sci. Hortic. 292, 110630 (2022).

Goel, M. & Schneeberger, K. plotsr: visualizing structural similarities and rearrangements between multiple genomes. Bioinformatics 38, 2922–2926 (2022).

Goel, M., Sun, H., Jiao, W.-B. & Schneeberger, K. SyRI: finding genomic rearrangements and local sequence differences from whole-genome assemblies. Genome Biol. 20, 277 (2019).

Grasso, F. et al. The transcriptional response to the olive fruit fly (*Bactrocera oleae*) reveals extended differences between tolerant and susceptible olive (*Olea europaea* L.) varieties. PLOS ONE 12, e0183050 (2017).

Graça, J. Suberin: The biopolyester at the frontier of plants. Frontiers in Chemistry, 3(OCT), 163798 (2015).

Gómez-Gómez, L. & Boller, T. FLS2: an LRR receptor-like kinase involved in the perception of the bacterial elicitor flagellin in Arabidopsis. Mol Cell. 5, 1003-1011 (2000).

Hallgren, J. et al. DeepTMHMM predicts alpha and beta transmembrane proteins using deep neural networks. Preprint at bioRxiv https://doi.org/10.1101/2022.04.08.487609v1 (2022).

Hawkins, T. J. et al. NET4 and RabG3 link actin to the tonoplast and facilitate cytoskeletal remodelling during stomatal immunity. Nat. Commun. 14, 5848 (2023).

Heese, A. et al. The receptor-like kinase SERK3/BAK1 is a central regulator of innate immunity in plants. Proc. Natl. Acad. Sci. 104, 12217–12222 (2007).

Hind, S. R. et al. Tomato receptor FLAGELLIN-SENSING 3 binds flgII-28 and activates the plant immune system. Nat. Plants 2, 16128 (2016).

Holst, F. et al. Helixer: ab initio prediction of primary eukaryotic gene models combining deep learning and a hidden Markov model. Nat. Methods 23, 732–739 (2026).

Hou, S. et al. The Arabidopsis MIK2 receptor elicits immunity by sensing a conserved signature from phytocytokines and microbes. Nat. Commun. 12, 5494 (2021).

Huot, B., Yao, J., Montgomery, B. L. & He, S. Y. Growth–Defense Tradeoffs in Plants: A Balancing Act to Optimize Fitness. Mol. Plant 7, 1267–1287 (2014).

Jacques Dainat et al. NBISweden/AGAT: AGAT v1.6.1. Zenodo (2026).

Jiménez-Ruiz, J. et al. Transposon activation is a major driver in the genome evolution of cultivated olive trees (*Olea europaea* L.). Plant Genome 13, e20010 (2020).

Jones, J. D. G. & Dangl, J. L. The plant immune system. Nature 444, 323–329 (2006).

Jones, P. et al. InterProScan 5: genome-scale protein function classification. Bioinformatics 30, 1236–1240 (2014).

Julca, I. et al. Genomic evidence for recurrent genetic admixture during the domestication of Mediterranean olive trees (*Olea europaea* L.). BMC Biol. 18, 148 (2020).

Funded by the European Union

Katoh, K. & Standley, D. M. MAFFT Multiple Sequence Alignment Software Version 7: Improvements in Performance and Usability. Mol. Biol. Evol. 30, 772–780 (2013).

Kemmerling, B. et al. The BRI1-Associated Kinase 1, BAK1, Has a Brassinolide-Independent Role in Plant Cell-Death Control. Curr. Biol. 17, 1116–1122 (2007).

Kileeg, Z., Haldar, A., Khan, H., Qamar, A. & Mott, G. A. Differential expansion and retention patterns of LRR-RLK genes across plant evolution. Plant Direct 7, e556 (2023).

Košćak, L. et al. Varietal Susceptibility of Olive to *Pseudomonas savastanoi* pv. *savastanoi* and the Antibacterial Potential of Plant-Based Agents. Microorganisms 12, 1301 (2024).

Kroj, T., Chanclud, E., Michel-Romiti, C., Grand, X. & Morel, J. Integration of decoy domains derived from protein targets of pathogen effectors into plant immune receptors is widespread. New Phytol. 210, 618–626 (2016).

Kunze, G. et al. The N Terminus of Bacterial Elongation Factor Tu Elicits Innate Immunity in Arabidopsis Plants. Plant Cell 16, 3496–3507 (2004).

Labroussaa, F., Ionescu, M., Zeilinger, A. R., Lindow, S. E. & Almeida, R. P. P. A chitinase is required for *Xylella fastidiosa* colonization of its insect and plant hosts. Microbiology 163, 502–509 (2017).

Landa, B.B., Saponari, M., Feitosa-Junior, O.R., Giampetruzzi, A., Vieira, F.J.D., Mor, E., Robatzek, S. *Xylella fastidiosa* 's relationships: the bacterium, the host plants, and the plant microbiome. New Phytol. 234, 1598–1605 (2022).

La Notte, P., Saponari, M., Mousavi, S., Mariotti, R., Abou Kubaa, R., Nikbakht, R., Melcarne, G., Specchia, F., Altamura, G., Ligorio, A. and Boscia, D. A survey in natural olive resources exposed to high inoculum pressure indicates the presence of traits of resistance to *Xylella fastidiosa* in 'Leccino' offspring. Frontiers in Plant Science 15, p.1457831 (2024).

Lee KP, Liu K, Kim EY, Medina-Puche L, Dong H, Duan J, Li M, Dogra V, Li Y, Lv R, Li Z, Lozano-Duran R, Kim C. PLANT NATRIURETIC PEPTIDE A and Its Putative Receptor PNP-R2 Antagonize Salicylic Acid-Mediated Signaling and Cell Death. Plant Cell. 32, 2237-2250 (2020).

Lee, S. A., Wallis, C. M., Rogers, E. E., & Burbank, L. P. Grapevine phenolic compounds influence cell surface adhesion of *Xylella fastidiosa* and bind to lipopolysaccharide. PLOS ONE, 15(10), e0240101 (2020).

Li, H. Aligning sequence reads, clone sequences and assembly contigs with BWA-MEM. Preprint available at arXiv 1303.3997 (2013).

Li, H. Minimap2: pairwise alignment for nucleotide sequences. Bioinformatics 34, 3094–3100 (2018).

Li, T. et al. Unlocking expanded flagellin perception through rational receptor engineering. Nat. Plants 11, 1628–1641 (2025).

Licciardello, G. et al. Cultivar Susceptibility to Olive Knot Disease and Association with Endophytic Microbiota Community. Agronomy 13, 468 (2023).

Love, M. I., Huber, W., & Anders, S. (2014). Moderated estimation of fold change and dispersion for RNA-seq data with DESeq2. Genome Biology 15, 550 (2014).

Funded by the European Union

Lucchese, P. G., Chiaromonte, E., Gerin, D., Agnusdei, A., Dalena, F., Cornacchia, D., Digiaro, D., Incampo, G., Salamone, D., Venerito, P., Faretra, F., Nigro, F., & Pollastro, S. (2026). Field Susceptibility of Almond (*Prunus dulcis*) Cultivars to Red Leaf Blotch Caused by *Polystigma amygdalinum* in Apulia (Italy) and Influence of Environmental Conditions. Plants 15(2), 188.

Lv, J., Jiang, C., Wu, W., Mao, K., Wei, Q., Zheng, Y., Gao, C., Niu, Z., Jin, G., Zhang, R., Mao, J., Chen, B., Ren, G., Yang, Y., Wan, D. The gapless genome assembly and multi-omics analyses unveil a pivotal regulatory mechanism of oil biosynthesis in the olive tree. Hortic Res. 21, 11(8):uhae168. (2024).

Macho, A. P. & Zipfel, C. Plant PRRs and the Activation of Innate Immune Signaling. Mol. Cell 54, 263–272 (2014).

Maddox, C. E., Laur, L. M., & Tian, L. Antibacterial Activity of Phenolic Compounds Against the Phytopathogen *Xylella fastidiosa*. Current Microbiology 60, 53 (2009).

Madsen, E. B. et al. A receptor kinase gene of the LysM type is involved in legume perception of rhizobial signals. Nature 425, 637–640 (2003).

Malinovsky, F. G., Fangel, J. U. & Willats, W. G. T. The role of the cell wall in plant immunity. Front. Plant Sci. 5, 178 (2014).

Manni, M., Berkeley, M. R., Seppey, M., Simão, F. A. & Zdobnov, E. M. BUSCO Update: Novel and Streamlined Workflows along with Broader and Deeper Phylogenetic Coverage for Scoring of Eukaryotic, Prokaryotic, and Viral Genomes. Mol. Biol. Evol. 38, 4647–4654 (2021).

Marçais, G. et al. MUMmer4: A fast and versatile genome alignment system. PLOS Comput. Biol. 14, e1005944 (2018).

Mariotti, R. et al. Genealogical tracing of *Olea europaea* species and pedigree relationships of var. *europaea* using chloroplast and nuclear markers. BMC Plant Biol. 23, 452 (2023).

Maroschek, J., Rösgen, Y., Rössner, C., Snoeck, S., Schwechheimer, C., Zipfel, C., Hückelhoven, R.. MIK2-clade receptor function in perception of a *Fusarium*-derived elicitor is conserved among different plant families. Preprint at bioRxiv.org doi: https://doi.org/10.1101/2025.05.22.655486 (2025).

Martin, M. Cutadapt removes adapter sequences from high-throughput sequencing reads. EMBnet. journal, 17, 10-12 (2011).

McKenna, A., Hanna, M., Banks, E., Sivachenko, A., Cibulskis, K., Kernytsky, A., Garimella, K., Altshuler, D., Gabriel, S., Daly, M. and DePristo, M.A. The Genome Analysis Toolkit: a MapReduce framework for analyzing next-generation DNA sequencing data. Genome research 20, 1297-1303 (2010).

McKinney, G.J., Waples, R.K., Seeb, L.W. and Seeb, J.E. Paralogs are revealed by proportion of heterozygotes and deviations in read ratios in genotyping-by-sequencing data from natural populations. Molecular Ecology Resources 17, 656-669 (2017).

McLaren, W., Gil, L., Hunt, S.E., Riat, H.S., Ritchie, G.R., Thormann, A., Flicek, P. and Cunningham, F. The ensembl variant effect predictor. Genome biology 17, 122 (2016).

Funded by the European Union

Mendes, F. K., Vanderpool, D., Fulton, B. & Hahn, M. W. CAFE 5 models variation in evolutionary rates among gene families. Bioinformatics 36, 5516–5518 (2021).

Mikheenko, A., Prjibelski, A., Saveliev, V., Antipov, D. & Gurevich, A. Versatile genome assembly evaluation with QUAST-LG. Bioinformatics 34, i142–i150 (2018).

Mitre, L. K. et al. The Arabidopsis immune receptor EFR increases resistance to the bacterial pathogens Xanthomonas and Xylella in transgenic sweet orange. Plant Biotechnol. J. 19, 1294–1296 (2021).

Miya, A. et al. CERK1, a LysM receptor kinase, is essential for chitin elicitor signaling in Arabidopsis. Proc. Natl. Acad. Sci. 104, 19613–19618 (2007).

Moll, L., Baró, A., Montesinos, L., Badosa, E., Bonaterra, A., & Montesinos, E. Induction of Defense Responses and Protection of Almond Plants Against Xylella fastidiosa by Endotherapy with a Bifunctional Peptide. Phytopathology 112, 1907–1916 (2022).

Montes-Osuna, N. & Mercado-Blanco, J. Verticillium Wilt of Olive and Its Control: What Did We Learn during the Last Decade? Plants 9, 735 (2020).

Ngou, B. P. M. et al. Systematic discovery and engineering of synthetic immune receptors in plants. Science 389, eadx2508 (2025).

Ngou, B. P. M., Ahn, H.-K., Ding, P. & Jones, J. D. G. Mutual potentiation of plant immunity by cell-surface and intracellular receptors. Nature 592, 110–115 (2021).

Ngou, B. P. M., Ding, P. & Jones, J. D. G. Thirty years of resistance: Zig-zag through the plant immune system. Plant Cell 34, 1447–1478 (2022).

Ngou, B. P. M., Heal, R., Wyler, M., Schmid, M. W. & Jones, J. D. G. Concerted expansion and contraction of immune receptor gene repertoires in plant genomes. Nat. Plants 8, 1146–1152 (2022).

Open2C et al. Pairtools: From sequencing data to chromosome contacts. PLOS Comput. Biol. 20, e1012164 (2024).

Pavan, S. et al. Screening of Olive Biodiversity Defines Genotypes Potentially Resistant to *Xylella fastidiosa*. Front. Plant Sci. 12, 723879 (2021).

Pedersen, B. S. & Quinlan, A. R. Mosdepth: quick coverage calculation for genomes and exomes. Bioinformatics 34, 867–868 (2018).

Pertea, G. & Pertea, M. GFF Utilities: GffRead and GffCompare. F1000 Research 9, 304 (2020).

Petutschnig, E. K., Jones, A. M. E., Serazetdinova, L., Lipka, U. & Lipka, V. The Lysin Motif Receptor-like Kinase (LysM-RLK) CERK1 Is a Major Chitin-binding Protein in Arabidopsis thaliana and Subject to Chitin-induced Phosphorylation. J. Biol. Chem. 285, 28902–28911 (2010).

Pierry, P.M., Feitosa-Junior, O.R., Martins-Junior, J., Barbosa, D., da Silva, A.M. and Zaini, P.A., Transcriptome profiling reveals differential expression of virulence genes in *Xylella fastidiosa* under nutrient-rich and xylem-like conditions. bioRxiv 2025.08.15.669762. https://doi.org/10.1101/2025.08.15.669762 (2025).

Purcell, S., Neale, B., Todd-Brown, K., Thomas, L., Ferreira, M.A., Bender, D., Maller, J., Sklar, P., De Bakker, P.I., Daly, M.J. and Sham, P.C., 2007. PLINK: a tool set for whole-genome

Funded by the European Union

association and population-based linkage analyses. The American journal of human genetics 81, 559-575.

Quesada, J. M. et al. Dissemination of *Pseudomonas savastanoi* pv. *savastanoi* populations and subsequent appearance of olive knot disease. Plant Pathol. 59, 262–269 (2010).

Quinlan, A. R. & Hall, I. M. BEDTools: a flexible suite of utilities for comparing genomic features. Bioinformatics 26, 841–842 (2010).

Raffaele, S., Vailleau, F., Léger, A., Joubès, J., Miersch, O., Huard, C., Blée, E., Mongrand, S., Domergue, F., & Roby, D. (2008). A MYB Transcription Factor Regulates Very-Long-Chain Fatty Acid Biosynthesis for Activation of the Hypersensitive Cell Death Response in Arabidopsis. The Plant Cell 20, 752–767.

Ramesh, K., Ruf, A. & Robatzek, S. Catch Me If You Can: How *Xylella fastidiosa* Thrives in the Xylem. Annu. Rev. Phytopathol. Epub ahead of print available at doi:10.1146/annurev-phyto-011325-110907 (2026).

Ramírez-Tejero, J.A., Jiménez-Ruiz, J., Serrano, A. et al. Verticillium wilt resistant and susceptible olive cultivars express a very different basal set of genes in roots. BMC Genomics 22, 229 (2021).

Rao, G., Zhang, J., Liu, X. et al. De novo assembly of a new *Olea europaea* genome accession using nanopore sequencing. Hortic Res 8, 64 (2021).

Rapicavoli, J. N., Blanco-Ulate, B., Muszyński, A., Figueroa-Balderas, R., Morales-Cruz, A., Azadi, P., Dobruchowska, J. M., Castro, C., Cantu, D., & Roper, & M. C. (n.d.). Lipopolysaccharide O-antigen delays plant innate immune recognition of *Xylella fastidiosa*. Nat. Commun. 9, 390 (2018).

Rhie, A. et al. Towards complete and error-free genome assemblies of all vertebrate species. Nature 592, 737–746 (2021).

Rhie, A., Walenz, B. P., Koren, S. & Phillippy, A. M. Merqury: reference-free quality, completeness, and phasing assessment for genome assemblies. Genome Biol. 21, 245 (2020).

Rhodes, J. et al. Perception of a divergent family of phytocytokines by the Arabidopsis receptor kinase MIK2. Nat. Commun. 12, 705 (2021).

Robatzek, S. et al. Molecular identification and characterization of the tomato flagellin receptor LeFLS2, an orthologue of Arabidopsis FLS2 exhibiting characteristically different perception specificities. Plant Mol. Biol. 64, 539–547 (2007).

Rodrigues, C. M., de Souza, A. A., Takita, M. A., Kishi, L. T., & Machado, M. A. (2013). RNA-Seq analysis of *Citrus reticulata* in the early stages of *Xylella fastidiosa* infection reveals auxin-related genes as a defense response. BMC Genomics, 14(1).

Roper, M. C., Greve, L. C., Warren, J. G., Labavitch, J. M. & Kirkpatrick, B. C. *Xylella fastidiosa* Requires Polygalacturonase for Colonization and Pathogenicity in *Vitis vinifera* Grapevines. Mol. Plant-Microbe Interactions® 20, 411–419 (2007).

Sabella, E., Luvisi, A., Aprile, A., Negro, C., Vergine, M., Nicolì, F., Miceli, A., De Bellis, L. *Xylella fastidiosa* induces differential expression of lignification related-genes and lignin accumulation in tolerant olive trees cv. 'Leccino'. J. Plant Physiol. 220, 60–68 (2018).

Funded by the European Union

Sabella, E., Aprile, A., Genga, A., Siciliano, T., Nutricati, E., Nicolì, F., Vergine, M., Negro, C., De Bellis, L., Luvisi, A. Xylem cavitation susceptibility and refilling mechanisms in olive trees infected by *Xylella fastidiosa*. Scientific Reports, 9(1), 9602 (2019).

Salman, M., Greenhut, R., Preece, J., Ferguson, L. & Kluepfel, D. Field evaluation of olive (*Olea europaea*) genotypes for resistance to *Pseudomonas savastanoi* pv. *savastanoi*. J. Plant Pathol. 102, 663–670 (2020).

Saponari, M., Boscia, D., Nigro, F. & Martelli, G. P. Identification of DNA sequences related to *Xylella fastidiosa* in oleander, almond and olive trees exhibiting leaf scorch symptoms in Apulia (southern Italy). J. Plant Pathol. 95, 668 (2013).

Saponari, M., Giampetruzzi, A., Loconsole, G., Boscia, D. & Saldarelli, P. *Xylella fastidiosa* in Olive in Apulia: Where We Stand. Phytopathology 109, 175–186 (2019).

Sarris, P. F., Cevik, V., Dagdas, G., Jones, J. D. G. & Krasileva, K. V. Comparative analysis of plant immune receptor architectures uncovers host proteins likely targeted by pathogens. BMC Biol. 14, 8 (2016).

Scaglione, D., Pinosio, S., Marroni, F., Di Centa, E., Fornasiero, A., Magris, G., Scalabrin, S., Cattonaro, F., Taylor, G. and Morgante, M., 2019. Single primer enrichment technology as a tool for massive genotyping: a benchmark on black poplar and maize. Annals of Botany 124, 543-551.

Schneider, K. van der Werf, W., a, M., Mourits, M.,Navas-Cortés, JA., Vicent, A., Oude Lansink, A. Impact of *Xylella fastidiosa* subspecies *pauca* in European olives. Proc. Natl. Acad. Sci. 117, 9250–9259 (2020).

Schulze, B. et al. Rapid Heteromerization and Phosphorylation of Ligand-activated Plant Transmembrane Receptors and Their Associated Kinase BAK1. J. Biol. Chem. 285, 9444–9451 (2010).

Sebastiani, L. et al. PacBio genome assembly of *Olea europaea* L. subsp. *europaea* cultivars Frantoio and Leccino. Sci. Data 12, 1095 (2025).

Shimizu, T. et al. Two LysM receptor molecules, CEBiP and OsCERK1, cooperatively regulate chitin elicitor signaling in rice: LysM receptors for rice chitin signaling. Plant J. 64, 204–214 (2010).

Shinya, T., Nakagawa, T., Kaku, H. & Shibuya, N. Chitin-mediated plant–fungal interactions: catching, hiding and handshaking. Curr. Opin. Plant Biol. 26, 64–71 (2015).

Sicard, A., Zeilinger, AR., Vanhove, M., Schartel, TE., Beal, DJ., Daugherty, MP., Almeida, RPP. *Xylella fastidiosa*: Insights into an Emerging Plant Pathogen. Annu. Rev. Phytopathol. 56, 181–202 (2018).

Simpson, AJ, et al. The Xylella fastidiosa Consortium of the Organization for Nucleotide Sequencing and Analysis. The genome sequence of the plant pathogen *Xylella fastidiosa*. Nature 406, 151–159 (2000).

Smith, S. A. & O'Meara, B. C. treePL: divergence time estimation using penalized likelihood for large phylogenies. Bioinformatics 28, 2689–2690 (2012).

Snoeck, S. Lee, HK., Schmid, MW., Bender, KW., Neeracher, MJ., Fernández-Fernández, AD., Santiago, J., Zipfel, C. Leveraging coevolutionary insights and AI-based structural

Funded by the European Union

modeling to unravel receptor–peptide ligand-binding mechanisms. Proc. Natl. Acad. Sci. 121, e2400862121 (2024).

Snoeck, S., Johanndrees, O., Nürnberger, T. & Zipfel, C. Plant pattern recognition receptors: from evolutionary insight to engineering. Nat. Rev. Genet. 26, 268–278 (2025).

Steidele, C.E., Gronnier, J., Stegmann, M., Hückelhoven, R. & Ried-Lasi, M. K. Promiscuity and specificity in ligand sensing by plant cell surface receptors. PLOS Pathog. 21, e1013548 (2025).

Steinegger, M. & Söding, J. MMseqs2 enables sensitive protein sequence searching for the analysis of massive data sets. Nat. Biotechnol. 35, 1026–1028 (2017).

Stevens, DM., Yang, D., Liang, TJ., Li, T., Vega, B., Coaker, GL., Krasileva, K. mamp-ml: A deep learning approach to epitope immunogenicity in plants. Preprint bioRxiv 15:2025.07.11.664399. doi: 10.1101/2025.07.11.664399 (2025).

Stevens, E.L., Heckenberg, G., Roberson, E.D., Baugher, J.D., Downey, T.J. and Pevsner, J., 2011. Inference of relationships in population data using identity-by-descent and identity-by-state. PLoS genetics, 7(9), p.e1002287.

Sun, L. & Zhang, J. Regulatory role of receptor-like cytoplasmic kinases in early immune signaling events in plants. FEMS Microbiol. Rev. 44, 845–856 (2020).

Sun, Y., Li, L., Macho, AP., Han, Z., Hu, Z., Zipfel, C., Zhou, JM., Chai, J. Structural Basis for flg22-Induced Activation of the Arabidopsis FLS2-BAK1 Immune Complex. Science 342, 624–628 (2013).

Tsalgatidou, P. C., Boutsika, A., Papageorgiou, A. G., Dalianis, A., Michaliou, M., Chatzidimopoulos, M., Delis, C., Tsitsigiannis, D. I., Paplomatas, E., & Zambounis, A. (2024). Global Transcriptome Analysis of the Peach (*Prunus persica*) in the Interaction System of Fruit–Chitosan–Monilinia fructicola. Plants, 13(5), 567.

Unver, T., Wu, Z., Sterck, L., Turktas, M., Lohaus, R., Li, Z., Yang, M., He, L., Deng, T., Escalante, FJ., Llorens, C., Roig, FJ., Parmaksiz, I., Dundar, E., Xie, F., Zhang, B., Ipek, A., Uranbey, S., Erayman, M., Ilhan, E., Badad, O., Ghazal, H., Lightfoot, DA., Kasarla, P., Colantonio, V., Tombuloglu, H., Hernandez, P., Mete, N., Cetin, O., Van Montagu, M., Yang, H., Gao, Q., Dorado, G., Van de Peer, Y. Genome of wild olive and the evolution of oil biosynthesis. Proc. Natl. Acad. Sci. 114 (2017).

Valverde, P., Barranco, D., López-Escudero, F. J., Díez, C. M. & Trapero, C. Efficiency of breeding olives for resistance to Verticillium wilt. Front. Plant Sci. 14, 1149570 (2023).

Van Sluys, M. A. et al. Comparative Analyses of the Complete Genome Sequences of Pierce's Disease and Citrus Variegated Chlorosis Strains of *Xylella fastidiosa*. J. Bacteriol. 185, 1018–1026 (2003).

Vatansever, R., Hernandez, P., Escalante, F. J., Dorado, G. & Unver, T. Genome-wide exploration of oil biosynthesis genes in cultivated olive tree varieties (Olea europaea): insights into regulation of oil biosynthesis. Funct. Integr. Genomics 22, 171–178 (2022).

Vetter, M. M. et al. Flagellin Perception Varies Quantitatively in Arabidopsis thaliana and Its Relatives. Mol. Biol. Evol. 29, 1655–1667 (2012).

Funded by the European Union

Vizzarri, V. et al. Comparative Assessment of *Verticillium dahliae* Tolerance in 77 Olive Cultivars. Crops 6, 9 (2026).

Vuruputoor, V. S. et al. Welcome to the big leaves: Best practices for improving genome annotation in non-model plant genomes. Appl. Plant Sci. 11, e11533 (2023).

Wallander, E. & Albert, V. A. Phylogeny and classification of Oleaceae based on rps16 and trnL-F sequence data. Am. J. Bot. 87, 1827–1841 (2000).

Wallis, C. M., & Chen, J. (2012). Grapevine phenolic compounds in xylem sap and tissues are significantly altered during infection by *Xylella fastidiosa*. Phytopathology 102(9), 816–826.

Wei, W., Sawyer, T. & Burbank, L. Csp1, a Cold Shock Protein Homolog in Xylella fastidiosa Influences Cell Attachment, Pili Formation, and Gene Expression. Microbiol. Spectr. 9, e01591-21 (2021).

Wickham H. ggplot2. WIREs Comput Stat. 2011;3:180–5. https://doi.org/10.1002/wics.147.

Willmann, R. et al. Arabidopsis lysin-motif proteins LYM1 LYM3 CERK1 mediate bacterial peptidoglycan sensing and immunity to bacterial infection. Proc. Natl. Acad. Sci. 108, 19824–19829 (2011).

Winkelmüller, T. M. et al. Gene expression evolution in pattern-triggered immunity within *Arabidopsis thaliana* and across Brassicaceae species. Plant Cell 33, 1863–1887 (2021).

Wong, T. K. F. et al. IQ-TREE 3: phylogenomic inference software using complex evolutionary models. Mol. Biol. Evol. 43, msag117 (2026).

Xiao, H., Huo, X., Wu, L., Zhong, L. & Cheng, Q. Gymnosperm FLS2 orthologues mediate conserved flg22 perception and divergent responses to flg22 variants. Prperint available at bioRxiv 2026.04.10.717846, doi: https://doi.org/10.64898/2026.04.10.717846 (2026).

Yuan, M. et al. Pattern-recognition receptors are required for NLR-mediated plant immunity. Nature 592, 105–109 (2021).

Zecharia, N., Krasnov, H., Vanunu, M., Castillo, A.I., Haberman, A., Dror, O., et al. *Xylella fastidiosa* outbreak in Israel: population genetics, host range and temporal and spatial distribution analysis. Phytopathology 112, 2296–2309 (2022).

Zhang, X., Henriques, R., Lin, S.-S., Niu, Q.-W. & Chua, N.-H. Agrobacterium-mediated transformation of *Arabidopsis thaliana* using the floral dip method. Nat. Protoc. 1, 641–646 (2006).

Zipfel, C. et al. Perception of the Bacterial PAMP EF-Tu by the Receptor EFR Restricts *Agrobacterium*-Mediated Transformation. Cell 125, 749–760 (2006).

Zipfel, C. Plant pattern-recognition receptors. Trends Immunol. 35, 345–351 (2014).

Funded by the European Union

7. SUPPLEMENTARY MATERIAL

Supplementary Table S1. Significantly upregulated DEGs in almond involved in phenolic compound biosynthesis.

Lc Vs. Uc					
Gene	**Gene Name**	**Function**	**Log2FC (Lc/Uc)**	**padj**	**Regulation**
4CL	4-coumarate:CoA ligase 3	Entry into the phenylpropanoid pathway	1.69	0.0027	Lc is Up
CHS	Chalcone-flavanone isomerase	Initiation of the flavonoid pathway	9.21	0.0008	Lc is Up
F3H	dihydroflavonol 4-reductase	Biosynthesis of dihydroflavonols / anthocyanins	6.51	0.0027	Lc is Up
FLS	flavonol synthase 1	Biosynthesis of flavonols	7.92	0.0005	Lc is Up
C4H	cinnamate 4-hydroxylase	Early step in the phenylpropanoid pathway	6.73	0.0029	Lc is Up
OMT	O-methyltransferase	Methylation of phenolic compounds	9.91	0.0002	Lc is Up
Gene	**Gene Name**	**Function**	**Log2FC (Ui/Uc)**	**padj**	**Regulation**
CHS	Chalcone-flavanone isomerase	Initiation of the flavonoid pathway	7.41	0.0006	Ui is Up
FLS	flavonol synthase 1	Biosynthesis of flavonols	5.6	0.0024	Ui is Up
C4H	cinnamate 4-hydroxylase	Early step in the phenylpropanoid pathway	7.33	0.0019	Ui is Up
OMT	O-methyltransferase	Methylation of phenolic compounds	7.7	0.001	Ui is Up

Genes represent those induced in the susceptible almond cultivar 'UEF' upon *Xylella fastidiosa* subsp. *fastidiosa* infection (Ui/Uc) and those constitutively upregulated in the resistant almond cultivar 'Lauranne' under basal conditions relative to the susceptible basal state (Lc/Uc).

Funded by the European Union

Supplementary Table S2. Significantly upregulated DEGs involved in callose formation.

Lc Vs. Uc					
Gene	**Gene Name**	**Function**	**log2FC (Lc/Uc)**	**padj**	**Regulation**
BBN70527	1,3-beta-glucan synthase	callose synthase	9.36337	0.0013	Lc is Up
BBN70526	glucan synthase-like 5	callose synthase	1.97315	8.17E-07	Lc is Up
BBN70191	beta-1,3-glucanase 1	callose degradation	7.44064	0.0008	Lc is Up
Ui Vs. Uc					
Gene	**Gene Name**	**Function**	**log2FC (Ui/Uc)**	**padj**	**Regulation**
BBN70527	1,3-beta-glucan synthase	callose synthase	9.25107	0.0009	Ui is Up

Genes represent those induced in the susceptible almond cultivar 'UEF' upon *Xylella fastidiosa* subsp. *fastidiosa* infection (Ui/Uc) and those constitutively upregulated in the resistant almond cultivar 'Lauranne' under basal conditions relative to the susceptible basal state (Lc/Uc).

Funded by the European Union

Supplementary Table S3. Significantly upregulated DEGs in almond involved in tylose formation.

Lc Vs. Uc					
Gene	**Gene Name**	**Function**	**log2FC (Lc/Uc)**	**padj**	**Regulation**
BBH00240	alpha-amylase-like 3	Amylase	7.50332	0.00044	Lc is Up
BBG92609	hypothetical protein	Amylase	7.07421	0.00044	Lc is Up
BBN68431	polyol/monosaccharide transporter 5	Monosaccharide transporter	9.89139	0.00022	Lc is Up
Ui Vs. Uc					
Gene	**Gene Name**	**Function**	**log2FC (Ui/Uc)**	**Padj**	**Regulation**
BBH02182	beta-amylase 4	Amylase	8.52847	0.00108	Ui is Up
BBG92609	hypothetical protein	Amylase	7.9748	0.00115	Ui is Up

Genes represent those induced in the susceptible almond cultivar 'UEF'upon *Xylella fastidiosa* subsp. *fastidiosa* infection (Ui/Uc) and those constitutively upregulated in the resistant almond cultivar 'Lauranne' under basal conditions relative to the susceptible basal state (Lc/Uc).

Funded by the European Union

Supplementary Table S4. Significantly upregulated DEGs in almond associated with the Plant-like hypersensitive response GO term.

Comparison	Gene id	log2FC	padj	Gene name	Regulation
Ui/Uc	BBG95704	9.2294	0.0012	F-box and associated interaction domains-containing protein	Up in Ui
	BBN67520	8.4860	0.0008	homolog of carrot EP3-3 chitinase	Up in Ui
	BBG98267	8.7119	0.0014	protein-binding protein	Up in Ui
	BBH05784	8.0326	0.0007	NB-ARC domain-containing disease resistance protein	Up in Ui
	BBH05778	6.2888	0.0389	NB-ARC domain-containing disease resistance protein	Up in Ui
	BBH01237	7.7947	0.0007	Ubiquitin carboxyl-terminal hydrolase family protein	Up in Ui
	BBH00319	6.3796	0.0006	myb domain protein 94	Up in Ui
	BBG96185	1.07E+12	0.0002	MAC/Perforin domain-containing protein	Up in Ui
	BBH05425	7.6891	0.0006	hypothetical protein	Up in Ui
	BBH01011	9.7142	0.0006	plant U-box 17	Up in Ui
	BBH03256	8.6619	0.0020	MAC/Perforin domain-containing protein	Up in Ui
Lc/Uc	BBH10359	5.6909	0.0035	RNA-binding protein-defense related 1	Up in Lc
	BBG96466	1.7899	0.0142	NB-ARC domain-containing disease resistance protein	Up in Lc
	BBG95704	8.4354	0.0009	F-box and associated interaction domains-containing protein	Up in Lc
	BBG98267	8.6965	0.0021	protein-binding protein	Up in Lc
	BBH05784	8.5021	0.0006	NB-ARC domain-containing disease resistance protein	Up in Lc
	BBH01237	7.08E+13	0.0005	Ubiquitin carboxyl-terminal hydrolase family protein	Up in Lc
	BBH00319	8.4936	0.0041	myb domain protein 94	Up in Lc
	BBG96185	10.6948	0.0000	MAC/Perforin domain-containing protein	Up in Lc
	BBH01011	9.8925	0.0004	plant U-box 17	Up in Lc
	BBH03256	8.7615	0.0007	MAC/Perforin domain-containing protein	Up in Lc

Genes represent those induced in the susceptible almond cultivar 'UEF' upon *Xylella fastidiosa* subsp. *fastidiosa* infection (Ui/Uc) and those constitutively upregulated in the resistant almond cultivar 'Lauranne' under basal conditions relative to the susceptible basal state (Lc/Uc). Matching colors indicate identical genes appearing in both comparisons.

Funded by the European Union

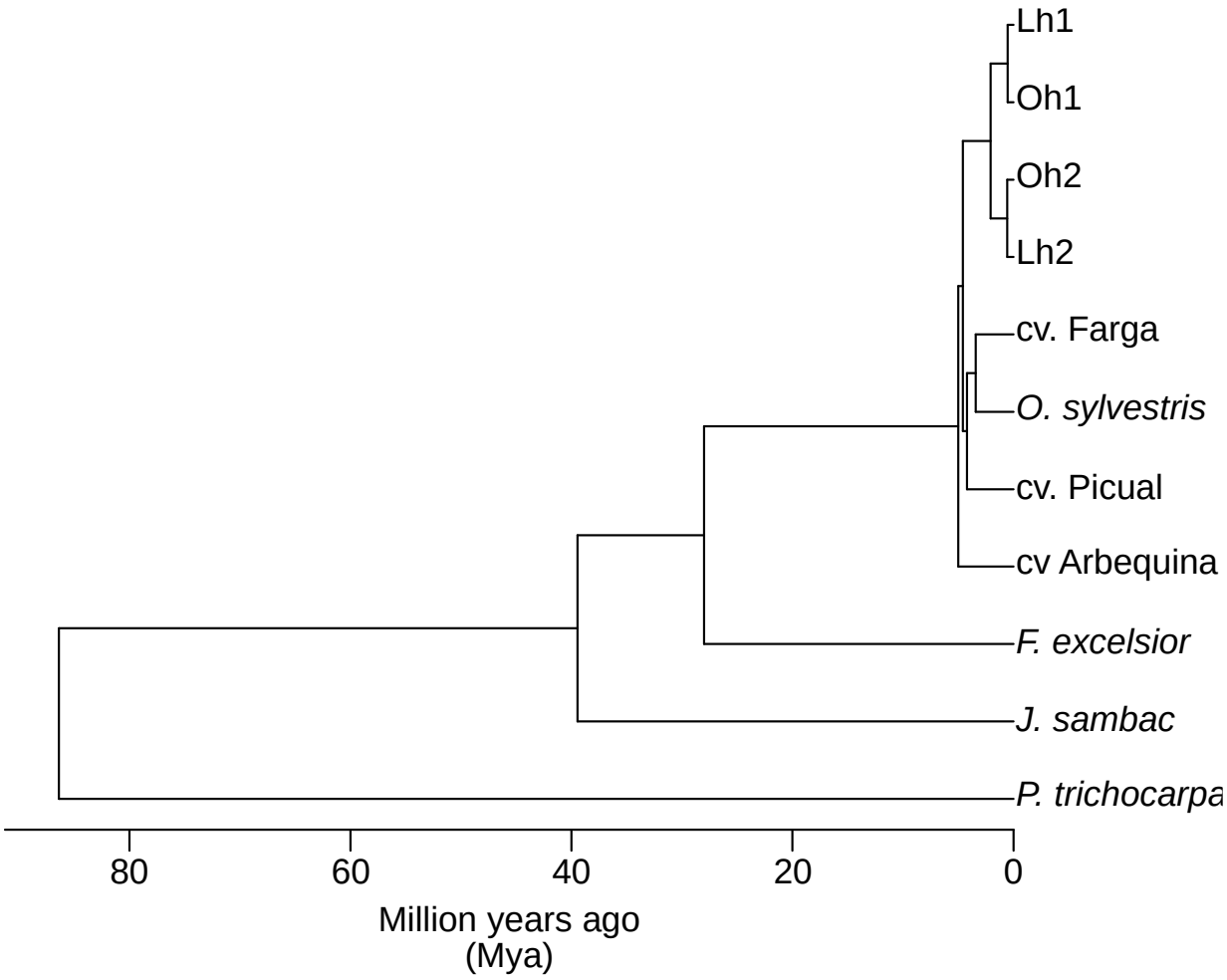
Supplementary Table S5. Disease susceptibility of olive cultivars

Pathogen (disease)	'Leccino'	'Ogliarola salentina'	References
Xylella fastidiosa (OQDS)	resistant	highly susceptible	Saponari et al., 2013, Giampetruzzi et al., 2016, Sabella et al., 2018, Saponari et al., 2019, Pavan et al., 2021
Pseudomonas savastanoi pv. *savastanoi* (olive knot)	moderately tolerant	moderately susceptible	Salman et al., 2020, Licciardello et al., 2023, Košćak et al., 2024
Verticillium dahliae (Verticillium wilt)	susceptible	moderately susceptible	Montes-Osuna et al., 2020, Ramírez-Tejero et al., 2021, Godena et al., 2022, Valverde et al., 2023, Vizzarri et al., 2026

Supplementary Table S6. Pairwise structural variations between olive haplotype assemblies detected by SyRI.

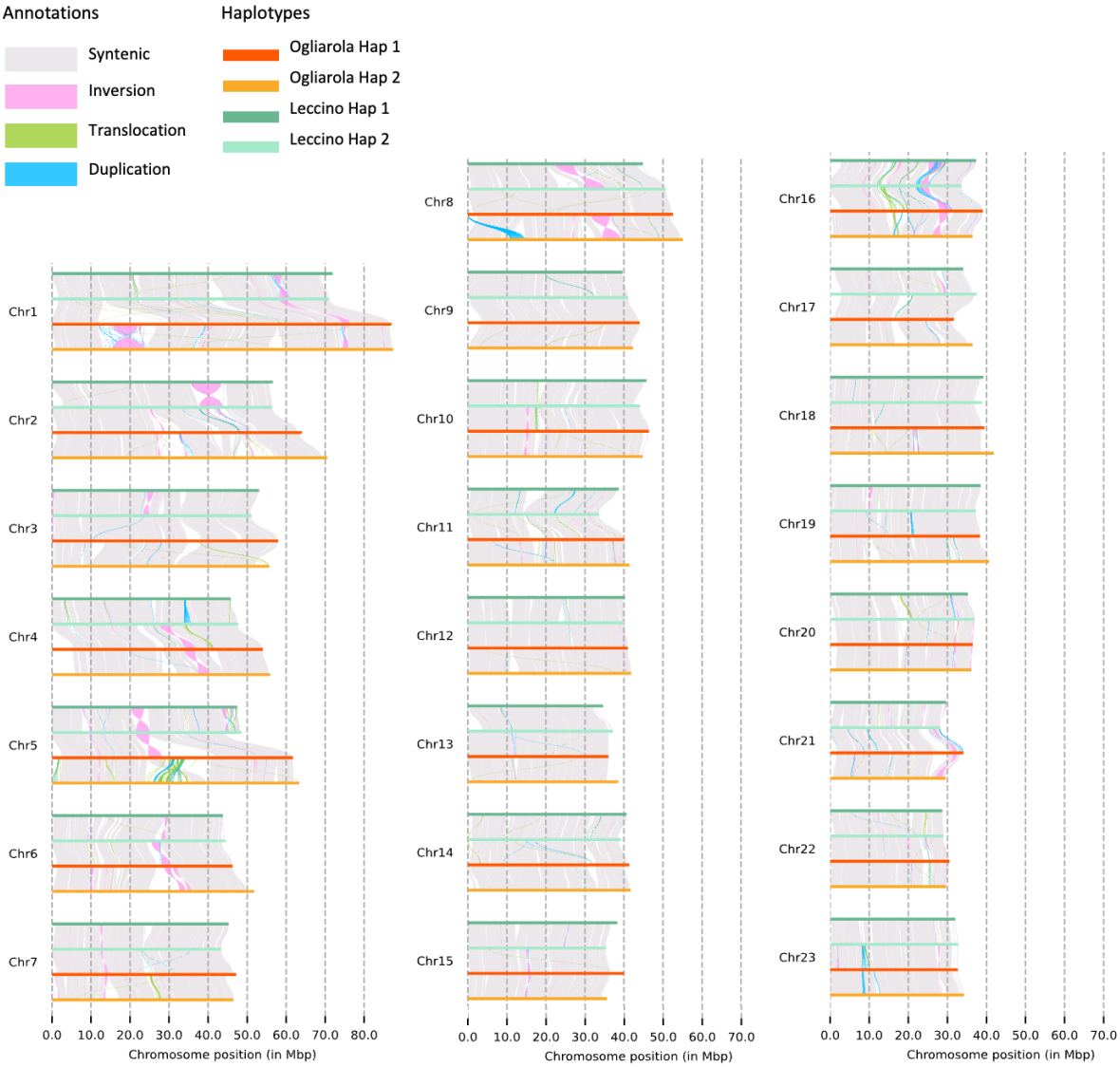
Pairwise comparison		Total nb of SVs	Inversions	Translocations	Inverted translocations	Duplications	Inverted duplications	Insertions (in query)	Deletions (in query)	Total genomic sequence affected (Mb) in ref	Total genomic sequence affected (Mb) in query
Reference	Query										
Leccino Hap 1	Leccino Hap 2	640827	129	427	457	489	498	319245	319582	55.23	50.68
Leccino Hap 1	Ogliarola Hap1	557395	100	481	423	797	748	277110	277736	53.57	48.32
Leccino Hap 1	Ogliarola Hap 2	479252	99	419	458	681	697	237746	239152	42.80	45.06
Leccino Hap 2	Ogliarola Hap2	565121	114	487	480	931	752	280956	281401	40.06	39.63
Ogliarola Hap 1	Ogliarola Hap 2	657716	149	668	592	997	1069	326878	327363	62.96	66.20
Ogliarola Hap 1	Leccino Hap 2	590056	115	452	413	723	744	293029	294580	44.84	44.24

Funded by the European Union



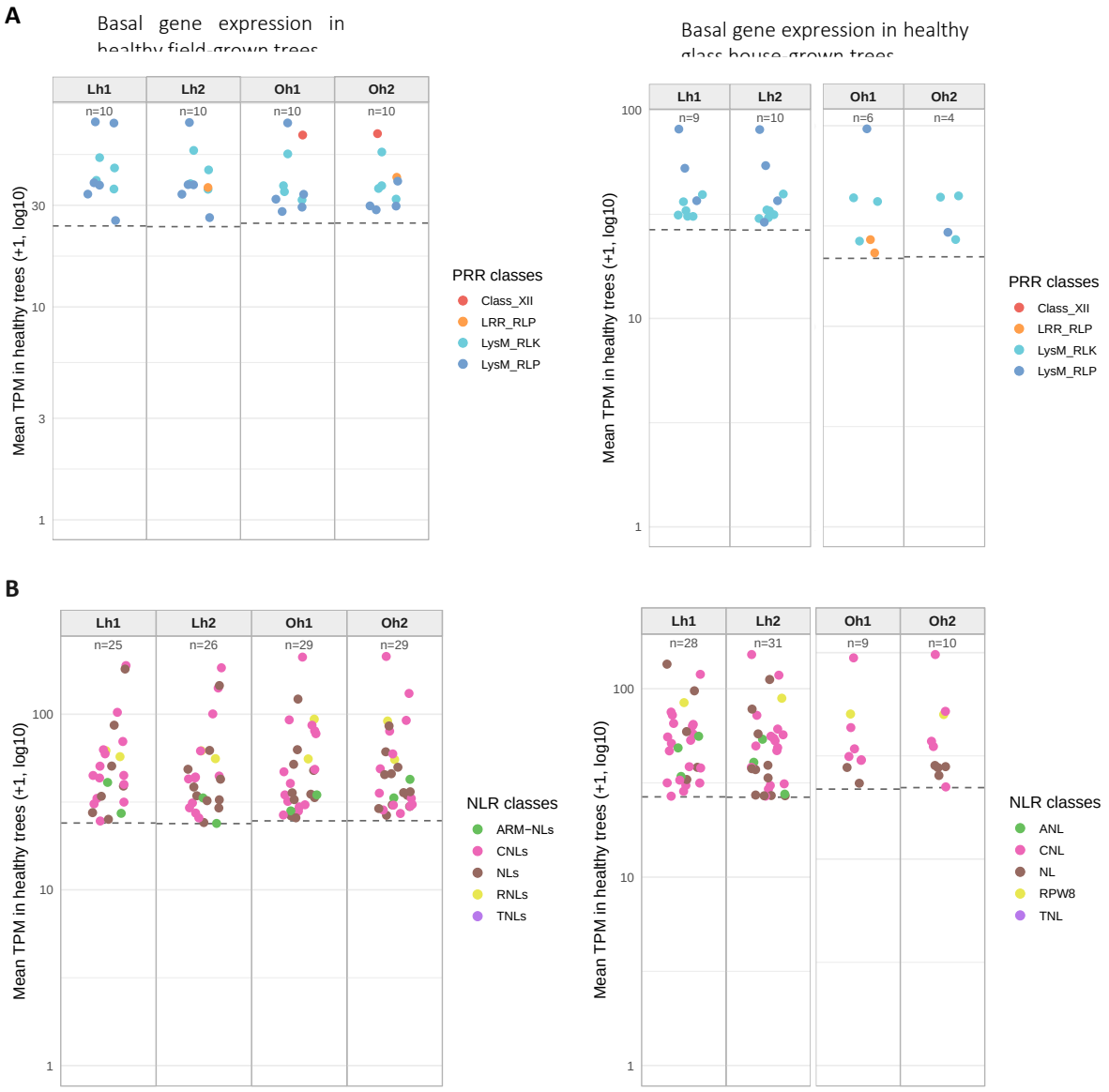
Supplementary Figure S1. Phylogenomic tree of 'Leccino', 'Ogliarola' and related *Olea* species. The species tree was inferred by OrthoFinder from single-copy orthologs using a gene tree-based approach and made ultrametric with treePL. Branch lengths reflect relative divergence time. The tree is rooted with *P. trichocarpa* as an outgroup.

Funded by
the European Union



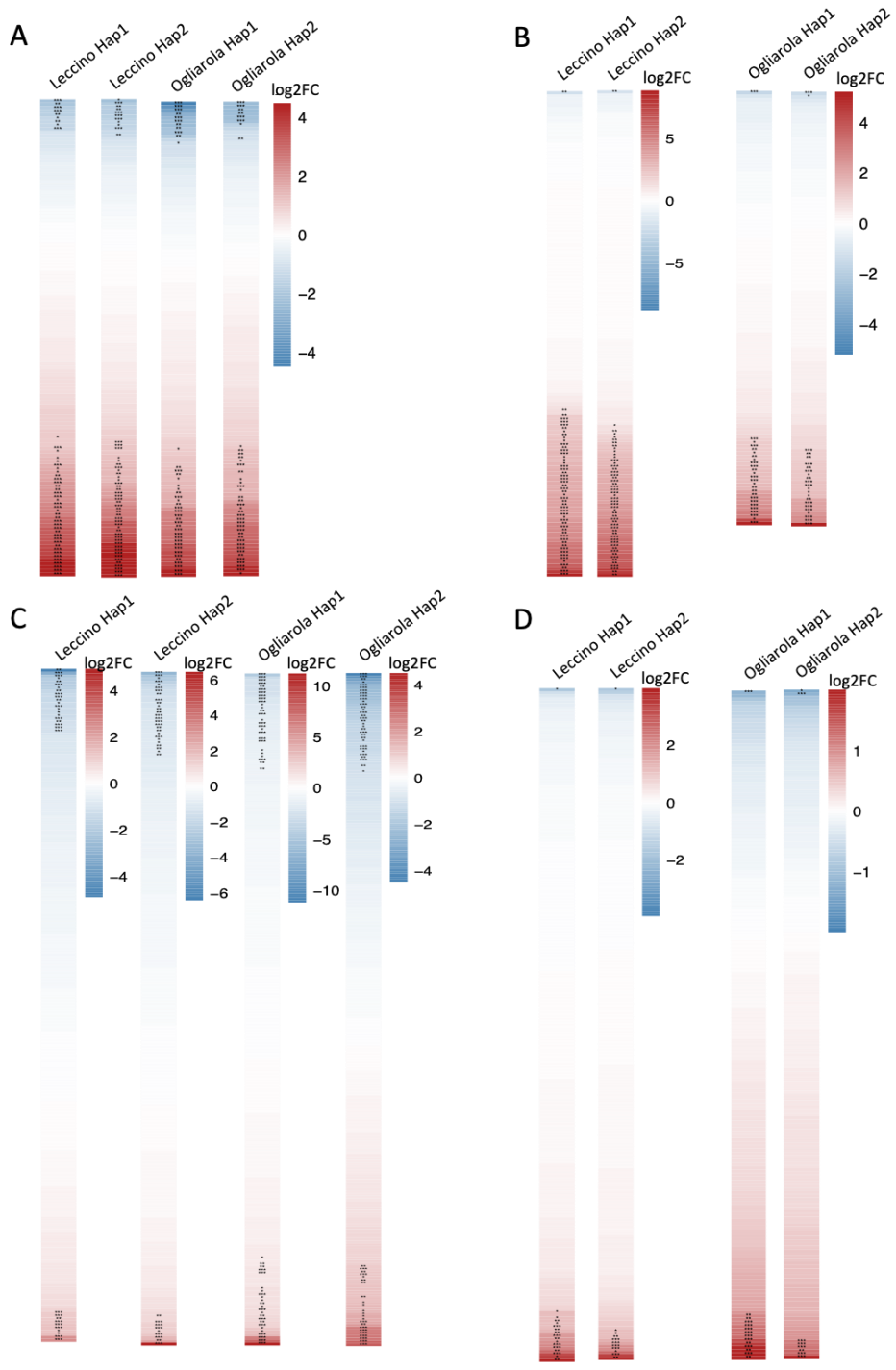
Supplementary Figure S2. Whole-genome synteny and structural variation analysis between 'Leccino' Haplotype 1, 'Leccino' Haplotype 2, Ogliarola Hap1 and Ogliarola Haplotype 2 (the previous one being the reference and the later the query, in a pairwise manner) detected with SyRI and visualized with plotsr. Genomic regions are color-coded as follows: syntenic regions (grey), inversions (pink), translocations (green), duplications (blue), and not-aligned regions (white). Chromosomes are represented as horizontal tracks and the connecting ribbons indicate homologous regions between the two assemblies.

Funded by the European Union



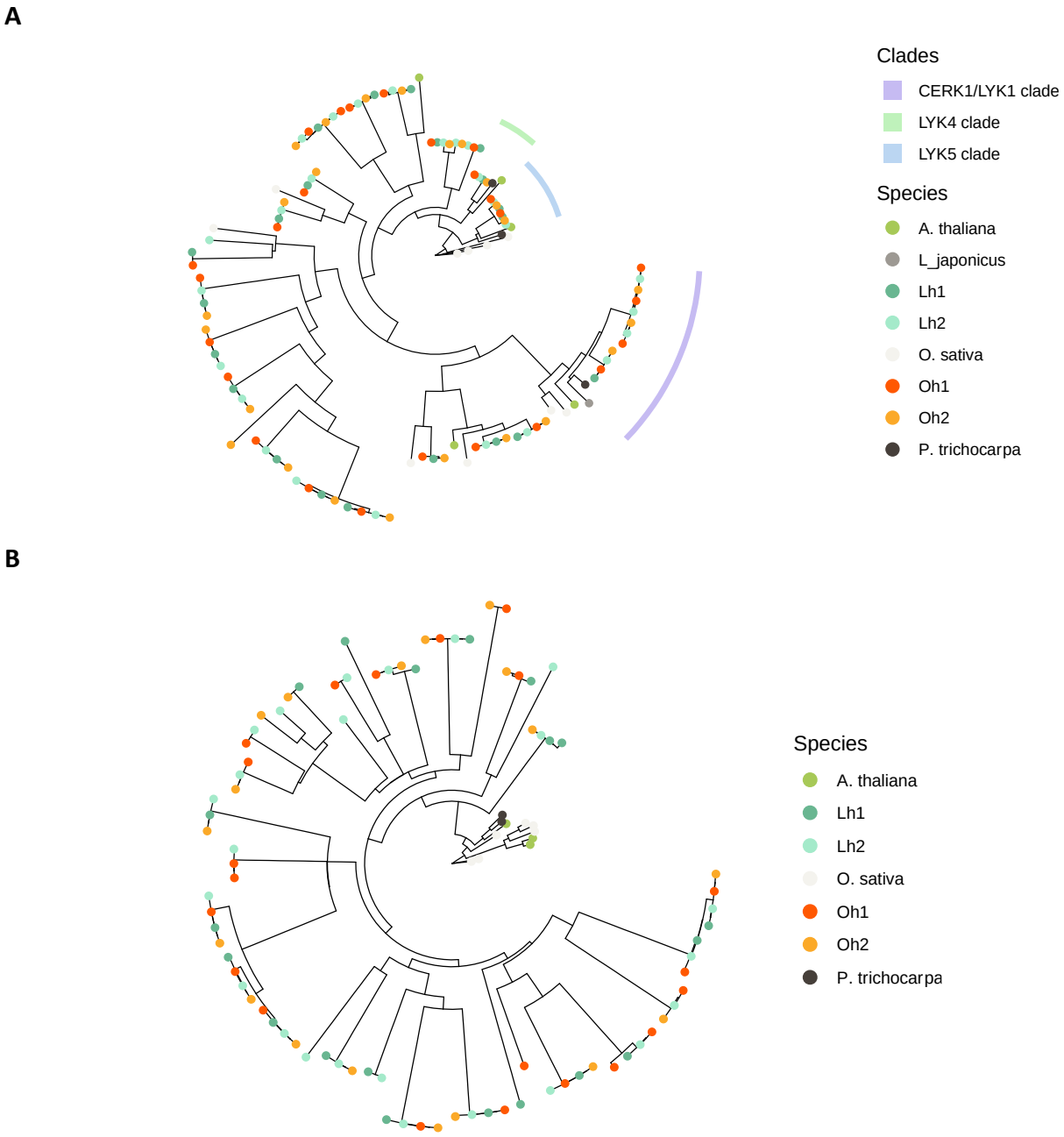
Supplementary Figure S3. Basal expression of *PRRs* and *NLRs* (A, B). Transcript abundance is shown as mean TPM (+1, log10) across healthy samples for each condition. 'Leccino' and 'Ogliarola salentina' reads were aligned to their respective haplotype assemblies (haplotypes 1 and 2). *PRRs* and *NLRs* are indicated by shaded colors; receptors falling within the top 20% most expressed genes are highlighted in bold color (black dashed line indicates the 20% expression cutoff).

Funded by the European Union



Supplementary Figure S4. Differential expression of *PRRs* and *NLRs* in healthy vs. *Xf*p-infected field-grown and greenhouse-grown trees. Log2 fold change (log2FC) in expression of PRR-encoding genes in healthy vs. *Xf*p-infected conditions in **A** field-grown trees and **B** greenhouse-grown trees. Log2FC in expression of NLR-encoding genes in healthy vs. *Xf*-infected conditions in **C** field-grown trees and **D** greenhouse-grown trees. Significance thresholds: * padj < 0.05, ** padj < 0.01, *** padj < 0.001 (with |log2FC| ≥ 1).

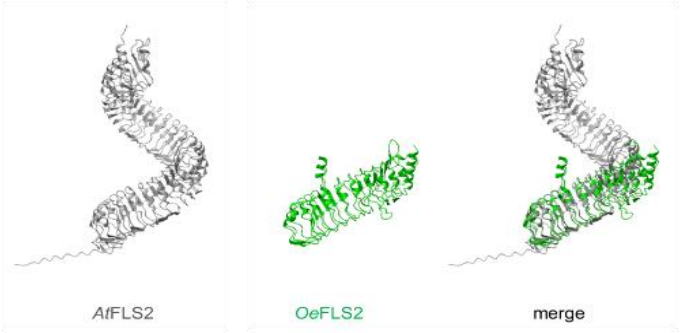
Funded by the European Union



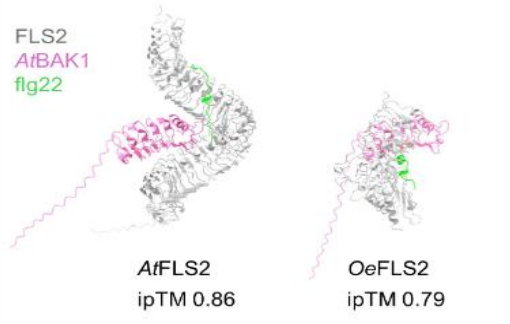
Supplementary Figure S5. LysM-RLK and LysM-RLP analysis. **A.** Phylogenetic tree of olive LysM-RLKs showing the relationship between the Arabidopsis and olive CERK1/LYK1, LYK5 and LYK4 orthologs, respectively. The triangle sectors indicate the clade clustering with known LRR-RLK-XII receptors from other plant species supported by OrthoFinder. The branch tip circles indicate the species and haplotypes. Lh1 = Leccino haplotype 1, Lh2 = Leccino haplotype 2, Oh1 = Ogliarola salentina haplotype 1, Oh2 = Ogliarola haplotype 2. **B.** Phylogenetic tree of LysM-RLPs from olive cultivars 'Leccino' and 'Ogliarola salentina' as well as reference plant species. Olive LysM-RLPs did not cluster with any functionally characterized LYPs, suggesting a divergent LysM-RLP repertoire in olive.

Funded by the European Union

A



B

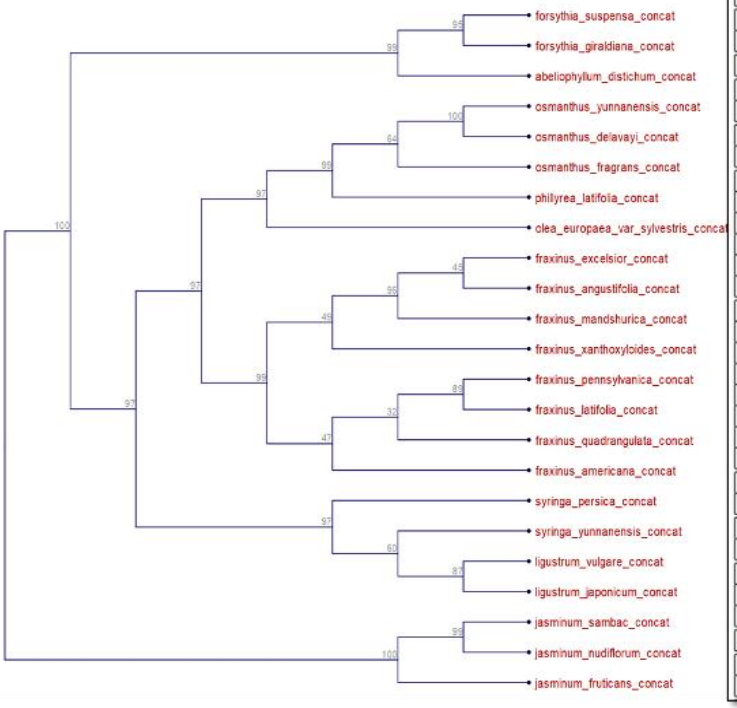


C

	flg22^{Pa}	flg15^{Pa}	flg15^{Ec}	flg22^{At}	flgII-28
*Oe*FLS2	1	1	1	1	**0**
*At*FLS2	**0**	2	2	1	1

Outcomes:
0 = immunogenic
1 = non-immunogenic
2 = weakly immunogenic

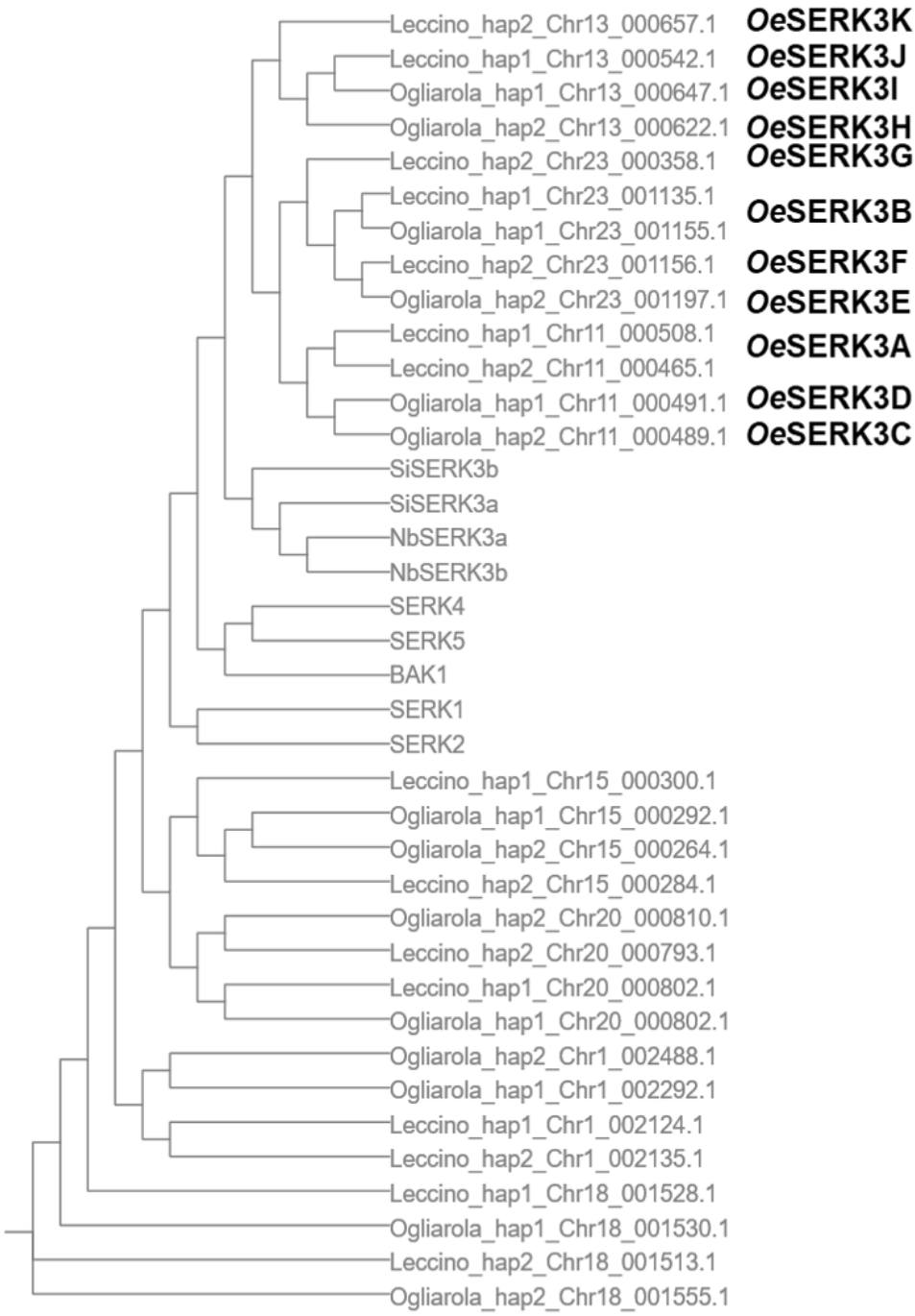
D



	flg22	chitin
Forsynthia suspensa	-	-
Forsynthia giraldiana	-	-
Abeliophyllum distichum	-	-
Osmanthus delavayi	-	-
Osmanthus fragrans	-	-
Phillyrea latifolia	-	-
Phillyrea angustifolia	-	-
Olea europaea ssp. *europaea*	-	-
var. *sylvestris*	-	-
var. *europaea*	-	-
cv. 'Leccino'	-	-
cv. 'Ogliarola'	-	-
cv. 'Frantoio'	-	-
Fraxinus excelsior	-	-
Fraxinus angustifolia	-	-
Fraxinus mandshurica	-	-
Fraxinus xanthoxyloides	-	-
Fraxinus pennsylvanica	-	-
Fraxinus latifolia	-	-
Fraxinus quadrangulata	-	-
Fraxinus americana	-	-
Syringa persica	-	-
Syringa yunnansensis	-	-
Ligustrum vulgare	-	-
Ligustrum japonicum	-	-
Jasminum sambac	-	-
Jasminum nudiflorum	-	-
Jasminum fructicans	-	-
Arabidopsis thaliana	+	+
Citrus limon	+	+
Citrus sinensis	(+)	+

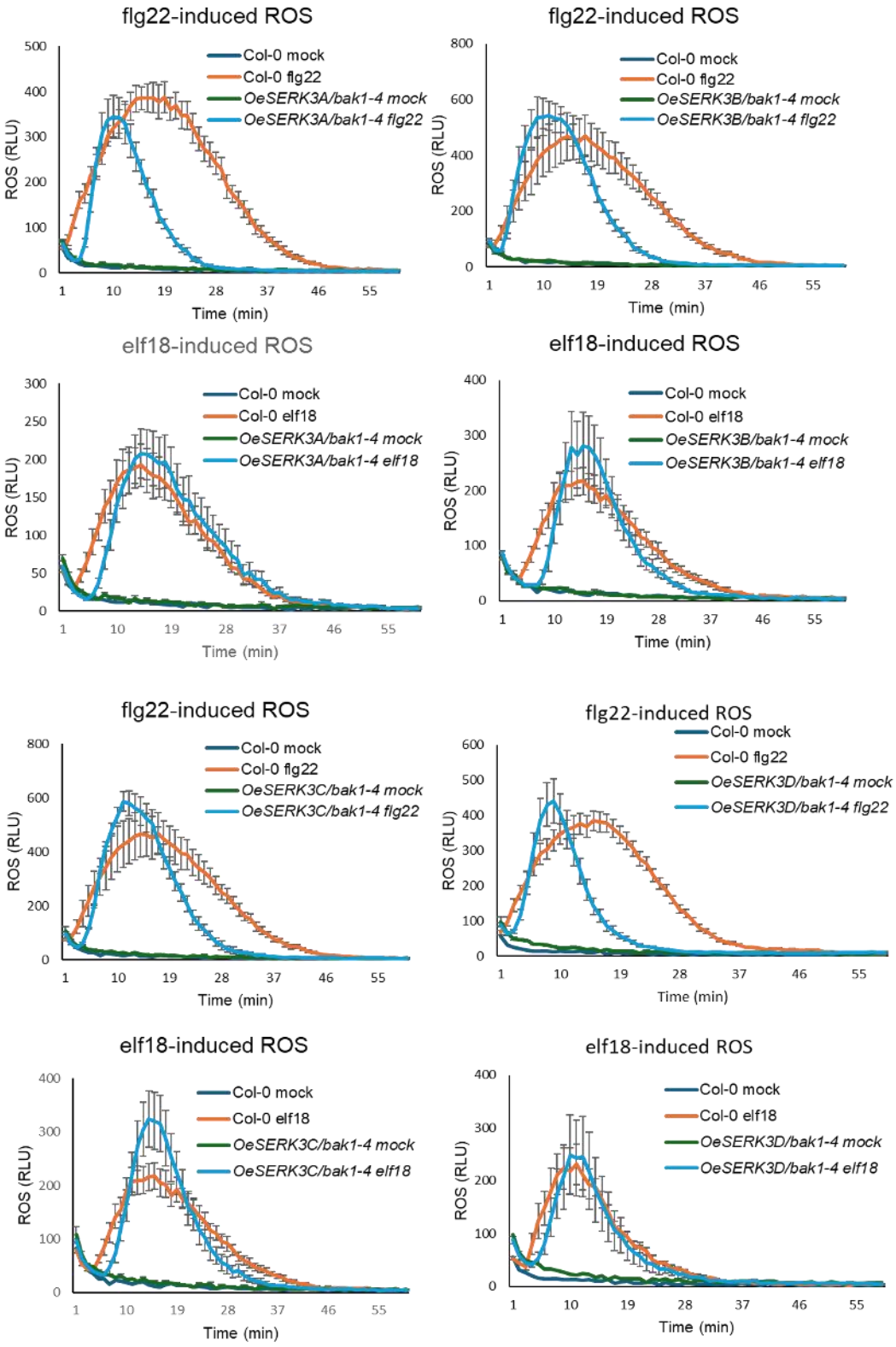
Supplementary Figure S6. Analysis of *OeFLS2*-like genes. **A, B.** Prediction of the indicated ectodomain structures without and with flg22 using AlphaFold2. **C.** Prediction of flg22 and flgII-28 peptide immunogenicity with OeFLS2-like and AtFLS2. **D.** Qualitative analysis of the ROS burst in response to flg22 in the indicated Oleaceae species.

Funded by the European Union



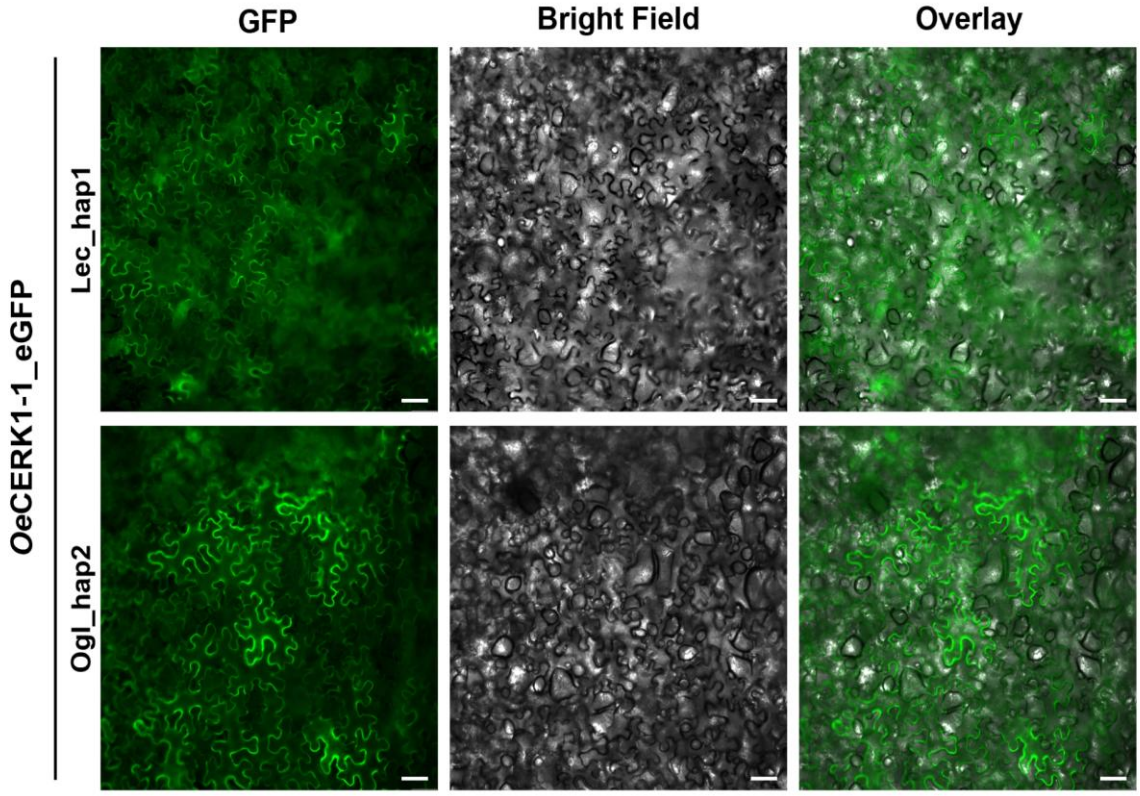
Supplementary Figure S7. OeSERK family analysis. Phylogenetic maximum-likelihood tree of SERK receptors from olive cultivars 'Leccino' and 'Ogliarola salentina' as well as reference plant species. OeSERK3s in bold were selected for functional validation.

Funded by the European Union



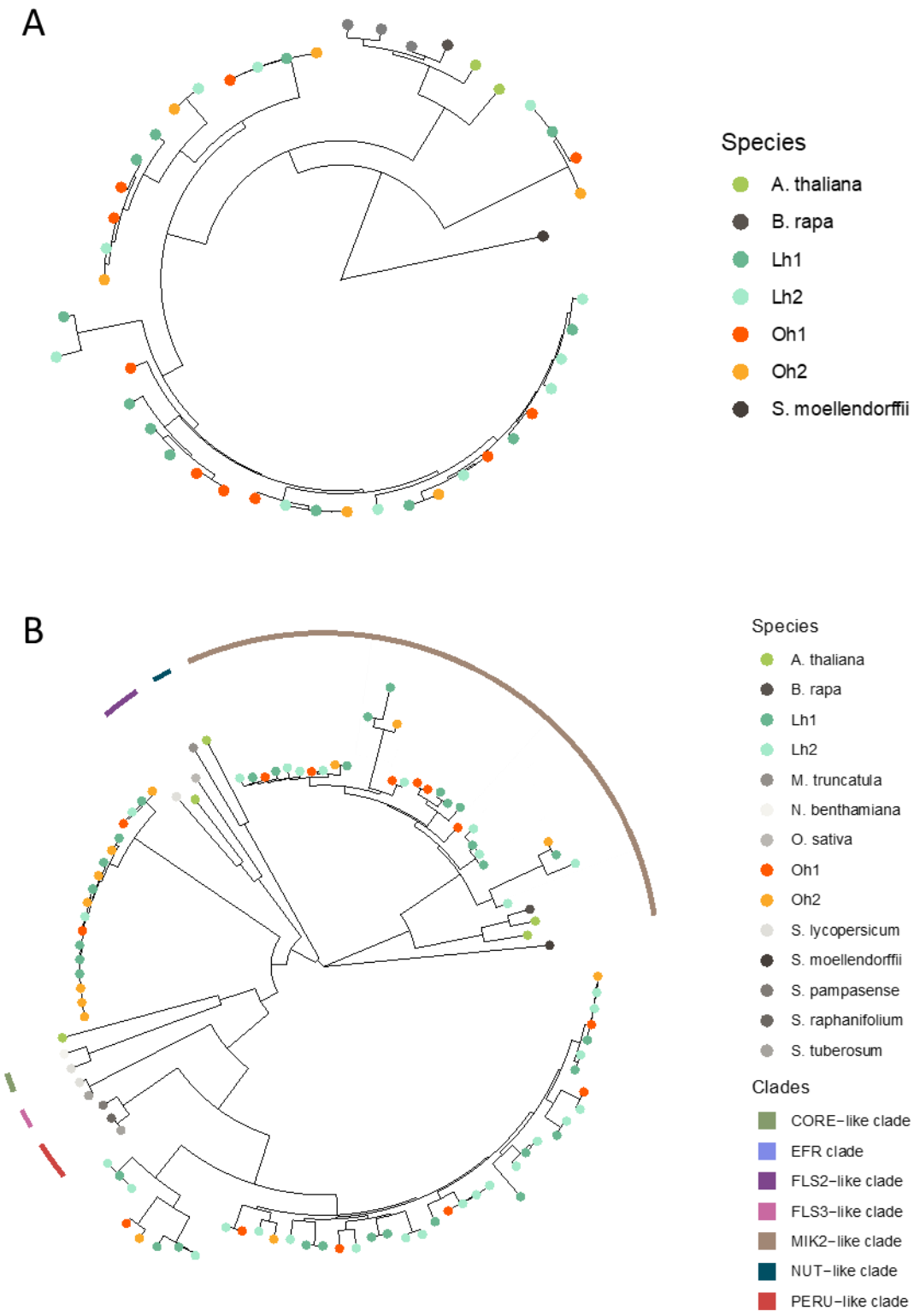
Supplementary Figure S8. Functional analysis of OeSERKs. *Arabidopsis thaliana bak1-4* mutant plants expressing the indicated OeSERK3s were generated and ROS burst was measured as RLU over time in leaves treated with the indicated elicitors.

Funded by the European Union



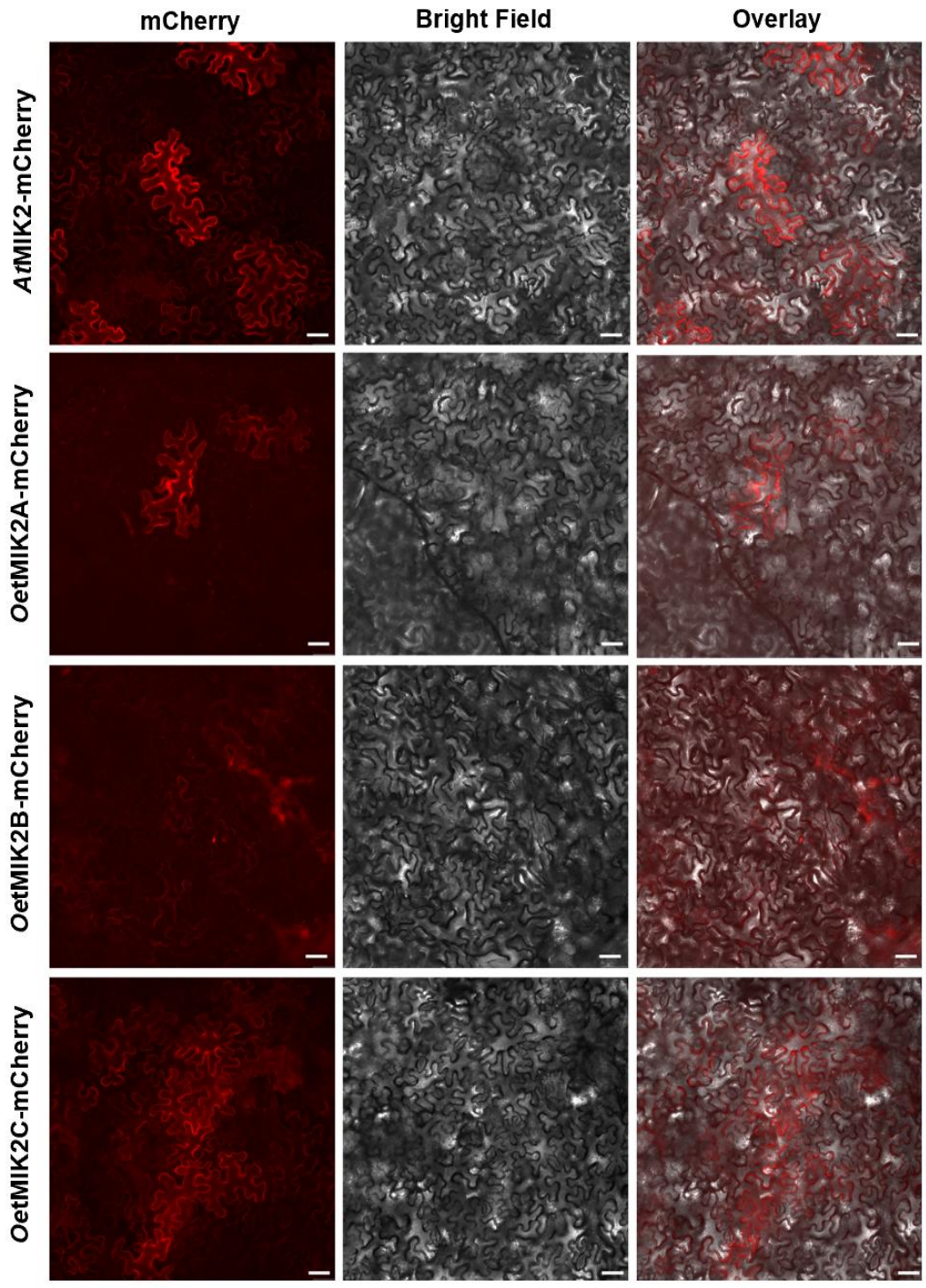
Supplementary Figure S9. Expression of *OeCERK1* genes in *Nicotiana benthamiana*. Microscopic images revealing that OeCERK1-1_eGFP localized on the cell periphery of *N. benthamiana* cells. The *pUBQ10::OeCERK1-1s_eGFP* construct was transiently expressed in *N. benthamiana*; (Scale bar = 50 µm).

Funded by
the European Union



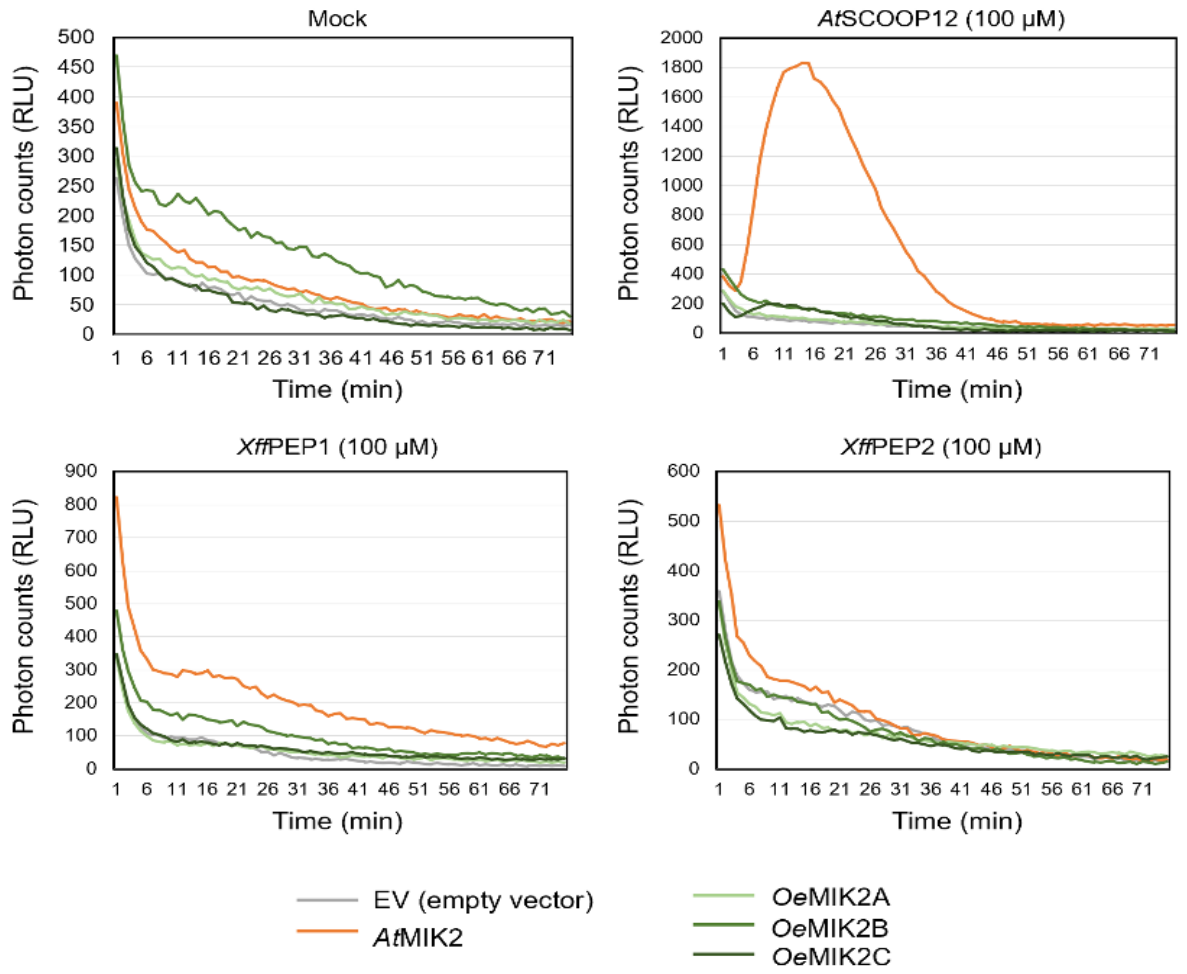
Supplementary Figure S10. Identification of *OeMIK2*-like genes and their expansion on the 'Leccino'-specific Chromosome 16 region. **A.** A phylogenetic tree was constructed based on the full-length protein sequences of all *OeMIK2*-like genes from the two olive cultivars and *At*MIK2 and known PRRs from other species. **B.** A phylogenetic tree based on olive LRR-RLK-XII only encoded on Chromosome 16.

Funded by the European Union



Supplementary Figure S11. Expression of *OeMIK2*-like genes in *Nicotiana benthamiana*. Microscopic images revealing that *Oe*MIK2s_mCherry is localized on the cell periphery of *N. benthamiana* cells. (weak signals for *Oe*MIK2B) The p*UBQ10::OeMIK2s_mCherry* construct was transiently expressed in *N. benthamiana*; scale bar = 50 µm.

Funded by the European Union



Supplementary Figure S12. Functional analysis of *OeMIK2*-like genes. ROS burst induced by different epitopes in *N. benthamiana* transiently expressing different *Arabidopsis* or olive MIK2-like candidates (EV, empty vector). ROS production was measured as relative luminescence units (RLU) over time. Only SCOOP12 triggered a detectable strong ROS burst in *At*MIK2 expressing discs, whereas *Oe*MIK2-likes did not respond to SCOOP12 or putative *Xff*-derived (PEP2) peptides.

Funded by the European Union